LBL-1007

PHENOMENOLOGY OF INCLUSIVE REACTIONS

Robert N. Cahn
(Ph.D. thesis)

July 18, 1972

AEC Contract No. W-7405-eng-48

PHENOMENOLOGY OF INCLUSIVE REACTIONS

Contents

PHENOMENOLOGY OF INCLUSIVE REACTIONS*

Robert N. Cahn

Lawrence Berkeley Laboratory
University of California
Berkeley, California 94720

July 18, 1972

ABSTRACT

Inclusive reactions are examined in the context of the Mueller formalism, which exploits the connection of the inclusive cross section with the six-point amplitude and Regge behavior. Some previous results of the model are reviewed. Internal symmetries together with the Mueller picture are used to produce a large number of testable predictions. The fundamental symmetries of the strong interactions yield predictions which test the validity of the basic assumptions of the model. SU(3) gives predictions which are expected to be violated, and thus furnish extensive information about symmetry breaking. Angular distributions yield information about behavior in the central rapidity region, if the transverse momentum distribution is known. The dual resonance model provides predictions for fragmentation and pionization, but the results are based on a naive model and do not agree with the data. Inclusive photon distributions are examined in detail. They provide information mainly about the inclusive π^0 distribution. In the low-transverse momentum region, bremsstrahlung is significant and can provide a measure of the charged multiplicity. The photon distribution arising from π^0 decays in the central region obeys an equality relating the spectrum at zero transverse momentum to the integral of the spectrum over all transverse momenta. A variety of experimental data are reviewed and compared with the predictions and prescriptions of the preceeding chapters.

PREFACE

As this thesis is the culmination of my formal education, I should like to take this opportunity to thank a number of people for their contributions to it. Professor J. D. Jackson has been more than generous with his time and his consistently reliable advice. In both his own work and his teaching, he has provided a model for thoroughness and clarity of insight which, if it cannot be copied, will certainly not be forgotten. Dr. Martin Einhorn has played a dual role as collaborator and teacher and his extensive assistance is gratefully acknowledged.

I should also like to thank some of those at Berkeley whom I have been privileged to learn from and/or work with: Professor Owen Chamberlain, Professor Geoffrey Chew, Professor Marvin Cohen, Professor William Chinowsky, Dr. Richard Field, Dr. Cristian Sorensen, Dr. Frank von Hippel, and Professor Eyvind Wichmann. In a variety of ways, these people have contributed to making my years in Berkeley exciting and rewarding.

Professor Charles Schwartz has contributed uniquely to my education and, I think, to the education of many of those who have been challenged by his dedication to the task of making physics humane.

I should like to thank Mrs. Christina Graham and Miss Georgella Perry for their efforts in the typing and preparation of this text.

Finally, I thank my family for their endurance and support.

BLANK

INTRODUCTION

This is not intended as a review of inclusive processes. Such an effort would be nearly futile in a field which is expanding as quickly as is this one. Fortunately, a few brave persons have undertaken such a task and the uninitiated reader is referred to their works for an introduction to the subject (Frazer et al., 1972; Berger, 1971a, 1971b; Quigg, 1971a, 1971b; Bjorken, 1971; Young, 1971; Arnold, 1971; Horn, 1971; Gasiorowicz, 1971). Among the original papers, those of DeTar (DeTar 1971) and Mueller (Mueller, 1970) provide an excellent starting point.

The title "Phenomenology of Inclusive Reactions" is meant to suggest that we shall focus on questions which are immediate to the interpretation of data. Consequently, we do not consider to any great extent a number of important topics such as the helicity structure of the six-point amplitude (Goddard and White, 1970, 1971, 1971a, 1972; DeTar et al., 1971a; Weis, 1971, 1972; Jones, Low, and Young, 1971). In addition, a number of important phenomenological topics are not discussed. One of these is the question of "exoticity." For this continuing controversy, the reader is referred to the original literature (Chan et al., 1971; Ellis et al., 1971; Chan and Hoyer, 1971a; Einhorn, Green, and Virasoro, 1972). An equally important topic is the analogue of finite energy sum rules for inclusive reactions (Dias De Deus, and Lam, 1972; Kwiecinski, 1972; Sanda, 1972; Einhorn, Ellis, and Finkelstein, 1972).

Phenomenological theories not based on the Mueller approach have been developed by several authors (Grote et al., 1971; G. Ranft, 1971; J. Ranft, 1971; Hwa and Lam, 1971, 1972; Jacob and Slansky, 1971, 1972; Jacob, Slansky, and Wu, 1972).[1]

There has been no attempt to review all the experimental data; only a portion of the data bearing on the theoretical developments of the text is discussed. The reader is referred to the review articles cited above for further experimental references.

CHAPTER ONE

PRELIMINARIES

A. Kinematics, Notation, and Definitions

An inclusive reaction or process is one in which not all the outgoing particles are specified. Thus the total cross section for $a + b$, $\sigma_{ab}(s)$, where s is the center-of-mass energy squared, might be called an inclusive measurement. The primary focus of this work is single particle inclusive processes, the archetype of which is $a + b \to c +$ anything. We shall develop notation and investigate the kinematics first for single particle inclusive processes and then consider generalizations to n-particle inclusive processes of the form $a + b \to c_1 + c_2 + \cdots + c_n +$ anything.

To begin, consider $a + b \to c +$ anything in a frame in which the momenta p_a and p_b are colinear. We can parameterize the momenta as

$$\begin{aligned} p_a &= (m_a \cosh \zeta_a,\ 0,\ 0,\ m_a \sinh \zeta_a) \\ p_b &= (m_b \cosh \zeta_b,\ 0,\ 0,\ m_b \sinh \zeta_b) \\ p_c &= (\omega_c \cosh \zeta,\ p_{xc},\ p_{yc},\ \omega_c \sinh \zeta) \end{aligned} \tag{1.1}$$

where

$$\begin{aligned} \omega_c^2 &= m_c^2 + p_{xc}^2 + p_{yc}^2 \\ &= m_c^2 + p_\perp^2 . \end{aligned} \tag{1.2}$$

Three frames have special significance: the rest frames of particles a and b, and the center of mass frame. Explicitly, in the rest frame of particle b (the "lab frame" if b is the target) we have:

$$\begin{aligned} p_a &= (m_a \cosh Y,\ 0,\ 0,\ m_a \sinh Y) \\ p_b &= (m_b,\ 0,\ 0,\ 0) \\ p_c &= (\omega_c \cosh y_c,\ p_{xc},\ p_{yc},\ \omega_c \sinh y_c) . \end{aligned} \tag{1.3}$$

On the other hand, in the center of mass frame, we have

$$\begin{aligned} p_a &= (m_a \cosh Z_a,\ 0,\ 0,\ m_a \sinh Z_a) \\ p_b &= (m_b \cosh Z_b,\ 0,\ 0,\ m_b \sinh Z_b) \\ p_c &= (\omega_c \cosh z,\ p_{xc},\ p_{yc},\ \omega_c \cosh z) . \end{aligned} \tag{1.4}$$

The variables ζ, y, and z are called rapidities. Their utility derives from their intimate connection with the Lorentz group. The rapidities of particles measured relative to two different frames moving colinearly with the momenta p_a and p_b are related by a constant which reflects the boost necessary to bring one frame into equivalence with the other. In particular, $Y = Z_a - Z_b$. Furthermore, the Lorentz invariant phase space factor, d^3p/E, is given by $d^2p_\perp\, dy$.

We can relate the rapidities defined above to the center of mass energy squared, $s = (p_a + p_b)^2$. Directly from (1.3) and (1.4) we find

$$s = m_a^2 + m_b^2 + 2m_a m_b \cosh Y$$

$$m_a \cosh Z_a = \frac{s + m_a^2 - m_b^2}{2(s)^{\frac{1}{2}}} \tag{1.5}$$

$$m_b \cosh Z_b = \frac{s + m_b^2 - m_a^2}{2(s)^{\frac{1}{2}}} \quad .$$

For large s, Eqs. (1.5) yield immediately

$$\begin{aligned} Y &\simeq \ell n\left(\frac{s}{m_a m_b}\right) \\ Z_a &\simeq \ell n[(s)^{\frac{1}{2}}/m_a] \\ Z_b &\simeq -\ell n[(s)^{\frac{1}{2}}/m_b] \quad . \end{aligned} \tag{1.6}$$

B. The Phase Space Boundary

The phase space boundary for $a + b \to c +$ anything can be determined by calculating the missing mass, M^*:

$$\begin{aligned} M^{*2} &= (p_a + p_b - p_c)^2 \\ &= s + m_c^2 - 2s^{\frac{1}{2}} \omega_c \cosh z \quad . \end{aligned} \tag{1.7}$$

There is a minimum value of M^* determined by the quantum numbers of a, b, and c. For example, for $p + K^- \to \Lambda^+ +$ anything, $M^* \geq m_\pi$ while for $p + p \to \pi^+ +$ anything, $M^* \geq$ mass of the deuteron. Let

$$\Delta = (M^*_{min})^2 - m_c^2 \quad . \tag{1.8}$$

Then from (1.4) we find that

$$\frac{\Delta}{s} = 1 - 2s^{-\frac{1}{2}} \omega_c \cosh z \tag{1.9}$$

is the equation of the phase space boundary. For large s, to lowest order in Δ/s, the curve has a universal shape in the center of mass, independent of particles a and b:

$$\cosh z = s^{\frac{1}{2}}/(2\omega_c) \quad . \tag{1.10}$$

For fixed ω_c and for large s, the extreme values of z permitted are

$$z_{ext} \simeq \pm \ell n\left(\frac{s^{\frac{1}{2}}}{\omega_c}\right) \quad . \tag{1.11}$$

Using Eq. (1.6) we can find equivalent forms in the rest frame of particle b:

$$\begin{aligned} y_{max} &\simeq Y + \ell n\left(\frac{m_a}{\omega_c}\right) \\ y_{min} &\simeq \ell n\left(\frac{\omega_c}{m_b}\right) \quad . \end{aligned} \tag{1.12}$$

C. Fragmentation and Pionization

We define three important domains for single particle inclusive processes:

1. $p_\perp$ fixed, $Z_a - z$ fixed, s increasing ,
2. $p_\perp$ fixed, $z - Z_b$ fixed, s increasing ,
3. $p_\perp$ fixed, z fixed, s increasing.

The first and second we call fragmentation of a and b respectively. The third we call pionization. We denote these three symbolically by $(b|c:a)$, $(b:c|a)$, and $(b|c|a)$. A colon indicates a fixed rapidity difference and a vertical slash a growing one. With b at rest in the laboratory, the process $(b:c|a)$ is a function of the lab rapidity, Y, of particle a, the lab rapidity, y, of particle c, and $p_\perp$, its transverse momentum. The hypothesis of limiting fragmentation (Benecke et al., 1969; Chou and Yang, 1970; Feynman, 1969) suggests that as $Y \to \infty$, $d\sigma/d^2p_\perp dy$ $(y, p_\perp, Y)$ approaches a limit which is independent of Y and which we shall indicate by $f(y, p_\perp)$. Similarly, $(b|c|a)$ is a function of $Z_a - Z_b = Y$, z, and $p_\perp$. As $Y \to \infty$, with z and $p_\perp$ fixed, it is expected that $d\sigma/d^2p_\perp dz$ $(z, p_\perp, Y)$ approaches a limit which is a function of $p_\perp$ only.

The generalization of these concepts is straightforward. Consider $(b:c_1|c_2,c_3|c_4|c_5:a)$. Here we are interested in the five-particle inclusive cross section with $z_2 - z_1$, $z_4 - z_3$, and $z_5 - z_4$ increasing while $z_1 - Z_b$, $z_3 - z_2$, and $Z_a - z_5$ are held fixed. It is understood that all the transverse momenta are fixed as well. We expect that at high values of s, $d\sigma/\prod_i(d^2p_{\perp_i} dz_i)$ becomes a function of the transverse momenta and the fixed, finite, rapidity differences only.

D. Kinematic Relations

While rapidities are generally the most useful longitudinal variables, in some applications, Feynman's variable (Feynman, 1969) $x = p_{zc}/[(s)^{\frac{1}{2}}/2]$ (z is the beam direction) has advantages. In this language, $x = 0$ corresponds to the pionization limit defined above.

As $s \to \infty$, with $p_\perp$ fixed, the phase space boundary is given simply by $|x| = 1$. The relation between x and z is easily determined:

$$x = \omega_c \sinh z/(2s^{\frac{1}{2}}) . \tag{1.13}$$

If we consider $x \neq 0$, as $s \to \infty$, we have

$$\begin{aligned} x &= \pm \frac{\omega_c}{m_a} e^{\frac{|z|}{Z_a}} \\ &= \pm \frac{\omega_c}{m_b} e^{\frac{|z|}{-Z_b}} . \end{aligned} \tag{1.14}$$

If $z > 0$

$$\begin{aligned} x &= \frac{\omega_c}{m_a} e^{-(Z_a - z)} \\ &= \frac{\omega_c}{m_a} e^{-y'} \end{aligned} \tag{1.15}$$

where y' is the rapidity of c in the rest frame of a. If, on the other hand, $z < 0$, then

$$x = -\frac{\omega_c}{m_b} e^{-y} \tag{1.16}$$

where y is the rapidity of c in the rest frame of b.

For $x > 0$, from (1.4) and (1.19), as $s \to \infty$

$$\begin{aligned} \frac{M^{*2} - m_c^2}{s} &= 1 - \left(x^2 + \frac{4\omega_c^2}{s}\right)^{\frac{1}{2}} \\ &\simeq 1 - |x| . \end{aligned} \tag{1.17}$$

It is also convenient to be able to express the standard invariants s, t, and u in terms of the rapidities or x. Of course one has the usual relation between the Mandelstam invariants:

$$s + t + u = m_a^2 + m_b^2 + m_c^2 + M^{*2} . \tag{1.18}$$

Using rapidities in the rest frame of a,

$$\begin{aligned} t &= (p_a - p_c)^2 \\ &= m_a^2 + m_c^2 - 2m_a\omega_c \cosh y' . \end{aligned} \tag{1.19}$$

Using (1.15) we find

$$\begin{aligned} t &\simeq m_a^2 + m_c^2 - m_a\omega_c\left(\frac{m_a x}{\omega_c} + \frac{\omega_c}{m_a x}\right) \\ &\simeq -p_\perp^2/x + m_a^2(1 - x) + m_c^2(1 - 1/x) . \end{aligned} \tag{1.20}$$

The analogous calculation for u yields:

$$u \simeq -xs . \tag{1.21}$$

In deriving (1.19) and (1.20), we have assumed $x > 0$ as $s \to \infty$. For $x > 0$, the roles of t and u would be interchanged. An interesting combination of Mandelstam invariants is given by tu/s. For fixed y' and $Y \to \infty$, we see that

$$\begin{aligned} tu &= (m_a^2 + m_c^2 - 2m_a\omega_c \cosh y')(m_b^2 + m_c^2 - 2m_b\omega_c \cosh[Y - y']) \\ &\simeq s(\omega_c^2 - [m_a^2 + m_c^2]x + m_a^2x^2) . \end{aligned} \tag{1.22}$$

Thus in the pionization domain,

$$\frac{tu}{s} \simeq \omega_c^2 . \tag{1.23}$$

For convenience we record here the phase-space volume in a variety of variables (the approximate relations are true asymptotically at high s):

$$\begin{aligned} \frac{d^3p}{E} &= d^2p_\perp\, dz \\ &= \pi dp_\perp^2\, dz \\ &\simeq \pi dp_\perp^2 \frac{dx}{x} \\ &\simeq \pi dx(-dt) \\ &\simeq \pi \frac{dM^{*2}}{s} dt . \end{aligned} \tag{1.24}$$

CHAPTER TWO

MODEL INDEPENDENT RELATIONS

Certain relations involving inclusive reactions may be derived without the introduction of models or assumptions such as Feynman scaling. These fundamental relations rely on kinematics and conservation laws, and their usefulness comes from the tests they provide on the consistency of both data and theories.

Let us abbreviate $dp_i = d^3p_i/E_i$. Then

$$\int dp_c \frac{d\sigma}{dp_c} = \langle n_c \rangle \sigma_{tot} . \tag{2.1}$$

The factor $\langle n_c \rangle$ is the mean multiplicity of particle type c. It arises because by integrating over dp_c we count up each particle of type c which occurs. We could define $\langle n_c \rangle$ independently of (2.1) by

$$\langle n_c \rangle \sigma_{tot} = \sum_{m=1}^{\infty} m \sigma_m \tag{2.2}$$

where σ_m is the cross section for producing precisely m particles of type c.

If c and d are distinct particle types, then

$$\int dp_c \, dp_d \frac{d\sigma}{dp_c \, dp_d} = \langle n_c n_d \rangle \sigma_{tot} . \tag{2.3}$$

If $c = d$, then

$$\int dp_c \, dp_d \frac{d\sigma}{dp_c \, dp_d} = \langle n_c^2 - n_c \rangle \sigma_{tot} \tag{2.4}$$

since each n-particle production event will be counted $n(n-1)$ times. Equations (2.3) and (2.4) can of course be generalized further.

Consider a conserved, additive quantity Q (such as charge). It is clear that

$$Q_a + Q_b = \sum_c \int dp_c \, Q_c \left(\frac{1}{\sigma_{tot}} \frac{d\sigma}{dp_c} \right) . \tag{2.5}$$

Four momentum conservation yields (DeTar, Freedman, and Veneziano, 1971; Predazzi and Veneziano, 1971)

$$(p_a + p_b)^\mu = \sum_c \int dp_c \, p_c^\mu \left(\frac{1}{\sigma_{tot}} \frac{d\sigma}{dp_c} \right) . \tag{2.6}$$

The extension to double inclusive cross sections is immediate:

$$\sum_d \int dp_d \, p_d^\mu \frac{1}{\sigma_{tot}} \frac{d\sigma}{dp_c \, dp_d} = (p_a + p_b - p_c)^\mu \frac{1}{\sigma_{tot}} \frac{d\sigma}{dp_c} . \tag{2.7}$$

We define

$$N(p_c) = \frac{1}{\sigma_{tot}} \frac{d\sigma}{dp_c}$$

$$N(p_c, p_d) = \frac{1}{\sigma_{tot}} \frac{d\sigma}{dp_c \, dp_c} \tag{2.9}$$

$$g(p_c, p_d) = N(p_c, p_d) - N(p_c) \, N(p_d) \tag{2.9}$$

where g is called the correlation function. Then from (2.6) and (2.7)

$$\sum_a \int dp_d \; p_d^{\mu} \; g(p_d, p_c) \;=\; -p_c^{\mu} \; N(p_c) \; . \qquad (2.10)$$

The case $\mu = 0$ shows that g cannot vanish identically.

Constraints are placed on inclusive reactions by the symmetries of the strong interactions. Certain of these are quite obvious. For example

$$(b{:}c|a) \;=\; (\bar{b}{:}\bar{c}|\bar{a}) \qquad (2.11)$$

where $\bar{a}$ is the conjugate, Ca, of particle a. Similarly, if I_i are the generators of isospin SU(2), and if

$$a' \;=\; \exp(-i\pi I_2)a \qquad (2.12)$$

then

$$(b{:}c|a) \;=\; (b'{:}c'|a') \; . \qquad (2.13)$$

This analysis has been extended by Lipkin and Peshkin (1972) to cover combinations of inclusive reactions involving various members of the same isomultiplets.

CHAPTER THREE

THE MUELLER FORMALISM

A. Mueller Diagram Rules

While the hypothesis of limiting fragmentation, Feynman scaling has an extensive history, its plausibility and attractiveness were enormously increased by the seminal work of Mueller (1970) and its elaboration by Abarbanel (1971a, 1971b). The key insight of Mueller was to recognize that inclusive cross sections are related to discontinuities of three-to-three amplitudes. While Mueller did not specify precisely the discontinuity required, that point has been investigated subsequently (Stapp, 1971; Tan, 1971; Polkinghorne, 1971). In most applications, the specification is inessential. We shall return to this point in Chapter Six.

The importance of this insight was enhanced by the introduction of Regge concepts to the analysis of the three-to-three amplitude. This was achieved through group theoretic analysis á la Toller. Just as two-body reggeology can be phrased in terms of $O(1,2)$ expansions, so can inclusive reaction phenomenology. Since the inclusive cross section is related to a discontinuity of the forward three-to-three amplitude, in fact $O(1,3)$ can be used, just as it can for forward two-to-two amplitudes.

In spite of much elegant phraseology concerning Plancherel measures and the like, at heart the basic Regge assumptions are still required--almost nothing can really be proved mathematically. Indeed, nearly all the content of these analyses can be summarized in terms of "Mueller diagrams" and some rules for the amplitudes they represent.

Consider $(b:c|a)$ in the rest frame of particle b. Let y and $p_\perp$ be fixed while $Y \to \infty$. Our rules for evaluating the cross section corresponding to the diagram in Fig. 3.1 are:

1. For each growing rapidity difference, insert a sum of Regge poles, each with a factor $\exp(\alpha_i \Delta y)$ where α_i is the Regge intercept at $t = 0$ and Δy is the growing rapidity difference.

2. Each Regge vertex has a residue which is a function of the rapidity difference of the particles attached to the vertex and the perpendicular momenta of those particles. For convenience we shall call the vertex with b entering and c exiting, and a reggeon i at $t = 0$ $f_i^{b\bar{c}}(y,p_\perp) \exp(y)$.

3. The invariant differential cross section is $\exp(-Y)$ times the amplitude obtained from 1. and 2.

Thus for $(b:c|a)$ in Fig. 3.1, we have

$$\frac{d\sigma}{dp_c} = \sum_i \beta_i^a \exp(-\Delta\alpha_i[Y - y]) f_i^{b\bar{c}}(y,p_\perp) \tag{3.1}$$

where $\Delta\alpha_i = 1 - \alpha_i$ and β_i^a is the two-body Regge vertex. If the leading pole is a Pomeron with $\alpha_P = 1$, then we find

$$\frac{d\sigma}{dp_c} = \beta_P^a f_P^{b\bar{c}}(y,p_\perp) + \sum_{i\neq P} \exp(-\Delta\alpha_i[Y - y])\beta_i^a f_i^{b\bar{c}}(y,p_\perp) . \tag{3.2}$$

This shows how Feynman scaling is related to the constancy of total cross sections at high energy.

As a second example consider $(b|c|a)$ as shown in Fig. 3.2. By our rules, using center of mass rapidities, we obtain:

$$\frac{d\sigma}{dp_c} = e^{-(Z_a - Z_b)} \sum \exp[\alpha_i(Z_a - z) + \alpha_j(z - Z_b)] f_{ij}^c(p_\perp)\beta_i^a\beta_j^b \tag{3.3}$$

$$= \beta_P^a\beta_P^b f_{PP}^c(p_\perp) + \sum_{j\neq P} \beta_j^a\beta_P^b f_{Pj}^c(p_\perp) \exp(-\Delta\alpha_j[Z_a - z])$$

$$+ \sum_{j\neq P} \beta_P^a\beta_j^b \exp(\Delta\alpha_j[Z_b - z]) f_{Pj}^c(p_\perp)$$

$$+ \sum_{\substack{i\neq P \\ j\neq P}} \beta_i^a\beta_j^b f_{ij}^c(p_\perp) \exp[-\Delta\alpha_i Z_a + \Delta\alpha_j Z_b + (\alpha_j - \alpha_i)z] . \tag{3.4}$$

Even if the rapidity separation between b and c is not growing, as long as it is large we might anticipate that an expansion like that in (3.4) would be appropriate. Clearly this requires

$$e^y f_j^{b\bar{c}}(y,p_\perp) \xrightarrow{y\to\infty} \sum_i \beta_i^b f_{ij}^c(p) e^{\alpha_i y} \tag{3.5}$$

or

$$f_j^{b\bar{c}}(y,p_\perp) \xrightarrow{y\to\infty} \sum_i \beta_i^b f_{ij}^c(p_\perp) e^{-\Delta\alpha_i y} . \tag{3.6}$$

With our conventions, the value of $\sigma_{ab}(s = \infty)$ is $\beta_P^a\beta_P^b$. Thus β has the dimensions of $(\text{mb})^{\frac{1}{2}}$ while f_{ij}^c has the dimensions of GeV^{-2}.

The Mueller expansion for $(b:c_1,c_2|a)$ can be derived similarly:

$$\frac{d\sigma}{dp_1\,dp_2} = \sum_j \beta_j^a\, f_j^{b,\bar{c}_1,\bar{c}_2}(y_1,y_2,p_{\perp 1},p_{\perp 2})\, e^{-\Delta\alpha_j(Y - y_2)} . \tag{3.7}$$

B. The Triple Regge Expansion

In a particular kinematic region, we can say something explicit about the residue $f_j^{b\bar{c}}$. Consider $t = (p_b - p_c)^2$ fixed, and $|x|$ near 1. Any particle c' other than c must have $|x'| < 1 - |x|$ by energy conservation. In terms of rapidity

$$\frac{\omega'_c}{m_b} e^{-y'} < 1 - \frac{\omega_c}{m_b} e^{-y}$$

$$y' > \log\left(\frac{\frac{\omega'_c}{m_b}}{1 - \frac{\omega_c}{m_b} e^{-y}}\right) \tag{3.8}$$

$$y' > \log\frac{\omega'_c}{m_b} - \log\left(1 - \frac{\omega_c}{m_b} e^{-y}\right) .$$

A fortiori, with $y(\omega) = \ell n\left(\frac{\omega_c}{m_b}\right)$

$$y' > \log\frac{m_c}{m_b} - \log\left(1 - e^{-[y-y(\omega)]}\right)$$

$$y' \gtrsim \log\frac{m_c}{m_b} - \log\left(y - y(\omega)\right) . \tag{3.9}$$

Thus by choosing y sufficiently near $y(\omega)$, we can insure that there must be a large rapidity separation between c and the nearest outgoing particle. This justifies inserting Regge pole in the $b\bar{c}$ channel. See Fig. 3.3a. If we now require M^{*2} to be large and consider the sum over final states we see that we should have a reggeized $a\bar{a}$ channel as well (Abarbanel et al., 1971a, 1971b; DeTar et al., 1971a). See Fig. 3.3b. What is the contribution of this so-called triple-Regge term to the invariant cross section? At fixed M^* it should behave as $s^{2\alpha_i(t)-1}$ if α_i is the Regge trajectory in the $b\bar{c}$ channel. This comes from $s^{\alpha_i(t)}$ for the reggeon in Fig. 3.3a, squared, times s^{-1} for a flux factor. On the other hand, from the general principles of fragmentation outlined above, we know that for fixed t and fixed x or y, it must go like $s^{\alpha_j(0)-1}$, where α_j is the trajectory in the $a\bar{a}$ channel. Thus the s and M^* dependence must be

$$\left(\frac{s}{M^{*2}}\right)^{2\alpha_i(t)-\alpha_j(0)} \left(\frac{s}{s_0}\right)^{\alpha_j(0)-1} \tag{3.10}$$

where $s_0 \simeq 1\ \mathrm{GeV}^2$ and thus sets the scale. If the two-body residues are β_i and β_j and if the triple-Regge coupling is $g_{iij}(t)$ we have, using a standard normalization,

$$\frac{d\sigma}{dp} = \frac{1}{16\pi} \sum_{i,j} |\beta_i(t)|^2\, \beta_j(0)\, g_{iij}(t) \left(\frac{s}{M^{*2}}\right)^{2\alpha_i(t)-\alpha_j(0)} \left(\frac{s}{s_0}\right)^{\alpha_j(0)-1} \tag{3.11}$$

$$= \frac{1}{16\pi} \sum_{i,j} |\beta_i(t)|^2\, \beta_j(0) g_{iij}(t)(1 - x)^{\alpha_j(0)-2\alpha_i(t)} \left(\frac{s}{s_0}\right)^{\alpha_j(0)-1} \tag{3.12}$$

$$\frac{d\sigma}{dp} \approx \sum_{i,j} |\beta_i(t)|^2 \beta_j(0) g_{iij}(t) \left(y - y(\omega)\right)^{\alpha_j(0)-2\alpha_i(t)} \left(\frac{s}{s_0}\right)^{\alpha_j(0)-1} \tag{3.13}$$

where in (3.13) we have expanded as in (3.9). We have defined the triple-Regge domain by

$$t \text{ fixed}$$

$$s \to \infty$$

$$M^{*2} \text{ large}$$

$$\frac{s}{M^{*2}} = \frac{1}{1-x} \text{ large} .$$

In terms of rapidity the last two conditions mean $y - y(\omega)$ is small and $s\left(y - y(\omega)\right)$ is large. Let us therefore say that the triple-Regge region is given by

$$\delta > y - y(\omega) > \frac{K}{\left(\frac{s}{s_0}\right)} \tag{3.14}$$

where δ is small and K is large. We now investigate the contribution of the triple-Regge region to the distribution in x and in y and its contribution to the multiplicity. In fact, its contribution to the multiplicity times the cross section is the same as its contribution to the cross section since no event can have two particles in the triple-Regge region as we showed above.

The most important result (Abarbanel et al., 1971a, 1971b) is that if $\alpha_P(0) = 1$, then $g_{PPP}(t = 0) = 0$. To prove this, we

integrate the contribution of the triple pomeron to find its contribution to the total cross section

$$\sigma_{PPP} = \frac{1}{16\pi} \int d^2p_\perp \int_{y(\omega)+K/(s/s_0)}^{y(\omega)+\delta} dy |\beta_P(t)|^2 \beta_P(0)\, g_{PPP}(t) \times \left(y - y(\omega)\right)^{1-2\alpha_P(t)} . \tag{3.15}$$

Let $\alpha_P(t) = 1 + \alpha_P' t$ and approximate all the couplings by their $t = 0$ values. Then we have

$$\sigma_{PPP} \simeq \frac{1}{16} |\beta_P(0)|^2 \beta_P(0)\, g_{PPP}(0) \int dp_\perp^2 \frac{1}{-2\alpha_P' t} \times \left\{ \delta^{-2\alpha_P' t} - \left[\frac{K}{\frac{s}{s_0}}\right]^{-2\alpha_P' t} \right\} . \tag{3.16}$$

In this region $t \simeq -p_\perp^2$, so that we can write

$$\sigma_{PPP} \simeq \frac{1}{16} |\beta_P(0)|^2 \beta_P(0)\, g_{PPP}(0) \int_{-\infty}^{0} \frac{dt}{-2\alpha_P' t} \left\{ \exp(-2\alpha_P' t \log \delta) - \exp\left(-2\alpha_P' t \log\left[\frac{K}{\frac{s}{s_0}}\right]\right) \right\} \tag{3.17}$$

$$\simeq \frac{1}{16} |\beta_P(0)|^2 \beta_P(0)\, g_{PPP}(0) \lim_{\epsilon \to 0} \frac{1}{2\alpha_P'} \left[E_1\left(2\epsilon\alpha_P' \log \frac{1}{\delta}\right) - E_1\left(2\epsilon\alpha_P' \log \frac{\frac{s}{s_0}}{K}\right) \right] \tag{3.18}$$

$$\sigma_{PPP} \simeq \frac{1}{16} |\beta_P(0)|^2 \beta_P(0)\, g_{PPP}(0)\, \frac{1}{2\alpha'_P} \left[\log \frac{\log \frac{\left(\frac{s}{s_0}\right)}{K}}{\log \frac{1}{\delta}} \right] . \qquad (3.19)$$

Thus this partial contribution to the cross section grows like $\log(\log s)$ while the cross section itself is constant by assumption. This contradiction shows that we must have $g_{PPP}(t = 0) = 0$ if the pomeron is a pole with unit intercept.

If we start with the ansatz

$$g_{PPP}(t) \simeq r_{PPP}(-t)^n \qquad (3.20)$$

we have

$$\sigma_{PPP} \simeq \frac{1}{16}|\beta_P(0)|^2 \beta_P(0)\, r_{PPP} \int_{-\infty}^{0} \frac{dt}{2\alpha'_P}(-t)^{n-1}$$

$$\times \left\{ \exp(-2\alpha'_P t \log \delta) - \exp\left(-2\alpha'_P t \log \frac{K}{\left(\frac{s}{s_0}\right)} \right) \right\} \qquad (3.21)$$

$$\simeq \frac{1}{16} |\beta_P(0)|^2 \beta_P(0)\, r_{PPP}\, \Gamma(n)\, \frac{1}{2\alpha'_P} \left\{ \left(2\alpha'_P \log \frac{1}{\delta} \right)^{-n} \right.$$

$$\left. - \left(2\alpha'_P \log \frac{\left(\frac{s}{s_0}\right)}{K} \right)^{-n} \right\} \qquad (3.22)$$

so that the triple pomeron contribution is $a + b(\log s)^{-n}$, which is consistent with a pomeron with unit intercept, provided $n > 0$.

We turn now to the contribution of the triple-Regge region to the inclusive cross section integrated over $p_\perp^2$. In this region, $t \simeq -p_\perp^2$ and we have

$$x \frac{d\sigma}{dx} \simeq \frac{1}{16} \int dt |\beta_i(t)|^2 \beta_j(0)\, g_{iij}(t)(1 - x)^{-2\alpha_i(t)+\alpha_j(0)}$$

$$\times \left(\frac{s}{s_0} \right)^{\alpha_j(0)-1} . \qquad (3.23)$$

The integral is dominated by the region near the largest t value, t_{max}. We have roughly,

$$x \frac{d\sigma}{dx} \simeq \frac{1}{16}|\beta_i(t_{max})|^2 \beta_j(0)\, g_{iij}(t_{max}) \left(\frac{s}{s_0} \right)^{\alpha_j(0)-1}$$

$$\times \frac{(1 - x)^{\alpha_j(0)-2\alpha_i(t_{max})}}{2\alpha'_i \log\left(\frac{1}{1 - x}\right)} . \qquad (3.24)$$

We can check that for $\alpha_j(0) = 1$ this gives a finite contribution to the cross section if $1 - 2\alpha_i(t_{max}) > -1$, i.e., if $i \neq P$.

If, on the other hand, $i = P$, and $g_{PPP} = r_{PPP}(-t)^n$

$$x \frac{d\sigma}{dx} \simeq \frac{1}{16}|\beta_P(0)|^2 \beta_P(0) r_{PPP} \int_{t_0}^{0} dt(-t)^n (1 - x)^{-1-2\alpha'_P t} \qquad (3.25)$$

$$\simeq \frac{1}{16}|\beta_P(0)|^2 \beta_P(0)\, r_{PPP}(1 - x)^{-1}\, \Gamma(n + 1) \left[2\alpha'_P \log \frac{1}{1 - x} \right]^{-n-1} .$$

(3.26)

Thus with a linear zero in g_{PPP}, the triple pomeron contribution goes like $(1 - x)^{-1}\big(-\log(1 - x)\big)^{-2}$, while a reggeon-reggeon-pomeron contribution with $\alpha_R = 1/2$ goes like $\big(-\log(1 - x)\big)^{-1}$. See Fig. 3.2.

C. Mean Multiplicity at High Energies

Let us see what Muellerism tells us about the average multiplicity of some species. For simplicity, we will consider the symmetric case a = b. Then

$$\langle n_c \rangle = 2 \int_{ymin}^{Y/2} dy \; d^2p_\perp \frac{1}{\sigma_{tot}} \frac{d\sigma}{dp}(y,p_\perp,s) \; . \tag{3.27}$$

Let us define

$$\frac{dN}{dy}(y,s) = \frac{1}{\sigma_{tot}} \int d^2p_\perp \frac{d\sigma}{dp}(y,p_\perp,s) \tag{3.28}$$

so that

$$\langle n_c \rangle = 2 \int_{ymin}^{Y/2} dy \; \frac{dN}{dy}(y,s) \; , \tag{3.29}$$

$$= Y \frac{dN}{dy}(\infty,\infty) - 2\int_0^\infty \left[dy \; \frac{dN}{dy}(\infty,\infty) - \frac{dN}{dy}(y,\infty)\right]$$

$$+ 2\int_{Y/2}^\infty dy \left[\frac{dN}{dy}(\infty,\infty) - \frac{dN}{dy}(y,\infty)\right] - 2\int_0^{Y/2} dy \left[\frac{dN}{dy}(y,\infty) - \frac{dN}{dy}(y,s)\right]$$

$$+ 2\int_{ymin}^0 dy \; \frac{dN}{dy}(y,\infty) - 2\int_{ymin}^0 dy \left[\frac{dN}{dy}(y,\infty) - \frac{dN}{dy}(y,s)\right] . \tag{3.30}$$

If we make the definitions:

$$F_{ij}{}^c = \int d^2p_\perp \, f_{ij}{}^c(p_\perp) \tag{3.31}$$

$$F_i{}^{b\bar{c}}(y) = \int d^2p_\perp \, f_i{}^{b\bar{c}}(y,p_\perp) \tag{3.32}$$

we can express the rapidity distributions as

$$\frac{dN}{dy}(\infty,\infty) = \beta_P{}^a \beta_P{}^b F_{PP}{}^c \tag{3.33}$$

$$\frac{dN}{dy}(y,\infty) = \beta_P{}^a F_P{}^{b\bar{c}}(y) \tag{3.34}$$

$$\frac{dN}{dy}(y,s) = \sum \beta_i{}^a \exp\big(-\Delta\alpha_i(Y - y)\big) F_i{}^{b\bar{c}}(y) \; . \tag{3.35}$$

Then for large y, we have by virtue of (3.1) and (3.6)

$$\frac{dN}{dy}(y,\infty) = \beta_P{}^a \sum_j \beta_j{}^b F_{Pj}{}^c \, e^{-\Delta\alpha_j y} \tag{3.36}$$

$$\frac{dN}{dy}(y,s) = \sum_{i,j} \beta_i{}^a \beta_j{}^b F_{ij}{}^c(y) \exp[-\Delta\alpha_i(Y - y) - \Delta\alpha_j y] \; . \tag{3.37}$$

Using (3.33) and (3.36) we find that

$$\int_0^\infty dy \left(\frac{dN}{dy}(\infty,\infty) - \frac{dN}{dy}(y,\infty)\right) < \infty \; . \tag{3.38}$$

For large Y we have

$$\int_{\frac{Y}{2}}^\infty dy \left(\frac{dN}{dy}(\infty,\infty) - \frac{dN}{dy}(y,\infty)\right) \simeq -\beta_P{}^a \sum_{j \neq P} \beta_j{}^b F_{Pj}{}^c \, \frac{e^{-\Delta\alpha_j \frac{Y}{2}}}{\Delta\alpha_j} \tag{3.39}$$

$$\int_0^{Y/2} dy\left(\frac{dN}{dy}(y,\infty) - \frac{dN}{dy}(y,s)\right) \simeq \sum_{j\neq P} \beta_j{}^a \int_0^{Y/2} dy\, F_j{}^{b\bar{c}}(y)\, e^{-\Delta\alpha_j(Y-y)} . \tag{3.40}$$

Now as $Y \to \infty$ the integral (3.40) over y up to some fixed y_0 gives a result of order $\exp(-\Delta\alpha_i Y)$. Now consider the contribution from large $y > y_0$

$$-\int_{y_0}^{Y/2} dy\left[\frac{dN}{dy}(y,\infty) - \frac{dN}{dy}(y,s)\right] = \sum_{\substack{i\neq P\\ j}} \beta_i{}^a\, \beta_j{}^b \int_{y_0}^{Y/2} dy\, F_{ij}{}^c$$

$$\times \exp\left(-\Delta\alpha_i(Y-y) - \Delta\alpha_j y\right) \tag{3.41}$$

$$= \sum_{j\neq P} \beta_j{}^a\, \beta_P{}^b\, F_{jP}{}^c\, e^{-\Delta\alpha_j Y}\left(\frac{e^{\Delta\alpha_j \frac{Y}{2}}}{\Delta\alpha_j} - \frac{e^{\Delta\alpha_j y_0}}{\Delta\alpha_j}\right)$$

$$+ \sum_{j\neq P} \beta_j{}^a\, \beta_j{}^b\, F_{jj}{}^c \left(\frac{Y}{2} - y_0\right) e^{-\Delta\alpha_j Y} ,$$

$$+ \sum_{\substack{i\neq P\\ j\neq P\\ i\neq j}} \beta_i{}^a\, \beta_j{}^b\, F_{ij}{}^c \left[\frac{e^{(\Delta\alpha_i-\Delta\alpha_j)\frac{Y}{2}}}{\Delta\alpha_i - \Delta\alpha_j} - \frac{e^{(\Delta\alpha_j-\Delta\alpha_j)y_0}}{\Delta\alpha_i - \Delta\alpha_j}\right] . \tag{3.42}$$

Combining the third and fourth terms of (3.30) yields,

$$- 2 \sum_{j\neq P} \left(\beta_P{}^a \beta_j{}^b - \beta_j{}^a \beta_P{}^b\right) F_{jP}{}^c\, e^{-\Delta\alpha_j \frac{Y}{2}} \Big/ \Delta\alpha_j$$

$$+ \sum_{j\neq P} \beta_j{}^a \beta_j{}^b\, F_{jj}{}^c\, Y\, e^{-\Delta\alpha_j Y} + \mathcal{O}\left(e^{-\Delta\alpha_j Y}, j \neq P\right) . \tag{3.43}$$

The last term in (3.30) is evaluated in the $s \to \infty$ limit:

$$\int_{ymin}^{0} dy\left[\frac{dN}{dy}(y,\infty) - \frac{dN}{dy}(y,s)\right] = \sum_{j\neq P} \beta_j{}^a \int_{ymin}^{0} dy\, F_j{}^{b\bar{c}}(y)\, e^{-\Delta\alpha_j(Y-y)} \tag{3.44}$$

which is of order $\exp(-\Delta\alpha_j Y)$.

Combining these results, we have for $a = b$,

$$\langle n_c \rangle = AY + B + CY\, e^{-\Delta\alpha_R Y} + \mathcal{O}\left(e^{-\Delta\alpha_R Y}\right) \tag{3.45}$$

where α_R is the leading non-pomeron pole and $\Delta\alpha_R = 1 - \alpha_R$ (so that $\Delta\alpha_R \simeq 1/2$). The coefficients A, B, and C are given by

$$A = \beta_P{}^a \beta_P{}^b F_{PP}{}^c$$

$$B = 2\int_0^{\infty} dy\, \beta_P{}^a \left(F_P{}^{b\bar{c}}(y) - F_{PP}{}^c \beta_P{}^b\right) \tag{3.46}$$

$$+ 2\int_{ymin}^{0} dy\, \beta_P{}^a\, F_P{}^{b\bar{c}}(y)$$

$$C = \beta_R{}^a \beta_R{}^b F_{RR}{}^c .$$

Even if $a \neq b$, the term proportional to $\exp(-\Delta\alpha_R Y/2)$ in Eq. (3.42) vanishes when the distribution for $y > Y/2$ is added in.[1]

The most relevant case is $a = b = p$. We can re-express (3.45) as

$$\langle n_c \rangle = A' \log s + B' + C' s^{-\Delta\alpha_R} \log s + \mathcal{O}(s^{-\Delta\alpha_R}) . \quad (3.47)$$

At first sight, the expansion for the average multiplicity seems to contradict the results for the triple-Regge region. There we found that the triple pomeron domain could contribute an amount $a + b(\log s)^{-n}$, while no such term turned up in the multiplicity expansion. A careful examination of our procedures reveals the cause of this discrepancy. In the triple pomeron case, we required M^{*2} to be large in order to insure that the $a\bar{a}$ channel had reggeized. This gave rise to the condition $\left(y - y(\omega)\right) > K/(s/s_0)$. On the other hand, in the multiplicity expansion, we assumed that for all values of y the $a\bar{a}$ channel had reggeized. This is equivalent to assuming in the triple-Regge estimate the integration continues right up to the phase-space boundary $(K \to 0)$. This would have the effect of eliminating the $(\log s)^{-n}$ term. Of course this may not be justified. The presence or absence of logarithmic terms causes difficulties as well for the sum rules discussed in Chapter 2. Most simply put, the problem is that in a pure pole model for two-body cross sections, the total cross section has terms of the form $s^{-\Delta\alpha}$, while the diffractive contributions (triple pomeron say) appear to give logarithmic contributions. Of course, these logarithmic contributions may be cancelled by other logarithmic contributions. On the other hand, this quandry may be an indication that pure pole models are inconsistent--that "dynamical" cuts are a necessity.

D. Sum Rule Constraints on Fragmentation Distributions

The energy-momentum conservation sum rule, (2.6), places constraints for the residues $f_j^{b\bar{c}}$. (Caneschi, 1971.) Let us work in the rest frame of a, and consider the $Y \to \infty$ limit. From (2.6),

$$p_a \cdot p_b + m_a^2 = \sum_c \int dp_c \; p_a \cdot p_c \; \frac{1}{\sigma} \frac{d\sigma}{dp_c} . \quad (3.48)$$

Considering only a pomeron with $\alpha_P = 1$, and an effective non-pomeron with intercept $\alpha_R < 1$,

$$\frac{d\sigma}{dp_c} = \beta_P^{\,a} f_P^{b\bar{c}}(Y - y, p_\perp) + \beta_R^{\,a} f_R^{b\bar{c}}(Y - y, p_\perp) e^{-\Delta\alpha_R y} \quad (3.49)$$

when y is large. This is the dominant region for (3.48), since

$$p_a \cdot p_c = m_a \omega_c \cosh y . \quad (3.50)$$

Thus as $Y \to \infty$ (3.48) yields

$$\frac{m_a m_b}{2} e^Y = \sum_c \int dp_c \frac{m_a \omega_c}{2} e^Y \frac{1}{\sigma}\left(\beta_P^{\,a} f_P^{b\bar{c}}(Y - y, p_\perp)\right) + \left(\beta_R^{\,a} f_R^{b\bar{c}}(Y - y, p_\perp) e^{-\Delta\alpha_R y}\right) . \quad (3.51)$$

Now in analogy with (3.49)

$$\sigma_{ab}(s) = \beta_P^{\,a}\beta_P^{\,b} + \beta_R^{\,a}\beta_R^{\,b} e^{-\Delta\alpha_R Y} . \quad (3.52)$$

Inserting this in (3.51) and expanding, we have

$$m_a m_b\, e^Y = \sum_c \int dp_c\, m_a \omega_c \frac{e^y}{\beta_P^a \beta_P^b}\left(1 - \frac{\beta_R^a \beta_R^b}{\beta_P^a \beta_P^b} e^{-\Delta\alpha_R Y}\right)$$

$$\times \left(\beta_P^a f_P^{b\bar{c}}(Y - y, p_\perp) + \beta_R^a f_R^{b\bar{c}}(Y - y, p_\perp)\, e^{-\Delta\alpha_R y}\right) . \qquad (3.53)$$

Let $y' = Y - y$, so that (3.53) becomes

$$1 = \sum_c \int_{Y-ymax}^{Y-ymin} dy' \int d^2p_\perp \frac{\omega_c}{mb}\, e^{-y'}\left(1 - \frac{\beta_R^a \beta_R^b}{\beta_P^a \beta_P^b} e^{-\Delta\alpha_R Y}\right)$$

$$\times \left(\frac{f_P^{b\bar{c}}(y', p_\perp)}{\beta_P^b} + \frac{\beta_R^a f_R^{b\bar{c}}(y', p_\perp)}{\beta_P^a \beta_P^b} e^{-\Delta\alpha_R (Y - y')}\right) \qquad (3.54)$$

Taking $Y \to \infty$, we obtain the fragmentation sum rules:

$$1 = \sum_c \int_{y'min}^{\infty} dy' \int d^2p_\perp \frac{\omega_c}{m_b} e^{-y'} \frac{f_P^{b\bar{c}}(y', p_\perp)}{\beta_P^b} \qquad (3.55)$$

and

$$1 = \sum_c \int_{y'min}^{\infty} dy' \int d^2p_\perp \frac{\omega_c}{m_b} e^{-\alpha_R y'} \frac{f_R^{b\bar{c}}(y', p_\perp)}{\beta_P^b} . \qquad (3.56)$$

Superficially, the sum rule (2.8) is a cause for concern. To see why, begin with (2.10) in the form

$$\sigma_{ab} \sum_d \int dp_d\, p_d \cdot p_c\, g(p_d, p_c) = -m_c^2 \frac{d\sigma}{dp_c} . \qquad (3.57)$$

Now

$$p_d \cdot p_c = \omega_d \omega_c \cosh(y_d - y_c) - p_{\perp d} \cdot p_{\perp c} . \qquad (3.58)$$

The right-hand side of (3.57) is bounded, so the integral on the left-hand side must converge. But for y_d large, $p_d \cdot p_c \simeq \omega_d \omega_c [\cosh(y_d - y_c)]/2$. Thus we must have some cancellation near the upper limit of the y integration. To see how this comes about, let us evaluate $g(p_d, p_c)$ for y_d large and y_c fixed. See Fig. 3.3. By our Mueller rules,

$$\frac{d\sigma}{dp_c\, dp_d} = f_P^{b\bar{d}}(Y - y_d, p_{\perp d})\, f_P^{a\bar{c}}(y_c, p_{\perp c}) + f_R^{b\bar{d}}(Y - y_d, p_{\perp d})$$

$$\times f_R^{a\bar{c}}(y_c, p_{\perp c})\, e^{-\Delta\alpha_R (y_d - y_c)} . \qquad (3.59)$$

From (2.10), (3.49), (3.52), and (3.59), we obtain

$$\sigma_{ab}(s)\, g(p_d, p_c) = f_P^{b\bar{d}} f_P^{a\bar{c}} + f_R^{b\bar{d}} f_R^{a\bar{c}}\, e^{-\Delta\alpha_R (y_d - y_c)}$$

$$- \frac{1}{\beta_P^a \beta_P^b}\left(1 - \frac{\beta_R^a \beta_R^b}{\beta_P^a \beta_P^b} e^{-\Delta\alpha_R Y}\right)\left(f_P^{b\bar{d}} \beta_P^a + f_R^{b\bar{d}} \beta_R^a\, e^{-\Delta\alpha_R y_d}\right)$$

$$\times \left(f_P^{a\bar{c}} \beta_P^b + f_R^{a\bar{c}} \beta_R^b\, e^{-\Delta\alpha_R (Y - y_c)}\right) \qquad (3.60)$$

$$= \left(f_R^{b\bar{d}}\, e^{-\Delta\alpha_R y_d} - \frac{\beta_R^b}{\beta_P^b} f_P^{b\bar{d}}\, e^{-\Delta\alpha_R Y}\right)\left(f_R^{a\bar{c}}\, e^{\Delta\alpha_R y_c} - \frac{\beta_R^a}{\beta_P^a} f_P^{a\bar{c}}\right)$$

$$+ \text{higher order in } Y \text{ and } y_d \qquad (3.61)$$

where the arguments are the same as those in (3.59). The terms shown explicitly in (3.61) are the ones which appeared to cause trouble on account of the $\exp(y_d)$ in the integrand. However, by virtue of the sum rules (3.55) and (3.56), the displayed terms in (3.61) cancel, leaving the high-order terms which permit the saturation of this sum rule (Ellis, Finkelstein, and Peccei, 1972; Cahn and Koplik, 1972).

E. Behavior in the Central Region

One of the most interesting consequences of Mueller analysis concerns the behavior at high energies of the inclusive differential cross section near $z = 0$. (Abarbanel, 1971, 1971a). From (3.4) we have for $(b|c|a)$

$$\frac{d\sigma}{dp_c} = \beta_P^{\,a}\beta_P^{\,b} f_{PP}^{\,c}(p_\perp) + \sum_{j\neq P} f_{Pj}^{\,c}(p_\perp)\Big[\beta_P^{\,a}\beta_j^{\,b} e^{\Delta\alpha_j(Z_b-z)} + \beta_j^{\,a}\beta_P^{\,b} e^{-\Delta\alpha_j(Z_a-z)}\Big] + \sum_{\substack{j\neq P\\ i\neq P}} \beta_i^{\,a}\beta_j^{\,b} e^{-\Delta\alpha_i Z_a} e^{\Delta\alpha_j Z_b} \times e^{z(\alpha_j-\alpha_i)} f_{ij}^{\,c}(p_\perp^{\,2}) \quad . \tag{3.62}$$

For simplicity consider only two Regge poles, P and R, with $\alpha_P = 1$, and $\alpha_R < 1$ and suppose $a = b$. Then the inclusive cross section is

$$\frac{d\sigma}{dp_c} = \beta_P^{\,2} f_{PP}^{\,c}(p_\perp) + 2\beta_P\beta_R \cosh \Delta\alpha_R z\, e^{-\Delta\alpha_R Z_a} f_{PR}^{\,c}(p_\perp) + \beta_R^{\,2} e^{-2\Delta\alpha_R Z_a} f_{RR}^{\,c}(p_\perp^{\,2}) \quad . \tag{3.63}$$

Since $s \propto \exp(2Z_a)$, the cross section at $z = 0$ approaches its asymptotic value as $s^{-(\Delta\alpha_R/2)}$ (typically $s^{-\frac{1}{4}}$). For fixed large s, the z dependence for small z is

$$\frac{d\sigma}{dp_c} = A(p_\perp) + B(p_\perp)\cosh \Delta\alpha_R z \quad . \tag{3.64}$$

It is clear that the sign of B is related to the rising or falling of $d\sigma/dp_c$ at $z = 0$ as s increases. A cross section increasing with s requires B to be negative and vice versa.

CHAPTER FOUR

CONSEQUENCES OF INTERNAL SYMMETRIES IN A MUELLER MODEL[1]

A. Quantum Numbers of the J-plane Singularities

In its simplest form the Mueller model assumes that $(a:c|b)$ is dominated by poles in the $b\bar{b}$ channel of the corresponding six-point function. The spirit of the model is more general though, and the existence of cuts as well as poles is expected. In a pure model with $\alpha_P(0) = 1$, scaling obtains [Eq. (3.2)]. In a pure pole model with $\alpha_P(0) < 1$, scaling holds for $\frac{1}{\sigma(s)} \frac{d\sigma}{dp}(s)$. By the factorizability of poles,

$$\frac{1}{\sigma_{ab}(s)} \frac{d\sigma}{dp} [(a:c|b),s]$$

is independent of b as $s \to \infty$. It is probably too much to ask that all the important j-plane singularities be poles and so factorizability may indeed be broken. This alone would not invalidate the Mueller approach any more than the existence of cuts in two-body reactions vitiates Regge phenomenology in that domain.

Whatever the nature of the j-plane singularities, they must have well-defined quantum numbers for certain symmetries of the strong interactions, including charge conjugation, C, and isospin. Thus we can decompose the cross section quite generally as

$$\frac{d\sigma}{dp}(a:c|b) = \sum_j f_j^{(a:c|b)}(y,p_\perp,Y) \qquad (4.1)$$

where the sum is over j-plane singularities in the $b\bar{b}$ channel. In a pure pole model, we have explicitly

$$f_j^{(a:c|b)} = f_j^{a\bar{c}}(y,p_\perp)\, \beta_j{}^b \exp(-\Delta\alpha_j[Y - y]) \ . \qquad (4.2)$$

If the charge conjugation eigenvalue of the singularity j is C_j, then

$$\frac{d\sigma}{dp}(\bar{a}:\bar{c}|b) = \sum_j C_j\, f_j^{(a:c|b)}(y,p_\perp,Y) \ . \qquad (4.3)$$

If $G = \exp(-i\pi I_2)x$ C is the G-parity operator and G_j the eigenvalue of the singularity j,

$$\frac{d\sigma}{dp}(Ga:Gc|b) = \sum G_j\, f_j^{(a:c|b)}(y,p_\perp,Y) \qquad (4.4)$$

and

$$\frac{d\sigma}{dp}(G\bar{a}:G\bar{c}|b) = \sum G_j\, C_j\, f_j^{(a:c|b)}(y,p_\perp,Y) \ . \qquad (4.5)$$

In a model in which cuts are generated by double pole exchange, it is easy to see how the cuts remain pure C and G objects while losing their factorizability. We might schematically represent the amplitude for Fig. 4.1 as

$$\int d^4q \exp\{\alpha_j(t)[Y - y] + \alpha_i(t)[Y - y]\}\, \beta_i{}^b(t)\, \beta_j{}^b(t)\, \frac{i}{-2p_b\cdot q}$$

$$\times\ \mathcal{M}(p_a,p_b,q) \qquad (4.6)$$

with $t = -q^2$, and where $\mathcal{M}$ is a forward four-particle, two-reggeon amplitude. Although factorizability is clearly lost, this contribution to the amplitude for $(\bar{a}:\bar{c}|b) = (a:c|\bar{b})$ is C_iC_j times the amplitude

for the $i \otimes j$ contribution to $(a:c|b)$. Of course the existence of well-defined C_j's and G_j's does not depend on such an explicit model, but is a consequence of the symmetries themselves.

By taking combinations of reactions, we can isolate certain singularities. For example $(\pi^+:\pi^-|b) - (\pi^-:\pi^+|b)$ is pure $G = +1$, $C = -1$ in the $b\bar{b}$ channel--what we would ordinarily call "ρ", but including singularities like the $\rho \otimes P$ cut as well.[2] Similarly $(K^+:\pi^-|b) - (K^-:\pi^+|b)$ is pure $C = -1$ with ρ-, ω-, and ϕ-like contributions.

The significance of this decomposition into amplitudes with well-defined quantum numbers in the $b\bar{b}$ channel is that it enables us to see whether or not the singularities correspond to those in two-body scattering. Does the $G = +1$, $C = +1$ amplitude dominate at high energies? Do the other amplitudes vanish as $s^{-\Delta\alpha_R}$ with $\Delta\alpha_R \simeq 1/2$? These are the fundamental points to be verified in establishing the correctness of the Mueller approach.

B. Isospin Equalities

Let us proceed under the assumption that the leading singularity--the pomeron--has $C = +1$ and $I = 0$. Then we may analyze the isospin structure of $f_P^{a\bar{c}}$. We turn again to the six-point function and see that, in effect, $f_P^{a\bar{c}}$ is a vertex which we may represent as

$$f_P^{a\bar{c}} \propto \langle a\bar{c}|P|a\bar{c}\rangle \ . \tag{4.7}$$

Because P is an $I = 0$ operator the Wigner-Eckart theorem gives us an especially simple decomposition:

$$\langle a\bar{c}|P|a\bar{c}\rangle = \sum_{\substack{I,I' \\ I_Z,I_Z'}} \langle a\bar{c}|I,I_Z\rangle\langle I,I_Z|P|I',I_Z'\rangle\langle I',I_Z'|a\bar{c}\rangle$$

$$= \sum_{I,I_Z} \langle a\bar{c}|I,I_Z\rangle^2 \, P_{A\bar{C}}^{\ I}$$

where $P_{A\bar{C}}^{\ I}$ represents the reduced matrix element for isomultiplets A and C of which a and c are members. Now the range of I is from $|I_A - I_C|$ to $I_A + I_C$, i.e. a range of $2I_{min} + 1$, where $I_{min} = \min(I_A,I_C)$. The number of fragmentations $(a:c)$ is $(2I_A + 1)\times(2I_C + 1)$ so there are $2I_{min} + 1$ independent amplitudes and $2I_{max}(2I_{min} + 1)$ linear relations. Thus for example as $s \to \infty$ (so that the $I = 0$ $b\bar{b}$ amplitude dominates)

$$(p:\pi^-) = (n:\pi^+) \tag{4.9a}$$

$$(p:\pi^+) = (n:\pi^-) \tag{4.9b}$$

$$(p:\pi^0) = (n:\pi^0) \tag{4.9c}$$

$$= \tfrac{1}{2}[(p:\pi^+) + (p:\pi^-)] \tag{4.9d}$$

where we have dropped b since it remains unchanged throughout. Of course these relations hold read either as fragmentation of nucleons into pions or vice versa: the isospin structure is the same in both instances.

Many of the isospin relations follow just from C and G. Of the relations (4.9), only (4.9d) requires $I = 0$ in the $b\bar{b}$

channel; the other follow from $C = G = 1$. The following asymptotic equalities follow just from $C = G = 1$:

$$\begin{aligned}
(K^+:\Lambda) &= (K^0:\Lambda) \\
(\pi^+:\Lambda) &= (\pi^-:\Lambda) \\
(\pi^+:\Sigma^-) &= (\pi^-:\Sigma^+) \\
(\pi^+:\Sigma^+) &= (\pi^-:\Sigma^-) \\
(\pi^+:\Sigma^0) &= (\pi^-:\Sigma^0) \quad .
\end{aligned} \tag{4.10}$$

C. SU(3) Equalities

In analogy to (4.7), we can find the relations which would follow from exact SU(3) and the assumption that the pomeron is a unitary singlet. The Wigner-Eckart theorem becomes slightly trickier to apply because the Clebsch Gordan series for SU(3) is more complex. For example we have the famous decomposition:
$8 \otimes 8 = 27 \oplus 10 \oplus 10^* \oplus 8 \oplus 8 \oplus 1$. Two 8's occur, while in the Clebsch Gordan series for SU(2) no irreducible representation occurs more than once. With this caveat we continue as in (4.8). For a and c members of octets A and C,[3]

$$\langle a\bar{c}|P|a\bar{c}\rangle = \sum_{\substack{\mu_\gamma,\nu \\ \mu_\gamma,\nu'}} \begin{pmatrix} 8 & 8 & \mu_\gamma \\ \nu_a & -\nu_c & \nu \end{pmatrix} \begin{pmatrix} 8 & 8 & \mu'_\gamma \\ \nu_a & -\nu_c & \nu' \end{pmatrix}$$

$$\times \langle \mu_\gamma,\nu|P_{A\bar{C}}|\mu'_\gamma\nu'\rangle \quad . \tag{4.11}$$

In general we have seven reduced matrix elements; $P^{27,27}$, $P^{10,10}$, P^{10*10*}, $P^{8_a,8_a}$, $P^{8_a,8_s}$, $P^{8_s,8_s}$, and $P^{1,1}$. By time reversal invariance for the six-point function, $P^{8_a,8_s} = P^{8_s,8_a}$. Let us consider first the case in which a is a pseudoscalar meson, and c is an octet baryon: (P:B). There are 64 reactions of this sort. By the isospin analysis above there are $2l_{min} + 1$ independent reactions for each isomultiplet fragmentation. Thus the number of independent reactions remaining after isospin equalities is

$$\begin{array}{llll}
(\pi:\Sigma) \to 3 & (K:\Sigma) \to 2 & (\bar{K}:\Sigma) \to 2 & (\eta:\Sigma) \to 1 \\
(\pi:N) \to 2 & (K:N) \to 2 & (\bar{K}:N) \to 2 & (\eta:N) \to 1 \\
(\pi:\Xi) \to 2 & (K:\Xi) \to 2 & (\bar{K}:\Xi) \to 2 & (\eta:\Xi) \to 1 \\
(\pi:\Lambda) \to 1 & (K:\Lambda) \to 1 & (\bar{K}:\Lambda) \to 1 & (\eta:\Lambda) \to 1
\end{array} \tag{4.12}$$

a total of 26. Since there are seven SU(3) invariant amplitudes, there are nineteen linear relations. These are determined from (4.12). The explicit decomposition into SU(3) invariant amplitudes is given in Table 4.1. One choice for the 19 independent relations is

$$\begin{aligned}
(\pi^-:p) &= (K^-:\Sigma^+) = (K^+:\Xi^0) \\
(\pi^+:p) &= (K :\Xi^0) = (K^+:\Sigma^+) \\
(\pi^-:\Sigma^+) &= (K^-:p) = (K^+:\Xi^-) \\
(\pi^-:\Sigma^-) &= (K^-:\Xi^-) = (K^+:p) \\
(\pi^-:\Xi^-) &= (K^-:\Sigma^-) = (K^+:n) \\
(\pi^+:\Xi^-) &= (K^-:n) = (K^+:\Sigma^-)
\end{aligned} \tag{4.13}$$

Equation (4.13) continued next page

Equation (4.13) continued

$$2(\pi^-:p) + 2(K^+:n) + 4(\pi^+:\Sigma^0) = (\pi^+:p) + (K^-:n) + 6(K^+:\Lambda)$$

$$2(\pi^+:p) + 2(K^-:n) + 4(\pi^+:\Sigma^0) = (\pi^-:p) + (K^+:n) + 6(K^-:\Lambda)$$

$$(\pi^+:p) + (\pi^-:p) + (K^-:n) + (K^+:n) = (\pi^+:\Sigma^0) + 3(\pi^-:\Lambda)$$

$$(\eta:\Sigma^+) = (\pi^+:\Lambda)$$

$$(\pi^+:\Sigma^0) + (\eta:\Lambda) = (\pi^+:\Sigma^+) + (\pi^+:\Sigma^-)$$

$$6(\eta:p) + (\pi^-:p) + (\pi^+:p) = 2(K^+:n) + 2(K^-:n) + 4(\pi^+:\Sigma^0)$$

$$6(\eta:\Xi^-) + (K^-:p) + (K^+:n) = 2(\pi^-:p) + 2(\pi^+:p) + 4(\pi^+:\Sigma^0) \quad . \tag{4.13}$$

We turn now to the case (P:P). Since the pomeron is C even, $P^{8_a,8_s} = 0$, and $P^{10^*,10^*} = P^{10,10}$. Consequently, there are only five SU(3) invariant amplitudes for (P:P) and (4.12) simplifies to

$$\langle a\bar{c}|P|a\bar{c}\rangle = \sum_{\mu_\gamma,\nu} \begin{pmatrix} 8 & 8 & \mu_\gamma \\ \nu_a & -\nu_c & \nu \end{pmatrix}^2 P^{\mu_\gamma,\mu_\gamma} \quad . \tag{4.14}$$

Since

$$\begin{pmatrix} 8 & 8 & \mu_\gamma \\ \nu_a & -\nu_c & \nu \end{pmatrix} = \pm \begin{pmatrix} 8 & 8 & \mu_\gamma \\ \nu_c & -\nu_a & -\nu \end{pmatrix} \quad , \tag{4.15}$$

we have

$$\langle a\bar{c}|P|ac\rangle = \langle c\bar{a}|P|c\bar{a}\rangle \tag{4.16}$$

where a and c are members of the same SU(3) multiplet. Thus asymptotically, where P dominates in the $b\bar{b}$ channel, (a:c) = (c:a).

We have as an example of the power of this SU(3) relation, the predictions for $s \to \infty$, $(\pi^+:K^-) = (K^-:\pi^+) = (\pi^-:K^+) = (K^+:\pi^-)$ using the charge conjugate variants of (a:c) = (c:a). Using C and isospin, the 64 reactions (P:P) can be reduced to 12:

$$(\pi:K) \to 2 \qquad (K:K) \to 2 \qquad (\eta:\eta) \to 1$$

$$(\pi:\pi) \to 3 \qquad (K:\bar{K}) \to 2$$

$$(\pi:\eta) \to 1 \qquad (K:\eta) \to 1 \quad . \tag{4.17}$$

Among the twelve independent amplitudes there must be seven more SU(3) relations beyond those of the form (a:c) = (c:a). We may choose them to be

$$(\pi^-:\pi^+) = (K^-:K^+)$$

$$(K^-:K^0) = (K^-:\pi^+)$$

$$(K^-:K^-) = (\pi^-:\pi^-)$$

$$(K^-:\pi^-) = (K^-:\bar{K}^0) \tag{4.18}$$

$$3(K^-:\eta) = 2(\pi^+:\pi^0) + (K^+:\pi^0)$$

$$3(\pi^-:\eta) = 4(K^+:\pi^0) - (\pi^+:\pi^0)$$

$$(\eta:\eta) = (\pi^+:\pi^+) + (\pi^+:\pi^-) - (\pi^+:\pi^0) \quad .$$

The last relation is written for completeness only. The others are experimentally accessible. Notice that it is unnecessary to observe $(K^-:\pi^0)$ since by isospin and C,

$$(K^-:\pi^0) = (K_L^0:\pi^-) = \tfrac{1}{2}[(K^-:\pi^+) + (K^-:\pi^-)] \quad .$$

By similar manipulations, these relations can be written in a variety of other forms.

A multitude of SU(3) relations can be derived for (B:B), (B:P), (P:B), etc. from (4.13) and (4.14) mutatis mutandis. Fragmentation into vector mesons can also be treated. If we consider the vector mesons as a degenerate nonet, designating the isosinglets by ω_1 and ω_B we find for the number of independent reactions after invoking C and isospin invariance in the case (P:V)

$$\begin{array}{lll} (\pi:K^*) \to 2 & (K:K^*) \to 2 & (\eta:K^*) \to 1 \\ (\pi:\rho) \to 3 & (K:\bar{K}^*) \to 2 & (\eta:\omega_1) \to 1 \\ (\pi:\omega_1) \to 1 & (K:\omega_1) \to 1 & (\eta:\omega_8) \to 1 \\ (\pi:\omega_8) \to 1 & (K:\omega_8) \to 1 & (\eta:\rho) \to 1 \\ & (K:\rho) \to 2 \ . & \end{array} \tag{4.19}$$

With seven SU(3) invariant amplitudes, there are twelve linear relations. It is possible to choose eight which do not involve ω_1 or ω_8, thus obviating the problem of the mixing angle. The relations involving the mixing angle are more complex and not accessible to tests. One choice of relations not involving ω_1 and ω_8 is

$$\begin{aligned} (K^+:\rho^+) &= (\pi^+:K^{*+}) \\ (K^+:\rho^-) &= (\pi^-:K^{*+}) \\ (K^-:K^{*0}) &= (K^-:\rho^+) \\ (K^-:K^{*-}) &= (\pi^-:\rho^-) \end{aligned}$$

Equation (4.20) continued next page

Equation (4.20) continued

$$\begin{aligned} (K^-:\rho^-) &= (K^-:\bar{K}^{*0}) \\ (K^-:K^{*+}) &= (\pi^-:\rho^+) \\ 3(\eta:K^{*+}) &= 2(\pi^+:\rho^0) + (K^+:\rho^0) \\ 3(\eta:\rho^+) &= 4(K^+:\rho^0) - (\pi^+:\rho^0) \ . \end{aligned} \tag{4.20}$$

Using isospin invariance in conjunction with these relations, one can generate other experimentally testable predictions, such as

$$2(K^-:\rho^0) = (K^-:\bar{K}^{*0}) + (K^-:K^{*0}) \ .$$

D. Symmetries in Pionization

From Fig. 3.2 and Eq. (3.7), we see that $(a|c|b)$ is controlled by double pomeron exchange. The residue $f_{PP}^{\ c}$ corresponds to a four-point amplitude for two pomerons at $t = 0$ and particle c coming in and going out. Thus the SU(3) content might be summarized as

$$f_{PP}^{\ c} \propto \langle c|PP|c\rangle \ . \tag{4.21}$$

If P is a unitary singlet, then $f_{PP}^{\ c}$ is the same for every c in the SU(3) multiplet. For members of the same isomultiplet, this relation should be exact (up to electromagnetic effects), as it should be for particles related by C.

A primitive model for SU(3) breaking in the pionization region can be obtained by assuming the pomeron has a small octet contribution:

$$P = P_0 + \epsilon P_8 \quad . \tag{4.22}$$

Then, to first order, (4.21) becomes

$$f_{PP}{}^{c} \propto \langle c|P_0P_0|c\rangle + 2\epsilon\langle c|P_0P_8|c\rangle \quad . \tag{4.23}$$

Of course (4.23) is analogous to the Gell-Mann-Okubo prescription for mass splittings. We can immediately conclude that (4.24) implies

$$\begin{aligned} \tfrac{1}{2}[(|N|) + (1\equiv1)] &= \tfrac{1}{4}[(|\Sigma|) + 3(|\Lambda|)] \\ (|K|) &= \tfrac{1}{4}[(|\pi|) + 3(|\eta|)] \end{aligned} \tag{4.24}$$

where N denotes any one member of the N isomultiplet, etc.

TABLE 4.1. $P \to B = \sum_{\Gamma} C_{\Gamma} P^{\Gamma}$

	$P^{27,27}$	$P^{10^*,10^*}$	$P^{10,10}$	$P^{8_s,8_s}$	$P^{8_a,8_a}$	$P^{8_a,8_s}$	$P^{1,1}$
$\pi^+ \to p$	1/5	1/6	1/6	3/10	1/6	$2\sqrt{5}/10$	0
$\pi^- \to p$	1/2	1/2	0	0	0	0	0
$K^+ \to p$	7/40	1/12	1/12	1/5	1/3	0	1/8
$K^+ \to n$	1/5	1/6	1/6	3/10	1/6	$-2\sqrt{5}/10$	0
$K^- \to p$	1	0	0	0	0	0	0
$K^- \to n$	1/2	0	1/2	0	0	0	0
$\eta \to p$	9/20	0	1/4	1/20	1/4	$-\sqrt{5}/10$	0
$\pi^- \to \Sigma^+$	1	0	0	0	0	0	0
$\pi^+ \to \Sigma^0$	1/2	1/12	1/12	0	1/3	0	0
$\pi^+ \to \Sigma^+$	7/40	1/12	1/12	1/5	1/3	0	1/8
$K^+ \to \Sigma^+$	1/5	1/6	1/6	3/10	1/6	$2\sqrt{5}/10$	0
$K^+ \to \Sigma^-$	1/2	0	1/2	0	0	0	0
$K^- \to \Sigma^+$	1/2	1/2	0	0	0	0	0
$K^- \to \Sigma^-$	1/5	1/6	1/6	3/10	1/6	$-2\sqrt{5}/10$	0
$\eta \to \Sigma^+$	3/10	1/4	1/4	1/5	0	0	0
$\pi^+ \to \Lambda$	3/10	1/4	1/4	1/5	0	0	0
$K^+ \to \Lambda$	9/20	1/4	0	1/20	1/4	$-\sqrt{5}/10$	0
$K^- \to \Lambda$	9/20	0	1/4	1/20	1/4	$\sqrt{5}/10$	0

Table 4.1 continued next page

Table 4.1 continued.

	$P^{27,27}$	$P^{10*,10*}$	$P^{10,10}$	$P^{8_s,8_s}$	$P^{8_a,8_a}$	$P^{8_a,8_s}$	$P^{1,1}$
$\eta \to \Lambda$	27/40	0	0	1/5	0	0	0
$\pi^+ \to \Xi^-$	1/2	0	1/2	0	0	0	0
$\pi^- \to \Xi^-$	1/5	1/6	1/6	3/10	1/6	$-2\sqrt{5}/10$	0
$K^+ \to \Xi^-$	1	0	0	0	0	0	0
$K^+ \to \Xi^0$	1/2	1/2	0	0	0	0	0
$K^- \to \Xi^-$	7/40	1/12	1/12	1/5	1/3	0	1/8
$K^- \to \Xi^0$	1/5	1/6	1/6	3/10	1/6	$2\sqrt{5}/10$	0
$\eta \to \Xi^-$	9/20	1/4	0	1/20	1/4	$\sqrt{5}/10$	0

CHAPTER FIVE

ANGULAR DISTRIBUTIONS IN THE CENTRAL REGION[1]

A. General Relations between Rapidity and Angular Distributions

In the previous chapters we have seen how the rapidity is a natural variable for the study of inclusive reactions. Some experimental data, however, cannot be treated in rapidity or Feynman's x variable because only the production angle is measured. This is frequently true for cosmic ray data, and is so for some accelerator data. In this chapter we shall investigate how distributions for which the rapidity is the natural variable appear when viewed only as angular distributions. Of course nothing precise can be said without specifying the actual distribution which is to be viewed as a function of production angle. Nevertheless, from the general behavior of the particle spectra as a function of transverse momentum we can form an adequate estimate of the modification of the spectra which occurs when the total particle momentum is averaged over.

The first step is to choose an angular variable which resembles the rapidity variable. The center of mass rapidity defined by Eq. (1.1) can be expressed as

$$z = \frac{1}{2} \ell n \left(\frac{E + p_{||}}{E - p_{||}} \right) \tag{5.1}$$

where E is the center of mass energy of the particle and $p_{||}$ is the momentum parallel to the beam direction. With $p_{||} = p \cos \theta$, this becomes

$$z = \frac{1}{2} \ell n \left(\frac{1 + \frac{P}{E} \cos \theta}{1 - \frac{P}{E} \cos \theta} \right) . \tag{5.2}$$

For $p \gg m_c$, z is evidently determined by the production angle and approximates the angular variable

$$\eta = \frac{1}{2} \ell n\left(\frac{1 + \cos\theta}{1 - \cos\theta}\right) \tag{5.3}$$

$$= \ell n\left(\cot\frac{\theta}{2}\right) . \tag{5.4}$$

Fixed angle behavior corresponds to $(b|c|a)$ since for fixed total momentum, it corresponds to fixed momentum parallel to the beam direction. Thus we begin with Eq. (3.64), which assumes two effective Regge poles--one pomeron with $\alpha_P = 1$, and one non-pomeron (which we call the reggeon here) with $\alpha_R = 1/2$. For simplicity we shall assume $a = b$, although this is certainly not necessary. Absorbing some kinematical factors, we can write

$$\frac{d\sigma}{dp} = f_{PP}(p_\perp) + f_{PR}(p_\perp)\, s^{-\frac{1}{4}} \cosh\left(\frac{z}{2}\right) + \mathcal{O}(s^{-\frac{1}{2}}) . \tag{5.5}$$

In Chapter 3 we pointed out that this form indicates a correlation between the cross section at $z = 0$ as a function of s and the variation with z near $z = 0$ at fixed s: rising cross sections must have a local maximum at the center while falling cross sections must develop a local minimum there. Clearly the same holds true for

$$\frac{d\sigma}{dz} = \int d^2p_\perp \frac{d\sigma}{dp} . \tag{5.6}$$

To investigate the nature of angular distributions we require some kinematical identities:

$$\operatorname{sech}\eta = \sin\theta \tag{5.7a}$$

$$\tanh\eta = \cos\theta \tag{5.7b}$$

$$p_\perp = p \operatorname{sech}\eta \tag{5.7c}$$

$$p_{||} = p \tanh\eta \tag{5.7d}$$

$$\frac{d^3p}{E} = d^2p_\perp\, dz \tag{5.7e}$$

$$= \pi\, dp_\perp^{\,2}\, dz \tag{5.7f}$$

$$= \pi\, dp_\perp^{\,2}\, d\eta \left(1 + \frac{m^2}{p_\perp^{\,2}\cosh^2\eta}\right)^{-\frac{1}{2}} . \tag{5.7g}$$

Equation (5.7g) follows from

$$z = \ell n\left[\frac{(p_\perp^{\,2}\cosh^2\eta + m^2)^{\frac{1}{2}} + p_\perp \sinh\eta}{m_\perp}\right] , \tag{5.8}$$

where $m_\perp^{\,2} = p_\perp^{\,2} + m^2$. Thus the cross section analogous to (5.6) is

$$\frac{d\sigma}{d\eta} = \int d^2p_\perp \left(1 + \frac{m^2}{p_\perp^{\,2}\cosh^2\eta}\right)^{-\frac{1}{2}} \frac{d\sigma}{dp} . \tag{5.9}$$

We define

$$\frac{d\sigma}{dz} = \frac{d\sigma}{dz}(P - P) + \frac{d\sigma}{dz}(P - R) \tag{5.10a}$$

$$\frac{d\sigma}{d\eta} = \frac{d\sigma}{d\eta}(P - P) + \frac{d\sigma}{d\eta}(P - R) \tag{5.10b}$$

with

$$\frac{d\sigma}{dz}(P - P) = \pi \int dp_\perp^2 \, f_{PP}(p_\perp) \tag{5.11a}$$

$$\frac{d\sigma}{dz}(P - R) = \pi \, s^{-\frac{1}{4}} \cosh\left(\frac{z}{2}\right) \int dp_\perp^2 \, f_{PR}(p_\perp) \tag{5.11b}$$

$$\frac{d\sigma}{d\eta}(P - P) = \pi \int dp_\perp^2 \, f_{PP}(p_\perp) \left(1 + \frac{m^2}{p_\perp^2 \cosh^2 \eta}\right)^{-\frac{1}{2}} \tag{5.11c}$$

$$\frac{d\sigma}{d\eta}(P - R) = \pi \, s^{-\frac{1}{4}} \int dp_\perp^2 \, f_{PF}(p_\perp) \left(1 + \frac{m^2}{p_\perp^2 \cosh^2 \eta}\right)^{-\frac{1}{2}} \times \left[\frac{1}{2} + \frac{1}{2}\left(1 + \frac{p_\perp^2 \sinh^2 \eta}{m^2}\right)^{\frac{1}{2}}\right]^{\frac{1}{2}} . \tag{5.11d}$$

Equation (5.11d) can be expanded for small η as

$$\frac{d\sigma}{d\eta}(P - R) = \pi \, s^{-\frac{1}{4}} \int dp_\perp^2 \, f_{PR}(p_\perp) \left(1 + \frac{m^2}{p_\perp^2}\right)^{-\frac{1}{2}} \left[1 + \frac{\eta^2}{8}\left(\frac{p_\perp^2}{m_\perp^2} + \frac{4m^2}{m_\perp^2}\right)\right] + \mathcal{O}(\eta^4) . \tag{5.12}$$

Thus we can make the comparisons,

$$\frac{\frac{d\sigma}{d\eta}(P - P)}{\frac{d\sigma}{dz}(P - P)} = \left\langle \left(1 + \frac{m^2}{p_\perp^2 \cosh^2 \eta}\right)^{-\frac{1}{2}} \right\rangle \tag{5.13a}$$

$$\frac{\frac{d\sigma}{d\eta}(P - R)}{\frac{d\sigma}{dz}(P - R)} = \frac{\left\langle \left[1 + \frac{\eta^2}{8}\left(\frac{p_\perp^2}{m_\perp^2} + \frac{4m^2}{m_\perp^2}\right)\right]\left(\frac{p_\perp}{m_\perp}\right)\right\rangle + \mathcal{O}(\eta^4)}{1 + \frac{z^2}{8} + \mathcal{O}(z^4)} . \tag{5.13b}$$

From (5.13a) we see that

$$\frac{d\sigma}{d\eta}(P - P) < \frac{d\sigma}{dz}(P - P) \tag{5.14}$$

for all η and $\frac{d\sigma}{d\eta}(P - P)$ approaches $\frac{d\sigma}{dz}(P - P)$ monotonically as $\eta \to \infty$. From (5.13b)

$$\left.\frac{d\sigma}{d\eta}(P - R)\right]_{\eta=0} < \left.\frac{d\sigma}{dz}(P - R)\right]_{z=0} . \tag{5.15}$$

From (5.11c) and (5.11d), for $\eta = z \to \infty$

$$\frac{e^{-\eta/2} \frac{d\sigma}{d\eta}(P - R)}{d^{-z/2} \frac{d\sigma}{dz}(P - R)} = \left\langle \left(\frac{p_\perp}{m_\perp}\right)^{\frac{1}{2}} \right\rangle . \tag{5.16}$$

Using (5.13b) and (5.16), for $\eta = z$

$$\frac{\frac{d\sigma}{d\eta}(P - R)_{\eta=0}}{\frac{d\sigma}{dz}(P - R)_{z=0}} < \frac{\frac{d\sigma}{d\eta}(P - R)_{\eta=\infty}}{\frac{d\sigma}{dz}(P - R)_{z=\infty}} < 1 . \tag{5.17}$$

B. Expansions about the Center

Asymptotically, the rapidity distribution becomes flat near $z = 0$. Its curvature comes from the pomeron-reggeon term what has $s^{-\frac{1}{4}}$ behavior. We can expand the rapidity distribution (5.10a) as

$$\frac{d\sigma}{dz} = \pi \int dp_\perp^2 \, f_{PP}(p_\perp) + \pi s^{-\frac{1}{4}} \left(1 + \frac{z^2}{8} + \cdots\right) \int dp_\perp^2 \, f_{PR}(p_\perp) \tag{5.18}$$

$$= A_0 + s^{-\frac{1}{4}}(B_0 + z^2 B_1 + \cdots) \tag{5.19}$$

with $B_1/B_0 = 1/8$.

The angular distribution on the other hand does not become flat asymptotically, but develops a local minimum at the center. We can write an analogous expansion for small η:

$$\frac{d\sigma}{d\eta} = (A_0' + A_1' \eta^2 + \cdots) + s^{-\frac{1}{4}}(B_0' + B_1' \eta^2 + \cdots) \tag{5.20}$$

where

$$A_0' = \pi \int dp_\perp^2 \, f_{PP}(p_\perp) \left(1 + \frac{m^2}{p_\perp^2}\right)^{-\frac{1}{2}} \tag{5.21a}$$

$$= A_0 \left\langle \frac{p_\perp}{m_\perp} \right\rangle \tag{5.21b}$$

$$A_1' = A_0 \left\langle \frac{m^2}{2m_\perp^2} \frac{p_\perp}{m_\perp} \right\rangle \tag{5.21c}$$

$$B_0' = B_0 \left\langle \frac{p_\perp}{m_\perp} \right\rangle \tag{5.22a}$$

$$B_1' = B_0 \left\langle \left(1 + \frac{3m^2}{m_\perp^2}\right) \frac{p_\perp}{m_\perp} \right\rangle \Big/ 8 \quad . \tag{5.22b}$$

Thus the center of the η distribution is depressed by a factor

$$\frac{A_0'}{A_0} = \left\langle \frac{p_\perp}{m_\perp} \right\rangle \quad . \tag{5.23}$$

The asymptotic curvature is given by

$$\frac{A_1'}{A_0'} = \frac{\left\langle \frac{m^2}{2m_\perp^2} \frac{p_\perp}{m_\perp} \right\rangle}{\left\langle \frac{p_\perp}{m_\perp} \right\rangle} \quad . \tag{5.24}$$

The curvature of the nonasymptotic reggeon-pomeron term is

$$\frac{B_1'}{B_0'} = \frac{1}{8} \frac{\left\langle \left(1 + \frac{3m^2}{m_\perp^2}\right) \frac{p_\perp}{m_\perp} \right\rangle}{\left\langle \frac{p_\perp}{m_\perp} \right\rangle} \quad . \tag{5.25}$$

As $m_c \to 0$, η and z become equivalent. It is easy to verify that in this limit, all the primed coefficients tend to the unprimed coefficients.

Because the asymptotic pomeron-pomeron term in the rapidity distribution is flat, the curvature of the distribution at finite s can be attributed to the nonasymptotic terms. For the angular distributions, the situation is not so simple. At finite s, the curvature depends on both the asymptotic and nonasymptotic terms. From (5.24) and (5.25) we see

$$0 < \frac{A_1'}{A_0'} < \frac{1}{2} \tag{5.26a}$$

$$\frac{1}{8} < \frac{B_1'}{B_0'} < \frac{1}{2} \quad . \tag{5.26b}$$

If at finite s we have

$$\frac{d\sigma}{d\eta} = C_0' + C_1'\eta^2 + \cdots \tag{5.27}$$

with $C_1' < 0$, then we can conclude $B_0' < 0$, since

$$C_1' = A_1' + s^{-\frac{1}{4}} B_0'\left(\frac{B_1'}{B_0'}\right) \quad . \tag{5.28}$$

If $C_1' > 0$, B_0' may be either positive or negative. No matter what the sign of B_0', eventually C_1' is simply determined by A_1', which is positive.

C. Numerical Examples

To clarify these ideas, consider a hypothetical distribution with

$$f_{PP}(p_\perp) = \frac{\sigma_{PP}}{m^2} e^{-ap_\perp^2} \tag{5.29a}$$

$$f_{PR}(p_\perp) = \frac{\sigma_{PR}}{m^{3/2}} e^{-ap_\perp^2} \quad . \tag{5.29b}$$

Then

$$\frac{d\sigma}{dz}(P - P) = \frac{\pi\sigma_{PP}}{am^2} \tag{5.30a}$$

$$\frac{d\sigma}{dz}(P - R) = \pi\left(\frac{s}{m^2}\right)^{-\frac{1}{4}} \frac{\sigma_{PR}}{am^2} \cosh\left(\frac{z}{2}\right) \tag{5.30b}$$

$$\frac{d\sigma}{d\eta}(P - P) = \frac{\pi\sigma_{PP}}{m^2} \int dp_\perp^2 \, e^{-ap_\perp^2} \left(1 + \frac{m^2}{p_\perp^2 \cosh^2\eta}\right)^{-\frac{1}{2}} \tag{5.30c}$$

$$\frac{d\sigma}{d\eta}(P - R) = \pi\left(\frac{s}{m^2}\right)^{-\frac{1}{4}} \frac{\sigma_{PR}}{m^2} \int dp_\perp^2 \, e^{-ap_\perp^2}$$

$$\times \left(1 + \frac{m^2}{p_\perp^2 \cosh^2\eta}\right)^{-\frac{1}{2}} \left(\frac{1}{2} + \frac{1}{2}\left[1 + \frac{p_\perp^2 \sinh^2\eta}{m_\perp^2}\right]^{\frac{1}{2}}\right)^{\frac{1}{2}} . \tag{5.30d}$$

The evaluation of (5.30c) is straightforward and yields

$$\frac{d\sigma}{d\eta}(P - P) = \frac{\pi\sigma_{PP}}{am^2} x\, e^x [K_1(x) - K_0(x)] \tag{5.31}$$

with $x = (am^2 \operatorname{sech}^2\eta)/2$ and where K_0 and K_1 are the usual modified Bessel functions. From (5.31) we find easily the expressions for A_0' and A_1'

$$A_0' = \frac{\pi\sigma_{PP}}{am^2} x\, e^x [K_1(x) - K_0(x)] \tag{5.32a}$$

$$A_1' = \frac{\pi \sigma_{PP}}{am^2} \times e^x [K_0(x) - 2x[K_1(x) - K_0(x)]] \qquad (5.32b)$$

where $x = am^2/2$. In a similar fashion we find

$$B_0' = \frac{\sigma_{PR}}{am^2} m^{\frac{1}{2}} \times e^x [K_1(x) - K_0(x)] \qquad (5.33a)$$

$$B_1' = \frac{\sigma_{PR}}{am^2} m^{\frac{1}{2}} \frac{1}{8} \times e^x \{K_1(x) - K_0(x) + 6\left[K_0(x) - 2x[K_1(x) - K_0(x)]\right]\}. \qquad (5.33b)$$

The ratios A_1'/A_0' and B_1'/B_0' are shown in Figs. 5.1 and 5.2 as a function of the parameter a. A full evaluation of the angular distributions arising from the pomeron-pomeron and pomeron-reggeon terms is shown in Figs. 5.3-6. The full expressions (5.11) have been evaluated numerically for transverse momentum distributions of the form $\exp(-ap_\perp^2)$ and $\exp(-bp_\perp)$. Clearly the general features are quite similar. At the center of the distributions, the angular distribution, $\frac{d\sigma}{d\eta}$, is about 70 to 90% as great as the rapidity distribution, $\frac{d\sigma}{dz}$.

CHAPTER SIX

INCLUSIVE REACTIONS IN A DUAL RESONANCE MODEL

A. Introduction

One of the most exciting and remarkable developments in particle physics has been the dual resonance model.[1] Not only has this model had success in representing theoretical concepts such as Regge behavior, factorization, crossing, and duality, but it has even had some success as a phenomenological tool. It was natural that it be applied to the problem of inclusive reactions.

Since the dual resonance model provides an explicit six-point amplitude, the inclusive cross sections can be deduced by examining the appropriate discontinuity. This suggests a lack of ambiguity which is unfortunately not real. In the Mueller framework, we know that scaling arises from a pomeron with intercept $\alpha_V = 1$. However, a trajectory with intercept $\alpha_V = 1$ in the simplest dual model is not believed to be the way to represent the pomeron. This belief relies on duality: the pomeron is supposed to the dual to nonresonant production in the crossed channel, while the "bare" Regge poles in the simple dual models are all dual to resonances. A more popular representation of the pomeron is the "twisted loop" which is, in fact dual to nonresonant production. Unfortunately, it is not yet possible to do calculations with the twisted loop pomeron--nor is it even clear that this is the proper representation for the pomeron. We are left with a choice: we can take $\alpha_V = 1$ so as to obtain scaling and ignore the complications mentioned above, or we can take $\alpha_V < 1$ and sacrifice scaling. Since both procedures have serious drawbacks, it is worthwhile to see what conclusions follow from one or the other, or perhaps both of the assumptions.

This chapter relies heavily on the work of Virasoro (1971) and of DeTar et al. (1971b). Independent, but similar work to that presented here has been performed by Thomas (1972). Virasoro and DeTar et al. give detailed explanations of the identification of the inclusive cross section with the appropriate six-point amplitude. The work of Thomas contains extensive numerical calculations. We shall pursue a middle course, half pedagogical, half phenomenological.

At this point it becomes necessary to delve slightly more seriously into the question of precisely which discontinuity of the six-point amplitude is connected with the inclusive cross section. (Stapp, 1971; Tan, 1971; Polkinghorne, 1971). We follow Tan, but present only the simplest heuristic arguments.

The optical theorem for two-body scattering relates the discontinuity of the forward amplitude to the total cross section. See Fig. 6.1a. The required inclusive cross section is represented in Fig. 6.1b. A discontinuity formula for three-to-three amplitudes can be written down (if not justified) by inspection. See Fig. 6.1c. In a region in which all channels except abc are below threshold, "extended" unitarity would give the relation shown in Fig. 6.1d, where the ab and a'b' channels have no + or - labels since they are below threshold.

To achieve the arrangement of Fig. 6.1b, we have to set s_{ab} above its cut and $s_{a'b'}$ below its cut as we raise s_{ab} from below threshold to above threshold. Thus we have the equality in Fig. 6.1e as our discontinuity relation for inclusive cross sections. The reader is referred to Stapp and Tan for further discussion.

The dual resonance model provides a prescription for evaluating the six-point amplitudes occurring in Fig. 6.1e. Even in the simple approach in which only tree diagrams are used, there are numerous contributions arising from the various permutations of the particles. As DeTar et al. show, the contributions of the various diagrams can be calculated in terms of a single configuration, say that given in Fig. 6.2a. If we consider $(a:x|b)$, it turns out that the contributing diagrams are those shown in Fig. 6.2c. This is, as DeTar et al. note, precisely what we expect from Mueller-like considerations. On the other hand, for $(a|x|b)$ we have contributions only from the diagram in Fig. 6.2d.

B. Explicit Calculations

For simplicity, we shall consider only the last diagram, 6.2a, both for $(a|x|b)$ and for $(a:x|b)$. This diagram alone possesses most of the properties we wish to discuss. In the small x region it should give an adequate representation of fragmentation since the other contributing diagrams vanish as $x \to 0$. Evaluation of the other fragmentation diagrams has been performed by Thomas.

We begin without assuming that the vacuum trajectory, α_V, necessarily has intercept unity. Accordingly, we define, as $s \to \infty$,

$$\bar{f}(x,\underline{p}_\perp) = \lim_{s\to\infty} \frac{1}{\sigma_{ab}} E \frac{d\sigma}{d^3p}(x,\underline{p}_\perp,s) \quad . \tag{6.1}$$

If $\alpha_t = \alpha_{a\bar{x}}(t)$ is the value of the Regge trajectory in the $a\bar{x}$ channel, then Eq. (3.3) of DeTar et al. may be written

$$\bar{f}(x,p_\perp) = (1-x)^{\alpha_V} \int_0^1 dz \int_0^{1-z} dy\, (yz)^{\alpha_V - 1}$$

$$\times \left[\left(1+\frac{r}{y}\right)\left(1+\frac{r}{z}\right)\right]^{\alpha_V+\alpha_t} (r+y+z)^{-2\alpha_V} (1-y-z)^{\alpha_V} \qquad (6.2)$$

where $r = x/(1-x)$. We assume that both the $a\bar{a}$ and $b\bar{b}$ channels have the same vacuum trajectory. The outgoing particle, x is assumed to be spinless and to lie on the trajectory of the $a\bar{a}x$ (or $\overline{aax}$) channel. We shall further assume that $\alpha_t = -1 + t$ so that particles a and b are spinless, with unit mass.

Next we transform variables until one integration in (6.2) can be done conveniently. Let

$$s = y + z$$
$$t = yz \ . \qquad (6.3a)$$

Calculating the Jacobian, we find

$$dy\, dz = (s^2 - 4t)^{-\frac{1}{2}}\, ds\, dt \ . \qquad (6.3b)$$

Thus

$$\bar{f}(x,p_\perp) = 2(1-x)^{\alpha_V} \int_0^1 ds \int_0^{s^2/4} dt\, (s^2-4t)^{-\frac{1}{2}}\, t^{\alpha_V - 1}$$

$$\times \left(1 + \frac{rs}{t} + \frac{r^2}{t}\right)^{\alpha_t+\alpha_V} (r+s)^{-2\alpha_V} (1-s)^{\alpha_V} \ . \qquad (6.4)$$

Letting $t = t's^2/4$, we can do the t' integration to get

$$\bar{f}(x,p_\perp) = 2(1-x)^{\alpha_V} 4^{-\alpha_V} \frac{\Gamma(\frac{1}{2})\Gamma(-\alpha_t)}{\Gamma(-\alpha_t+\frac{1}{2})} \int_0^1 ds\ s^{2\alpha_V - 1} (r+s)^{-2\alpha_V}$$

$$\times (1-s)^{\alpha_V} \left(1+\frac{2r}{s}\right)^{2(\alpha_t+\alpha_V)} F\left(-\alpha_t-\alpha_V, \tfrac{1}{2}; -\alpha_t+\tfrac{1}{2}; \left(1+\frac{2r}{s}\right)^{-2}\right) \qquad (6.5)$$

where $F(a,b,c;z)$ is the usual hypergeometric function. Equation (6.5) is a convenient form for numerical integration since the argument of the hypergeometric function has a modulus less than unity and thus the power series for F converges.

Typical results are shown in Fig. 6.3. In these calculations, the vacuum trajectory was taken to have an intercept of 0.5 (the choice of DeTar et al.). Each fixed $p_\perp$ curve rises from zero at the kinematical boundary, attains a maximum value and then falls to its asymptotic value which is only a fraction of the maximum. The asymptotic value is, of course, the $x = 0$ result. In particular, this naive model predicts that the central value is a local minimum.

C. Limiting Cases

From Eq. (6.5) we can evaluate certain limiting cases. First consider $p_\perp \gg 1$ (Our units are always determined by the slope of the trajectories, which we assume to be about 1 GeV^{-2}). From (1.29) for fixed x, as $p \to \infty$ we find that $t \to -\infty$. This can be exploited by using the properties of the hypergeometric function:

$$F\left(-\alpha_t - \alpha_V, \tfrac{1}{2}; -\alpha_t + \tfrac{1}{2}; \left(1 + \frac{2\gamma}{s}\right)^{-2}\right)$$

$$= \left(1 - \frac{1}{\left(1 + \frac{2\gamma}{s}\right)^2}\right)^{-\frac{1}{2}} F\left(\alpha_V + \tfrac{1}{2}, \tfrac{1}{2}; -\alpha_t + \tfrac{1}{2}; \frac{1}{1 - \left(1 + \frac{2\gamma}{s}\right)^2}\right) . \tag{6.6}$$

Now the hypergeometric function on the right hand side goes to unity as $t \to -\infty$ ($\alpha_t \to \infty$) (Erdelyi et al., 1953, p. 76) if $\gamma > 0$. Thus we have

$$\bar{f}(x, p_\perp \gg 1) \simeq 2(1 - x)^{\alpha_V} 4^{-\alpha_V} \frac{\Gamma(\frac{1}{2})\,\Gamma(-\alpha_t)}{\Gamma(-\alpha_t + \frac{1}{2})} \int_0^1 ds\; s^{2\alpha_V - 1}$$

$$\times (\gamma + s)^{-2\alpha_V} (1 - s)^{\alpha_V} \left(1 + \frac{2\gamma}{s}\right)^{2(\alpha_t + \alpha_V)} \left(\frac{4\gamma}{s} + \frac{4\gamma^2}{s^2}\right)^{-\frac{1}{2}} \left(1 + \frac{2\gamma}{s}\right). \tag{6.7}$$

Since $-\alpha_t \gg 1$, the integral is dominated by s near 1, so that we may write

$$\bar{f}(x, p_\perp \gg 1) \simeq 2(1 - x)^{\alpha_V} 4^{-\alpha_V} \frac{\Gamma(\frac{1}{2})\,\Gamma(-\alpha_t)}{\Gamma(-\alpha_t + \frac{1}{2})} (4\gamma)^{-\frac{1}{2}} (1 + \gamma)^{-\frac{1}{2} - 2\alpha_V}$$

$$\times \int_0^1 ds'\; (s')^{\alpha_V} \left(1 + \frac{2\gamma}{1 - s'}\right)^{2(\alpha_t + \alpha_V) + 1} \tag{6.8}$$

where we have put $s = 1 - s'$. The integral now is dominated by s' near zero and we find

$$\bar{f}(s, p_\perp \gg 1) \simeq 2(1 - x)^{\alpha_V} 4^{-\alpha_V} \frac{\Gamma(\frac{1}{2})\,\Gamma(-\alpha_t)}{\Gamma(-\alpha_t + \frac{1}{2})} (4\gamma)^{-\frac{1}{2}} (1 + \gamma)^{-\frac{1}{2} - 2\alpha_V}$$

$$\times (1 + 2\gamma)^{2(\alpha_t + \alpha_V) + 1} \left(\frac{2\gamma}{1 + 2\gamma}\right)^{-\alpha_V - 1} \left(-2(\alpha_t + \alpha_V) - 1\right)^{-\alpha_V - 1}$$

$$\times \Gamma(\alpha_V + 1) \tag{6.9}$$

With

$$Q^2 = -(1 + \alpha_t)x$$

$$= p_\perp^2 - m_a^2 x(1 - x) - m_c^2 (x - 1) , \tag{6.10}$$

we have, for $Q^2 \gg 1$

$$\bar{f}(x, p_\perp \gg 1) \simeq \Gamma(\tfrac{1}{2})\,\Gamma(\alpha_V + 1)\, 2^{-4\alpha_V - 2} (Q^2)^{-\alpha_V - 3/2}$$

$$\times (1 - x)^{2 + \alpha_V} (1 - x)^{3\alpha_V} \left(\frac{1 + x}{1 - x}\right)^{-2Q^2/x} . \tag{6.11}$$

Thus the $p_\perp$ behavior is essentially $\exp(-bp_\perp^2)$ times a power of $p_\perp$ with

$$b = \frac{2}{x} \log\left(\frac{1 + x}{1 - x}\right) . \tag{6.12}$$

From (6.5) we can also derive an expression for pionization ($x = 0$). As $\gamma \to 0$, with $p_\perp$ fixed,

$$F\left(\alpha_V + \frac{1}{2},\ \frac{1}{2};\ -\alpha_t + \frac{1}{2};\ -\left(\frac{4\gamma}{s} + \frac{4\gamma^2}{s^2}\right)^{-1}\right) \rightarrow$$

$$\rightarrow \left(\frac{4Q^2}{s}\right)^{\alpha_V + \frac{1}{2}} \Psi\left(\alpha_V + \frac{1}{2},\ \alpha_V + 1;\ \frac{4Q^2}{s}\right) \qquad (6.13)$$

where $\Psi(a,c;\ z)$ is the usual confluent hypergeometric function whose integral representation is (Erdelyi, 1953)

$$\Psi(a,c;\ z) = \frac{1}{\Gamma(a)} \int_0^\infty dt\ e^{-zt}\ t^{a-1}(1+t)^{c-a-1}\ .$$

In this limit, $-\alpha_t \rightarrow Q^2/\gamma$ and we have

$$\bar{f}(x=0,\ p_\perp) = 2\pi^{\frac{1}{2}}\ (Q^2)^{\alpha_V} \int_0^1 ds\ s^{-\alpha_V - 1}(1-s)^{\alpha_V}$$

$$\times\ e^{-4Q^2/s}\ \Psi(\alpha_V + \tfrac{1}{2},\ \alpha_V + 1;\ 4Q^2/s) \qquad (6.14a)$$

$$= 2\pi^{\frac{1}{2}}\ (Q^2)^{\alpha_V} \int_0^\infty ds\ s^{\alpha_V}(1+s)^{-1}\ e^{-4Q^2(1+s)}$$

$$\times\ \Psi\left(\alpha_V + \tfrac{1}{2},\ \alpha_V + 1;\ 4Q^2(1+s)\right)\ . \qquad (6.14b)$$

Numerical evaluation of the pionization distribution is shown in Fig. 6.4 for two values of the vacuum intercept: $\alpha_V = 0.5$ and $\alpha_V = 0.9$. Both give rather steep behavior which is compared with

experimental data in the final chapter (see Fig. 8.8a). The asymptotic form of the pionization can be found easily from (6.11):

$$\bar{f}(x=0, p_\perp \gg 1) \simeq \Gamma(\tfrac{1}{2})\ \Gamma(\alpha_V + 1)\ 2^{-4\alpha_V - 2}\ (Q^2)^{-\alpha_V - 3/2}\ e^{-4m_\perp^2}\ . \qquad (6.15)$$

For small values of the transverse momentum, the distribution is much steeper, and in fact diverges for $m_\perp = 0$.

CHAPTER SEVEN

INCLUSIVE PHOTON DISTRIBUTIONS[1]

A. Introduction

The most extensively studied inclusive processes are the single-particle inclusive reactions of the form $(a:c|b)$. If particle c is not a hadron, but rather the decay product of a hadron, d, the observed spectrum is an indirect image of the original inclusive process $(a:d|b)$. In particular, the observation of $(a:\gamma|b)$ yields information primarily about $(a:\pi^0|b)$. Of course the information is not as precise as would be a direct measurement of $(a:\pi^0|b)$ in a coincidence experiment.

There are further complications in interpreting the photon spectrum. Some photons arise from the decays of hadrons other than π^0's, most notably from the decays of η's. The $\eta \to 3\pi^0$ mode is an especially copious source of photons. Each η yields an average of 3.2 photons. Because of the much greater production of π^0's and because the photons from the $\eta \to 3\pi^0$ mode are essentially indistinguishable from "true" π^0 photons we shall generally ignore the complication introduced by η decays.

A second complication is the production of photons by charged particle bremsstrahlung. For soft photons bremsstrahlung must be taken into account. We shall do this in Sec. F in the context of a model.

The basic assumption of the paper is that at high energies hadronic processes exhibit Feynman scaling. Beyond this, we shall need little more than kinematics. Since these kinematics are

essential and somewhat unfamiliar, we present them in some detail in Sec. B. These results are combined with Feynman scaling in Sec. C. A numerical example is presented in Sec. D to clarify the preceding sections. The prescription of Sternheimer (1955) for extracting the π^0 spectrum from the observed photon spectrum is examined in Sec. E. The bremsstrahlung contribution to the photon distribution is analyzed in Sec. F. Finally, the principles derived are applied to an analysis of the CERN ISR data on $(p:\gamma|p)$ in Chapter 8.

The principal results are

1. If $(a:\pi^0|b)$ scales, so that the inclusive π^0 differential cross section gives

$$\lim_{s\to\infty} \frac{E}{\sigma_{inel}} \frac{d\sigma}{d^3p}(x,p_\perp^2,s) = \frac{1}{\sigma_{inel}} f_{\pi^0}(x,p_\perp^2)$$

$$= \bar{f}_{\pi^0}(x,p_\perp^2) ,$$

where $p_\perp$ is the component of the π^0 momentum perpendicular to the beam direction and $x = p_{||}/[(s)^{\frac{1}{2}}/2]$, then the photon spectrum resulting from the π^0 decays also scales:

$$\lim_{s\to\infty} \frac{k}{\sigma_{inel}} \frac{d\sigma}{d^3k}(x,k_\perp^2,s) = \frac{1}{\sigma_{inel}} f_\gamma(x,k_\perp^2)$$

$$= \bar{f}_\gamma(x,k_\perp^2)$$

where $k_\perp$ is the component of photon momentum perpendicular to the beam direction and $x = k_{||}/[(s)^{\frac{1}{2}}/2]$.

2. $f_\gamma(x,k_\perp^2)$ is continuous as $x \to 0$ except for $k_\perp^2 = 0$, where we have

$$\lim_{x\to 0}\lim_{k_\perp\to 0} f_\gamma(x,k_\perp^2) = \frac{1}{2}\lim_{k_\perp\to 0}\lim_{x\to 0} f_\gamma(x,k_\perp^2) .$$

3. For the photon spectrum arising from π^0 decays,

$$\lim_{k_\perp\to 0} f_\gamma(x=0,k_\perp^2) = \frac{2}{m^2}\int_0^\infty dk_\perp^2\, f_\gamma(x=0,k_\perp^2)$$

on the assumption that the π^0 distribution has scaled.

4. For the photon spectrum arising from bremsstrahlung, we derive the result for large s, small $k_\perp$, and $x = 0$,

$$\frac{k d\sigma}{\sigma d^3k}(k_\perp,s) \approx \frac{\alpha}{4\pi^2 k_\perp^2}\langle n_c\rangle$$

where α is the fine structure constant, and $\langle n_c\rangle$ is the mean charged multiplicity.

B. DECAY KINEMATICS

The calculation of the photon distribution from a known π^0 distribution is straight-forward. If a single π^0 with four-momentum p and mass m decays into two photons, the distribution of photons is given, in invariant form, by

$$k\frac{dN}{d^3k}(p,k) = \frac{1}{\pi}\delta\left(p\cdot k - \frac{m^2}{2}\right) . \tag{7.1}$$

Consequently, the Lorentz invariant cross section for photon production is

$$k\frac{d\sigma}{d^3k} = \int \frac{d^3p}{E}\left(E\frac{d\sigma}{d^3p}(p,s)\right)\frac{1}{\pi}\delta\left(p\cdot k - \frac{m^2}{2}\right) \tag{7.2}$$

where

$$E\frac{d\sigma}{d^3p}(p,s)$$

is the invariant differential cross section for the production of π^0's at a center-of-mass energy squared equal to s. For definiteness we shall assume that the π^0's result from p-p collisions, and the center of mass is that of the p-p system. It will be apparent that all the results apply equally to $(a{:}\pi^0|b)$ with only trivial modifications, if any.

The π^0's which contribute to the photon spectrum at a given momentum, k, are constrained by Eq. (7.1) to satisfy

$$E - p'_{\parallel} = \frac{m^2}{2k} \tag{7.3}$$

where $p'_{||}$ is the component of π^0 momentum parallel to the photon momentum. From (7.3) we find

$$p'_{||} = p_0 + \frac{k}{m^2} p'^2_{\perp} \tag{7.4}$$

where $p'_{\perp}$ is component of π^0 momentum perpendicular to the photon momentum and where

$$p_0 = k - \frac{m^2}{4k} . \tag{7.5}$$

See Fig. 7.1. In momentum space, the π^0's contributing at a given photon momentum are confined to a paraboloid whose axis is along the direction of the photon, and whose apex is at $p'_{||} = p_0$. For large k/m the paraboloid becomes very narrow. The limit $k \to 0$ is degenerate and must be handled with care.

The delta function in (7.2) can be eliminated by integrating over Θ, the angle between the π^0 and the photon, with the result

$$k \frac{d\sigma}{d^3k} = \frac{1}{\pi k} \int_{E_0}^{\infty} dE \int_0^{2\pi} d\phi \; E \frac{d\sigma}{d^3p} (p,s) \tag{7.6}$$

where ϕ is the azimuthal angle in the plane perpendicular to the photon, and where

$$E_0 = (p_0^2 + m^2)^{\frac{1}{2}}$$

$$= k + \frac{m^2}{4k} . \tag{7.7}$$

In (7.6) we have taken the upper in the E integration to be infinite and assumed the kinematical limits are incorporated into the π^0 differential cross section. The π^0 three momentum in (7.6) is given,

in co-ordinates relative to the photon, by

$$\underset{\sim}{p} = \left\{ p'_{||}, p'_x = \cos\phi \left[\frac{m^2}{k} (p'_{||} - p_0) \right]^{\frac{1}{2}}, p'_y = \sin\phi \left[\frac{m^2}{k} (p'_{||} - p_0) \right]^{\frac{1}{2}} \right\} . \tag{7.8}$$

The π^0 inclusive cross section is a function of s, p_z the component of momentum parallel to the beam direction, and $p_{\perp}$, the component perpendicular to it. If the azimuthal angle ϕ is measured away from the plane containing the photon and the beam direction, and if the photon has components of momentum parallel and perpendicular to the beam direction $k_{||}$ and $k_{\perp}$ respectively, then

$$p_{\perp}^2 = \left\{ \left[\frac{m^2}{k} (E - E_0) \right]^{\frac{1}{2}} \frac{k_{||}}{k} \cos\phi + \left(E - \frac{m^2}{2k} \right) \frac{k_{\perp}}{k} \right\}^2 + \frac{m^2}{k} (E - E_0) \sin^2\phi \tag{7.9}$$

where E is the π^0 energy. See Fig. 7.2. Thus we have explicitly

$$k \frac{d\sigma}{d^3k} (k,s) = \frac{1}{\pi k} \int_{E_0}^{\infty} dE \int_0^{2\pi} d\phi \; E \frac{d\sigma}{d^3p} \left\{ E, p_{\perp}^2 \right.$$

$$= \left(\left[\frac{m^2}{k} (E - E_0) \right]^{\frac{1}{2}} \frac{k_{||}}{k} \cos\phi + \left(E - \frac{m^2}{2k} \right) \frac{k_{\perp}}{k} \right)^2$$

$$\left. + \frac{m^2}{k} (E - E_0) \sin^2\phi, s \right\} . \tag{7.10}$$

For $k/m \gg 1$, the paraboloid over which the integration takes place becomes narrow. If it is approximated by one of vanishing width, Eq. (7.10) becomes

$$k \frac{d\sigma}{d^3k}(k,s) \approx \frac{2}{k}\int_{E_0}^{\infty} dE\, E \frac{d\sigma}{d^3p}(\bar{p},s) \tag{7.11}$$

where $\bar{\underset{\sim}{p}}$ lies in the same direction as $\underset{\sim}{k}$. In this limit we can also approximate E_0 by k. Then we have the approximation of Sternheimer (1955):

$$\frac{\partial}{\partial k}\left[k^2 \frac{d\sigma}{d^3k}(\underset{\sim}{k},s)\right] = -2\, E \frac{d\sigma}{d^3p}(\underset{\sim}{p} = \underset{\sim}{k},s) . \tag{7.12}$$

We postpone until Sec. E an evaluation of the reliability of Sternheimer's approximation.

C. SCALING

The scaling hypothesis is that as $s \to \infty$, the invariant differential production cross-section becomes a function of $p_\perp^2$ and $x = p_{||}/[(s)^{\frac{1}{2}}/2]$ only. (See Sec. A) To see how this scaling manifests itself in the photon spectrum arising from π^0 decay, we being with Eq. (7.10) and introduce new co-ordinates:

$$\begin{aligned} Q^2 &= \frac{m^2}{k}(E - E_0) \\ Q_x &= Q \cos\phi \\ Q_y &= Q \sin\phi \ . \end{aligned} \tag{7.13}$$

Then we have

$$k \frac{d\sigma}{d^3k}(\underset{\sim}{k},s) = \frac{2}{\pi m^2}\int d^2Q\, E \frac{d\sigma}{d^3p}\left(E = \frac{kQ^2}{m^2} + E_0,\right.$$

$$\left. p_\perp^2 = \left\{\left[\frac{k_{||}}{k} Q_x + \left(\frac{kQ^2}{m^2} + p_0\right)\frac{k_\perp}{k}\right]^2 + Q_y^2\right\}, s\right) . \tag{7.14}$$

If we take $s \to \infty$ with $x_\gamma \neq 0$, in the notation of Sec. A we have

$$f_\gamma(x_\gamma, k_\perp^2) = \frac{2}{\pi m^2}\int d^2Q\, f_\pi\left(x_\pi = x_\gamma\left(1 + \frac{Q^2}{m^2}\right)\right.,$$

$$\left. p_\perp^2 = \left\{\left[Q_x + k_\perp\left(1 + \frac{Q^2}{m^2}\right)\right]^2 + Q_y^2\right\}\right) . \tag{7.15}$$

Equation (7.15) makes manifest the scaling of the photon distribution for $x \neq 0$.

The π^0 spectrum is expected to become a function of $p_\perp$ alone as $s \to \infty$ with $p_\perp$ and $p_{||}$ fixed. This carries over to the photon spectrum as we show below. From (7.14), we have in the $x_\gamma = 0$ limit (with $k_\perp$ and $k_{||}$ fixed),

$$f_\gamma(0,k_\perp^2) = \frac{2}{\pi m^2}\int d^2Q\, f_\pi\left(0,p_\perp^2 = \left\{\left[\frac{k_{||}}{k}Q_x + \left(\frac{kQ^2}{m^2} + p_0\right)\frac{k_\perp}{k}\right]^2 + Q_y^2\right\}\right) . \tag{7.16}$$

Only π^0's with $x_\pi = 0$ contribute, since from (7.14), π^0's with $x_\pi \neq 0$ would have $p_\perp^2 \propto s$, and we assume the cross section falls off in $p_\perp^2$. We can change variables in (7.16) to

$$\begin{aligned} Q_x' &= Q_x + \frac{m^2}{2k_\perp}\frac{k_{||}}{k} \\ Q_y' &= Q_y \end{aligned} \tag{7.17}$$

to get

$$f_\gamma(0,k_\perp^2) = \frac{2}{\pi m^2}\int d^2Q'\, f_\pi\left(0,p_\perp^2 = \left\{\left[p_0(k_\perp) + \frac{k_\perp}{m^2}Q'^2\right]^2 + Q_y'^2\right\}\right) \tag{7.18}$$

where

$$p_0(k_\perp) = k_\perp - \frac{m^2}{4k_\perp} .$$

From (7.18), we see that the photon spectrum in the central region is indeed independent of $k_{||}$.

If $k_\perp \neq 0$, then $f_\gamma(x_\gamma,k_\perp^2)$ [Eq. (7.15)] joins smoothly to $f_\gamma(0,k_\perp^2)$ [Eq. (7.18)]. To prove this, let

$$\begin{aligned} Q_x' &= Q_x + \frac{m^2}{2k_\perp} \\ Q_y' &= Q_y \end{aligned} \tag{7.19}$$

in Eq. (7.15) and let $x_\gamma \to 0$. Then we find

$$\lim_{x_\gamma \to 0} f_\gamma(x_\gamma,k_\perp^2) = \frac{2}{\pi m^2}\int d^2Q'\, f_\pi\left(0,p_\perp^2 = \left\{\left[p_0(k_\perp) + \frac{k_\perp}{m^2}Q'^2\right]^2 + Q_y'^2\right\}\right) \tag{7.20}$$

$$= f_\gamma(0,k_\perp^2) .$$

On the other hand, if $k_\perp = 0$, the transformation given by (7.19) cannot be used. Instead, we have from (7.15),

$$f_\gamma(x_\gamma,0) = \frac{2}{\pi m^2}\int d^2Q\, f_\pi\left(x_\pi = x_\gamma\left(1 + \frac{Q^2}{m^2}\right),\ p_\perp^2 = Q^2\right) . \tag{7.21}$$

Evaluation of the $k_\perp \to 0$ limit of $f_\gamma(0,k_\perp^2)$ requires some care. Because $p_0(k_\perp) \approx -\frac{m^2}{4k_\perp}$, $p_\perp^2$ is large unless [see Eq. (7.18)]

$$\frac{k_\perp Q_x'^2}{m^2} - \frac{m^2}{4k_\perp} \approx 0 . \tag{7.22}$$

With

$$\begin{aligned} Q_x' &= Q_x'' \pm \frac{m^2}{2k_\perp} \\ Q_y' &= Q_y'' , \end{aligned} \tag{7.23}$$

we have from (7.18),

$$p_\perp^2 = Q''^2 \pm 2Q''_x k_\perp\left(1 + \frac{Q''^2}{m^2}\right) + k_\perp^2\left(1 + \frac{Q''^2}{m^2}\right)^2 \quad . \qquad (7.24)$$

Hence there are two identical contributions to the photon spectrum. We can write (7.18) as

$$f_\gamma(0,k_\perp^2) = \frac{4}{\pi m^2}\int_{-\infty}^{\infty} dQ''_y \int_{-\frac{m^2}{2k_\perp}}^{\infty} dQ''_x\, f_\pi\left(0,p_\perp^2 = Q''^2 + 2Q''_x k_\perp\right.$$

$$\left. \times \left(1 + \frac{Q''^2}{m^2}\right) + k_\perp^2\left(1 + \frac{Q''^2}{m^2}\right)^2\right). \qquad (7.25)$$

For $k_\perp/m \ll 1$, we separate out an integral over the entire Q'' plane

$$f_\gamma(0,k_\perp^2) = \frac{4}{\pi m^2}\int d^2Q''\, f_\pi\left(0,p_\perp^2 = Q''^2 + 2Q''_x k_\perp\left(1 + \frac{Q''^2}{m^2}\right)\right.$$

$$\left. + k_\perp^2\left(1 + \frac{Q''^2}{m^2}\right)^2\right) + E \qquad (7.26)$$

where we anticipate that E will die exponentially in $m/k_\perp$. In particular,

$$\lim_{k_\perp^2 \to 0} f_\gamma(0,k_\perp^2) = \frac{4}{\pi m^2}\int d^2Q''\, f_\pi(0,p_\perp^2 = Q''^2) \; . \qquad (7.27)$$

But from (7.21)

$$\lim_{x \to 0} f_\gamma(x,0) = \frac{2}{\pi m^2}\int d^2Q\, f_\pi(0,p_\perp^2 = Q^2) \; . \qquad (7.28)$$

Thus $f_\gamma(x,k_\perp^2)$ is not continuous at the point $x = 0$, $k_\perp = 0$. To understand how this comes about, examine Eq. (7.15). Contributions to the integral come from small values of $p_\perp^2$. For $Q_y = 0$,

$$p_\perp^2 = \left[Q_x + k_\perp\left(1 + \frac{Q_x^2}{m^2}\right)\right]^2 \qquad (7.29)$$

while the integral in Eq. (7.15) extends to $x_\pi = 1$, or

$$\frac{Q_x^2}{m^2} = \frac{1}{x_\gamma} - 1 \; . \qquad (7.30)$$

The condition $p_\perp^2 = 0$ yields, for $(k_\perp/m) \ll 1$,

$$Q_x \approx k_\perp \quad \text{or} \quad -\frac{m^2}{k_\perp} \; .$$

Thus the small $p_\perp^2$ regions are near $(Q_x = k_\perp,\ Q_y = 0)$ and $(Q_x = -m^2/k_\perp,\ Q_y = 0)$. If $x > (k_\perp/m)^2$, then by (7.30), the second region falls outside the integration domain determined by the kinematical limits. Thus as x decreases to values less than about $(k_\perp/m)^2$, the second region is introduced into the integrations, giving rise to the factor of two between (7.27) and (7.28)

We can reformulate (7.27) in an interesting fashion. To do this we first note that

$$\int_0^\infty dp_\perp^2\, f_{\pi^0}(0,p_\perp^2) = \frac{1}{2}\int_0^\infty dk_\perp^2\, f_\gamma(0,k_\perp^2) \; . \qquad (7.31)$$

This relation can be proved directly from (7.1). It reflects the fact that the central rapidity region for the photons must be twice as heavily populated as the central region for pions.

As a consequence, we have a theorem for the photon spectrum arising from the decays of a scaled π^0 spectrum:

$$\lim_{k_\perp \to 0} f_\gamma(0,k_\perp^2) = \frac{2}{m^2}\int_0^\infty dk_\perp^2 \, f_\gamma(0,k_\perp^2) \quad . \tag{7.32}$$

Equation (7.32) is a striking consequence of scaling in hadronic collisions, relating the photon spectrum in the central region at zero transverse momentum, to the spectrum in the central region integrated over transverse momentum. Since the equation is linear in the photon cross section, it is unaffected by uncertainties in overall normalization.

The integral in Eq. (7.26) can be expanded in powers of $k_\perp/m$:

$$f_\gamma(0,k_\perp^2) = \frac{4}{\pi m^2}\int_0^\infty \frac{dQ^2}{2}\int_0^{2\pi} d\phi \left\{ f_\pi(0,Q^2) + \left[2Q\cos\phi\, k_\perp\left(1+\frac{Q^2}{m^2}\right) + k_\perp^2\left(1+\frac{Q^2}{m^2}\right)^2\right] f_\pi'(0,Q^2) + \frac{1}{2}\left[2Q\cos\phi\, k_\perp\left(1+\frac{Q^2}{m^2}\right)\right]^2 f_\pi''(0,Q^2) + \mathcal{O}(k_\perp^4/m^4)\right\} \tag{7.33}$$

$$= \frac{4}{m^2}\int_0^\infty dQ^2 \left\{ f_\pi(0,Q^2) + k_\perp^2\left(1+\frac{Q^2}{m^2}\right) f_\pi'(0,Q^2) + Q^2 k_\perp^2\left(1+\frac{Q^2}{m^2}\right) f_\pi''(0,Q^2) + \mathcal{O}(k_\perp^4/m^4)\right\} \tag{7.34}$$

where primes denote differentiation with respect to Q^2. Assuming $Q^2 f_\pi(0,Q^2)$ and $Q^2 f_\pi'(0,Q^2)$ vanish for $Q^2 = 0$, we integrate by parts

to get

$$f_\gamma(0,k_\perp^2) = \frac{4}{m^2}\int_0^\infty dQ^2 \, f_\pi(0,Q^2)\left\{ 1 + \frac{k_\perp^2}{m^2}\left[2 + \frac{4Q^2}{m^2}\right] + \mathcal{O}\left(\frac{k_\perp^4}{m^4}\right)\right\}. \tag{7.35}$$

As $k_\perp$ increases, the E term in Eq. (7.26) must be considered as well. From Eq. (7.35), though, we expect a rise in the photon spectrum for transverse momenta increasing from zero to small values. For larger values of $k_\perp$, the E term reduces the value of the right-hand side of (7.26). We expect E to become significant when $(m^2/2k_\perp) \approx \langle p_\perp \rangle$, where $\langle p_\perp \rangle$ is the average transverse pion momentum.

The general principles outlined here are displayed explicitly in the next section.

D. A SIMPLE EXAMPLE

An appreciation for the results of the preceding sections can be gained by considering an especially simple example. Suppose that the scaled π^0 distribution is independent of x and given by

$$f_{\pi^0}(x,p_\perp^2) = e^{-ap_\perp^2} \qquad 0 < |x| < 1 . \tag{7.36}$$

From (7.15) we find

$$f_\gamma(x,k_\perp^2) = \frac{2}{\pi m^2}\int_0^{m^2(\frac{1}{x}-1)} \frac{dQ^2}{2}\int_0^{2\pi} d\theta$$

$$\times \exp\left\{-a\left[Q^2 + 2k_\perp Q\cos\theta\left(1+\frac{Q^2}{m^2}\right) + k_\perp^2\left(1+\frac{Q^2}{m^2}\right)^2\right]\right\} \tag{7.37}$$

$$= \frac{2}{m^2}\int_0^{m^2(\frac{1}{x}-1)} dQ^2 \exp\left\{-a\left[Q^2 + k_\perp^2\left(1+\frac{Q^2}{m^2}\right)^2\right]\right\}$$

$$\times I_0\left(2ak_\perp Q\left[1+\frac{Q^2}{m^2}\right]\right) \tag{7.38}$$

where I_0 is the usual modified Bessel function. Similarly, from (7.18) we find

$$f_\gamma(0,k_\perp^2) = \frac{4}{am^2}\int_0^\infty dz \exp\left(-a\left[\frac{2k_\perp z}{am^2} + p_0(k_\perp)\right]^2\right)e^{-z} I_0(z) . \tag{7.39}$$

We can find the $k_\perp \to 0$ limit of the two expressions. From (7.38),

$$f_\gamma(x,k_\perp^2 = 0) = \frac{2}{am^2}\left\{1 - \exp\left(-am^2\left[\frac{1}{x}-1\right]\right)\right\} , \tag{7.40}$$

while from (7.39)

$$\lim_{k_\perp \to 0} f_\gamma(0,k_\perp^2) = \frac{4}{am^2} . \tag{7.41}$$

This shows explicitly the factor of two associated with interchanging the order of the limits $x \to 0$ and $k_\perp \to 0$, which we proved generally in Eqs. (7.27) and (7.28).

The numerical evaluation of Eq. (7.39) with $am^2 = 0.3$ is shown in Figs. (7.3) and (7.4). In Fig. (7.3) we see that the fall-off in $k_\perp$ is much steeper than that of the generating π^0 spectrum. For $k_\perp/m \gg 1$, (7.39) becomes

$$f_\gamma(0,k_\perp^2 \gg m^2) \approx \frac{e^{-ak_\perp^2} e^{am^2/2}}{ak_\perp^2} . \tag{7.42}$$

In Fig. 7.4, the quadratic rise away from $k_\perp = 0$ is clearly visible in confirmation of Eq. (7.35). Also shown is the $x = 0$ spectrum arising from a π^0 distribution

$$f_{\pi^0}(0,p_\perp^2) = e^{-bp_\perp} \tag{7.43}$$

with the value of b chosen to give the same $\langle p_\perp^2\rangle$ as (7.36) ($b^2m^2 = 1.8$ corresponds to $am^2 = 0.3$).

Figure (7.4) shows that two rather different π^0 spectra can give rise to quite similar photon spectra, provided the $\langle p_\perp^2\rangle$ values are roughly the same. It also shows the turn-over as the E term in Eq. (7.26) becomes significant, around $(m^2/2k_\perp)^2 = \langle p_\perp^2\rangle$. Numerical

calculations reveal that $f_\gamma(0,k_\perp^2)$ is not terribly sensitive to the parameter a in Eq. (7.36), if the results are normalized to the same value at $k_\perp = 0$. For example, with $am^2 = 0.2$ the curve differs from that with $am^2 = 0.3$ by no more than 15% in the range $0 \leq k_\perp/m \leq 1$.

The evaluation of $f_\gamma(x,k_\perp^2)$ [Eq. (7.38)] is shown in Fig. 7.5. For small $k_\perp/m$ and x not too small, Eq. (7.40) is a good representation of the photon spectrum. For very small x, the distribution rises towards the value dictated by Eq. (7.39). The transition takes place in the region $x \approx m^2/k_\perp^2$.

E. STERNHEIMER'S PRESCRIPTION

At any finite energy, Sternheimer's prescription, Eq. (7.12), may be used to derive the π^0 spectrum from a known photon spectrum if $k/m \gg 1$. A scaled form of Sternheimer's prescription is also easily obtained. From Eq. (7.12),

$$2E\frac{d\sigma}{d^3p}(\underset{\sim}{p} = \underset{\sim}{k},s) = -\left\{\frac{\partial}{\partial k}\left[k^2\frac{d\sigma}{d^3k}(\underset{\sim}{k},s)\right]\right\}_{\underset{\sim}{k}=\underset{\sim}{p}_\pi} \tag{7.44}$$

In terms of $k_\perp$ and $k_{||}$ we have

$$2E\frac{d\sigma}{d^3p}(\underset{\sim}{p} = \underset{\sim}{k},s) \simeq -\left(1 + k_{||}\frac{\partial}{\partial k_{||}} + k_\perp\frac{\partial}{\partial k_\perp}\right)\left[k\frac{d\sigma}{d^3k}(k,s)\right] . \tag{7.45}$$

Passing to the scaling limit,

$$2f_{\pi^0}(\underset{\sim}{p} = \underset{\sim}{k},s) = -\left(1 + x\frac{\partial}{\partial x} + k_\perp\frac{\partial}{\partial k_\perp}\right) f_\gamma(x,k_\perp) . \tag{7.46}$$

If $k_\perp = \beta x$ and if

$$F_\gamma(x,\beta) = f_\gamma(x,k_\perp) \tag{7.47}$$

then

$$\frac{\partial}{\partial x}\left[xF_\gamma(x,\beta)\right] = \frac{\partial}{\partial x}\left[xf_\gamma(x,k_\perp = \beta x)\right]$$

$$= \left(1 + x\frac{\partial}{\partial x} + x\beta\frac{\partial}{\partial k_\perp}\right) f_\gamma(x,k_\perp = \beta x) . \tag{7.48}$$

Thus we can write (7.46) as

$$2f_{\pi^0}(x,k_\perp) = -\frac{\partial}{\partial x}\left[xF_\gamma(x,\beta)\right] \quad . \tag{7.49}$$

In effect, k has been replaced by x, and $\tan\theta = k_\perp/k_\parallel$ by $\beta = k_\perp/x$. From (7.46) the $x = 0$ analogue is

$$2f_{\pi^0}(0,k_\perp) = -\frac{\partial}{\partial k_\perp}\left[k_\perp f_\gamma(0,k_\perp)\right] \quad . \tag{7.50}$$

We can test this prescription with the model of the previous section. From (7.42)

$$\frac{\partial}{\partial k}\left[k_\perp f_\gamma(0,k_\perp)\right] \approx -2\, e^{am^2/2}\, e^{-ak_\perp^2} \quad . \tag{7.51}$$

Thus the value of the pion distribution we would infer from Sternheimer's prescription differs from the true expression by a constant. It is easy to see how this has happened. The approximation $p_0 \approx k$ is inadequate since $\exp(-ap_0^2)$ differs by a constant factor from $\exp(-ak^2)$. For less rapidly varying π^0 distributions this problem would not arise.

F. BREMSSTRAHLUNG

While π^0 decays are the primary source of photons in hadronic collisions, in a restricted kinematic region bremsstrahlung is an important source also. The bremsstrahlung arises primarily from the sudden creation of charged particles, i.e., inner bremsstrahlung analogous to radiative beta-decay. The general features of the bremsstrahlung contribution can be anticipated by considering the classical formula for the intensity of inner bremsstrahlung from a particle created suddenly with a velocity $\underset{\sim}{\beta}$:

$$k\frac{dN}{d\Omega dk} = \frac{\alpha}{4\pi^2}\beta^2\frac{\sin^2\theta}{(1-\beta\cos\theta)^2} \tag{7.52}$$

where k is the photon energy and θ is the angle between the photon direction and the direction of $\underset{\sim}{\beta}$. For the Lorentz invariant form we have

$$k\frac{dN}{d^3k} = \frac{\alpha}{4\pi^2k^2}\beta^2\frac{\sin^2\theta}{(1-\beta\cos\theta)^2} \quad . \tag{7.53}$$

Consider the special case of photons emitted at 90 degrees to the beam direction. As the value of s (the center of mass energy square) increases, more and more charged particles are produced in the forward and backward directions. While the bremsstrahlung from these particles peaks also in the forward and backward directions, a contribution at 90 degrees persists. Indeed, it can be seen from (7.53) that, with the assumption of incoherence, each particle gives a contribution to the soft photon spectrum at 90° of $(\alpha/4\pi^2k^2)$. Thus at 90° the bremsstrahlung contribution is

$$\frac{kd\sigma}{\sigma d^3k} \approx \frac{\alpha}{4\pi^2k^2}\langle n_c\rangle \tag{7.54}$$

where $\langle n_c \rangle$ is the mean multiplicity of charged particles. Since $\langle n_c \rangle$ is believed to grow like log s, this contribution, unlike that from π^0 decay does not scale, but increases with increasing s.

We shall now treat the bremsstrahlung in a more complete fashion. Our model will be based on a number of assumptions. Firstly, we shall assume that the photons are emitted incoherently from the charged particles. Secondly, we shall assume that all the created charged particles are pions. Thirdly, we shall neglect bremsstrahlung from the incident particles. Finally, we shall assume that the relevant diagrams are like that in Fig. 7.6. We shall restrict ourselves to low photon momenta and assume that the extrapolation of the hadronic matrix element is negligible. Thus a typical matrix element squared is

$$|M(p_a,p_b,q_1 - k,q_2,\cdots,q_n)|^2 \; e^2 \; \frac{1}{|(q_1 - k)^2 - m^2|^2} \times \sum_i |(2q_i - k)\cdot\epsilon_i|^2 \qquad (7.55)$$

where $M(p_a,p_b,q_1,\cdots,q_n)$ is the matrix element for the nonradiative process. The sum is over the photon polarizations. Because we have assumed incoherent production of the photons, and negligible extrapolation of the matrix element, after summing over exclusive processes, we get a form which factorizes between the hadronic production and the emission of bremsstrahlung:

$$\left[2(2\pi)^3\right]^2 kq_0 \frac{d\sigma}{d^3k d^3q} = 2(2\pi)^3 \, q_0 \frac{d\sigma}{d^3q} \, 4\pi\alpha \, \frac{|\underset{\sim}{q} \times \hat{k}|^2}{(q\cdot k)} \; . \qquad (7.56)$$

Making manifest the correspondence with the classical result, we have

$$kq_0 \frac{d\sigma}{d^3k d^3q} = \frac{\alpha}{4\pi^2 k^2} \beta^2 \frac{\sin^2\theta'}{(1 - \beta\cos\theta')^2} q_0 \frac{d\sigma}{d^3q} \; , \qquad (7.57)$$

where $\beta = |\underset{\sim}{q}|/q_0$ and θ' is the angle between $\hat{q}$ and $\hat{k}$. The bremsstrahlung spectrum them is

$$k \frac{d\sigma}{d^3k} = \frac{\alpha}{4\pi^2 k^2} \int \frac{d^3q}{q_0} \left(q_0 \frac{d\sigma}{d^3q}\right)\left(\frac{q}{q_0}\right)^2 \frac{\sin^2\theta'}{\left(1 - \frac{q}{q_0}\cos\theta'\right)^2} \; . \qquad (7.58)$$

Specializing to the case of photons at 90° to the beam direction, we can re-express the result in terms of angles relative to the beam direction rather than the photon direction. Thus we have

$$\frac{k}{\sigma}\frac{d\sigma}{d^3k} = \frac{\alpha}{4\pi^2 k^2} \int \frac{dq_{\parallel} dq_{\perp}^2}{2q_0} \left(\frac{q_0}{\sigma}\frac{d\sigma}{d^3q}\right) \int_0^{2\pi} d\phi \, \frac{1 - \frac{q_{\perp}^2}{q^2}\cos^2\phi}{\left(\frac{q_0}{q} - \frac{q_{\perp}}{q}\cos\phi\right)^2}$$

Equation (7.59) continued next page

Equation (7.59) continued.

$$\frac{k}{\sigma}\frac{d\sigma}{d^3k} = \frac{\alpha}{4\pi^2k^2}\int \frac{dq_{\parallel}\,\pi dq_{\perp}^2}{q_0}\left(\frac{q_0}{\sigma}\frac{d\sigma}{d^3q}\right)$$

$$\left\{1 + 2\left[\left(1 - \frac{q_{\perp}^2}{q_0^2}\right)^{-3/2}\left(1 - \frac{q_{\perp}^2}{q_0^2} - \frac{m^2}{2q_0^2}\right) - 1\right]\right\} \qquad (7.59)$$

$$= \frac{\alpha}{4\pi^2k^2}\langle n_c\rangle\{1 + R\}\,. \qquad (7.60)$$

As we shall see, R is a small correction. The basic result is simply that at 90 degrees, each charged particle contributes to the bremsstrahlung according to the classical 90° result for relativistic particles:

$$k\frac{dN}{d^3k} = \frac{\alpha}{4\pi^2k^2}\,. \qquad (7.61)$$

We can derive an estimate for R by considering a model in which $(q_0/\sigma)\,(d\sigma/d^3q)$ is a function of $q_{\perp}$ only, except that it vanishes for $|q_{\parallel}| > P$, with $s = 4P^2$. With $(q_0/\sigma)(d\sigma/d^3q) = g(q_{\perp}^2)$, we have

$$R = \frac{2\int dq_{\perp}^2\int_{-P}^{P} dq_{\parallel}\left([q_0^2-q_{\perp}^2]^{-\frac{1}{2}} - q_0^{-1} - \frac{m^2}{2}[q_0^2-q_{\perp}^2]^{-\frac{3}{2}}\right)g(q_{\perp}^2)}{\int dq_{\perp}^2\int_{-P}^{P} dq_{\parallel}\; g(q_{\perp}^2)q_0^{-1}} \qquad (7.62)$$

$$R \simeq \frac{2\int dq_{\perp}^2\, g(q_{\perp}^2)\left(\log\frac{m_{\perp}^2}{m^2} - 1\right)}{\int dq_{\perp}^2\, g(q_{\perp}^2)\left(\log\frac{s}{m^2} - \log\frac{m_{\perp}^2}{m^2}\right)}$$

$$\simeq 2\left(\left\langle\log\frac{m_{\perp}^2}{m^2}\right\rangle - 1\right)\Big/\log(s/m^2) \qquad (7.63)$$

where $m_{\perp}^2 = q_{\perp}^2 + m^2$ and where we have assumed $s \gg m^2$. In addition to the $\log(s/m^2)$ suppression, R is reduced by cancellation between the two terms in the numerator. For example, if $g(q_{\perp}^2) = \exp(-aq_{\perp}^2)$,

$$\left\langle\log\frac{m_{\perp}^2}{m^2}\right\rangle = e^{am^2}E_1(am^2) \qquad (7.64)$$

where E_1 is the usual exponential integral function. For a reasonable value of am^2, say $am^2 = 0.3$, $\left\langle\log\frac{m_{\perp}^2}{m^2}\right\rangle = 1.2$ so that $R \approx 0.4/\log(s/m^2)$.

For photons with fixed center of mass momentum, but not necessarily perpendicular to the beam direction, we have similarly,

$$\frac{k}{\sigma}\frac{d\sigma}{d^3k} = \frac{\alpha}{4\pi^2k_{\perp}^2}\langle n_c\rangle[1 + R'] \qquad (7.65)$$

where R' is given by the previous expression for R except that the argument of the pion inclusive differential cross section is shifted by the amount necessary to bring the photon to a 90° orientation.

CHAPTER EIGHT

COMPARISON OF THEORY AND EXPERIMENT

A. The Nature of Inclusive Data

An extraordinary variety of experimental data on inclusive reactions has appeared in the past two years. Much of the data is from bubble chamber experiments. A smaller fraction is from counter experiments. There are in addition angular data from cosmic ray experiments and from the CERN Intersecting Storage Rings (ISR). Each type of data has certain advantages and disadvantages.

Bubble chamber data have the advantage that they provide results over a continuous kinematic range. They also allow the detection of hyperons and K_0's which are not as amenable to counter experiments. On the other hand, there are severe problems of particle identification for high momentum particles of the same charge. Rejection of events with ambiguities of identification can be a source of bias in the data. Since it is impossible to obtain high statistics in a small kinematic interval, the bubble chamber data is particularly suitable for comparison of integrated spectra, e.g., $d\sigma/dz$ or $d\sigma/dy$.

Counter data basically provide information only on long-lived particles. On the other hand, it is possible to make precise comparisons, say, of particle ratios at fixed values of the kinematic parameters.

Cosmic ray data have had the advantage of providing the highest energy reactions, but their usefulness in this regard may have come to an end with the completion of the ISR. The ISR has provided during the past year the most exciting data on inclusive reactions. Its range of s, from about 400 to 2800 GeV^2, is

invaluable for testing predictions about the approach to (or existence of!) scaling. Of course, the ISR data are limited in accuracy by normalization problems more severe than those of conventional accelerators.

NAL's 200-500 GeV machine should make a substantial contribution to the understanding of inclusive reactions. While not reaching as high a c.m. energy as the ISR, it should provide high quality data in the near asymptotic region, as well as giving data on processes other than proton-proton collisions.

In this chapter we review some of the inclusive data bearing on the assumptions and conclusions of the preceding chapters. This is by no means a comprehensive review of the inclusive data, but it should provide a means of evaluating our present understanding of these processes.

B. Do Inclusive Reactions Scale?

Apparently they do. Figure 8.1 shows data (Allaby, 1971) for $(p:\pi^+|p)$ at $p_{inc} = 14$ and 24 GeV/c at $p_\perp = 0.1$ GeV/c. The data for the two energies are strikingly similar as functions of x. Figure 8.2 and 8.3 show data for $(p:\pi^+|p)$ and $(p:\pi^-|p)$ as a function of the lab rapidity, y, with $p_\perp$ fixed, at incident (or equivalent) momenta from 12 to 1500 GeV/c. (Sens, 1972.) The data show no sign of having a local minimum at $z = 0$, as anticipated by the dual resonance model (see Fig. 6.3, and Brower and Ellis, 1972), or by some multiperipheral models (Pignotti and Ripa, 1971).

None of these data are precise enough to determine whether the cross section is really independent of s. Certainly a behavior like $(\log s)^{-1}$ or $s^{-0.02}$ cannot be excluded. As we emphasized in

Chapter Four, the Mueller picture does not require a pure pole pomeron with intercept one. We might consider four possibilities:

1. The leading singularity does not have vacuum quantum numbers. For example there could be two cuts which coincide, one having $C = +1$ and $G = +1$ and another weaker one with $C = -1$ and $G = +1$.

2. The leading singularity has vacuum quantum numbers, but is not factorizable.

3. The leading singularity has pure vacuum quantum numbers and is a factorizable pole with intercept less than one.

4. The leading singularity has vacuum quantum numbers and is a factorizable pole with intercept one.

Possibility #4 is the simplest and was implicitly assumed in most of Chapter 3 and 5. Possibility #3 is quite similar if we consider everywhere the differential cross section normalized by the total cross section at the appropriate value of s. Possibility #1 is clearly undesirable, but how can it be distinguished from #2?

Consider $(\pi^{\pm}:\pi^{\pm}|p)$, $(\pi^{\pm}:\pi^{\mp}|p)$, $(\pi^{\pm}|\pi^{+}:p)$, and $(\pi^{\pm}|\pi^{-}:p)$. If the leading singularity is purely $C = +1$, then (see footnote 2, Chapter 4)

$$(\pi^{+}:\pi^{-}|p) = (\pi^{-}:\pi^{+}|p) \tag{8.1a}$$

$$(\pi^{+}:\pi^{+}|p) = (\pi^{-}:\pi^{-}|p) \tag{8.1b}$$

$$(\pi^{+}|\pi^{+}:p) = (\pi^{-}|\pi^{+}:p) \tag{8.1c}$$

$$(\pi^{+}|\pi^{-}:p) = (\pi^{-}|\pi^{-}:p) \tag{8.1d}$$

at high s, independent of whether there is factorization. These relations would be a consequence of a Pomeranchuk-type Theorem for

inclusive processes. In Fig. 8.4 these proposed equalities are displayed schematically. Data for six of the eight processes are shown in Fig. 8.5 (Alston-Garnjost, 1972; Alston-Garnjost et al., 1972). The data of Fig. 8.5 are at relatively low energy and a good deal of energy dependence is apparent. The curves have yet to coalesce at $x = 0$. At $x < 0$ $(\pi^{-}|\pi^{-}:p)$ and $(\pi^{+}|\pi^{-}:p)$ are not equal, but lie distinctly below $(\pi^{+}|\pi^{+}:p)$. The overall appearance, nevertheless, is similar to that of Fig. 8.4. Further study of these reactions could demonstrate that the leading singularity has $C = +1$. Later we shall mention a test of isospin nature of the leading singularity.

Evidence on the factorization of the leading singularity is inconclusive at present. In Fig. 8.6 (Chen et al., 1971) we see $(1/\sigma)d\sigma/dp$ for $(p:\pi^{-}|\pi^{+})$, $(p:\pi^{-}|\pi^{-})$, $(p:\pi^{-}|K^{+})$, and $(p:\pi^{-}|p)$ at 7, 24.8, 12.7, and 28.5 GeV/c respectively. If all reactions had reached their limiting values and if the leading singularity were factorizable, the curve would coincide. While this is clearly not realized, the largest discrepancy is between $(p:\pi^{-}|\pi^{-})$ and $(p:\pi^{-}|\pi^{+})$ whose asymptotic equality depends not on factorization, but only on the leading singularity having $C = +1$ as we noted above.

On the basis of the exoticity requirement of Chan et al. (1971), Chen et al. (1971) interpreted the data to indicate the $(p:\pi^{-}|\pi^{+})$ had reached its scaling limit while the other reactions had not. Whether this is true or not, the comparison of $(p:\pi^{-}|\pi^{+})$ with $(p:\pi^{-}|\pi^{-})$ is not a test of factorization, but of the C quantum number of the leading j-plane singularity.

C. Symmetry Relations

Some of the relations derived in Chapter Four have been discussed in connection with the quantum number of the leading trajectory. We continue these considerations turning to the data from the ISR. In the pionization limit, we have the C invariance predictions:

$$(|p|) = (|\bar{p}|) \tag{8.2a}$$

$$(|\pi^+|) = (|\pi^-|) \tag{8.2b}$$

$$(|K^+|) = (|K^-|) \tag{8.2c}$$

and by isosinglet dominance,

$$(|\pi^+|) = (|\pi^0|) = (|\pi^-|) \ . \tag{8.3}$$

In the fragmentation region we have the weaker statement:

$$(p{:}\pi^0) = \tfrac{1}{2}[(p{:}\pi^+) + (p{:}\pi^-)] \ . \tag{8.4}$$

In Fig. 8.7 we show the data of the Saclay-Strasbourg group (Sens, 1972) for $(p|p|p)$ and $(p|\bar{p}|p)$ at 90 degrees to the beam direction and $s = 2800$ GeV^2. The p curve is similar in shape to, but about a factor of two higher than, the $\bar{p}$ curve. If the asymptotic term is given by $P \otimes P$ (a pomeron in both the $a\bar{a}$ and $b\bar{b}$ channels), we have, up to lowest order in nonleading terms

$$(p|p|p) = P \otimes P + 2P \otimes (P' + \rho + \omega + A_2) \tag{8.5a}$$

$$(p|\bar{p}|p) = P \otimes P + 2P \otimes (P' - \rho - \omega + A_2) \tag{8.5b}$$

where we use ρ to indicate the $G = +1$, $C = -1$ contribution, etc. If we accept the two-body Regge lore that $p\bar{p}$ couples weakly to $I = 1$ exchanges we have

$$(p|p|p) \simeq P \otimes P + 2P \otimes (P' + \omega) \tag{8.6a}$$

$$(p|\bar{p}|p) \simeq P \otimes P + 2P \otimes (P' - \omega) \ . \tag{8.6b}$$

The discrepance between $(p|p|p)$ and $(p|\bar{p}|p)$ indicates large P' and ω contributions which tend to cancel for $\bar{p}$ production. In this same framework, we would have for neutron and anti-neutron production

$$(p|n|p) = P \otimes P + 2P \otimes [P' - \rho + \omega - A_2] \tag{8.7a}$$

$$(p|\bar{n}|p) = P \otimes P + 2P \otimes [P' + \rho - \omega - A_2] \ . \tag{8.7b}$$

In the approximation in which we ignore all but $I = 0$ exchanges, we have

$$(p|p|p) \simeq (p|n|p) \tag{8.8a}$$

$$(p|\bar{p}|p) \simeq (p|\bar{n}|p) \ . \tag{8.8b}$$

These relations have not yet been tested.

Data for $(p|\pi^+|p)$ and $(p|\pi^-|p)$ at $x = 0$ are in excellent agreement. In Figs. 8.8 we again show data of the Saclay Strasbourg Group at 90 degrees. A simple exponential in $p_\perp$ gives an excellent fit to the data, while the dual resonance model with $\alpha_V = 0.9$ gives behavior which is too steep. To terms of order $s^{-\frac{1}{4}}$

$$(p|\pi^+|p) = P \otimes P + 2P \otimes (P' + \rho) \tag{8.9a}$$

$$(p|\pi^-|p) = P \otimes P + 2P \otimes (P' - \rho) \ . \tag{8.9b}$$

If the near equality of the data for s from 960 to 2800 GeV^2 indicates an absence of $s^{-\frac{1}{4}}$ terms, then we must have [see Eq. (3.3)]

$$f^{\pi^\pm}_{PP'}(p_\perp) \simeq f^{\pi^+}_{P\rho}(p_\perp) \simeq 0 . \tag{8.10}$$

There is no obvious reason for expecting this. In Fig. 8.9 we show data for the ratio π^+/π^- as a function of x (Albrow et al., 1972). We expect the ratio to approach unity as $x \to 0$. This is consistent within the errors.

While the vanishing of the $s^{-\frac{1}{4}}$ terms for $(p|\pi|p)$ seems surprising, it is consistent with the flatness of the rapidity distributions shown in Fig. 8.2 and 8.3. The absence of the $s^{-\frac{1}{4}}$ behavior implies the absence of the $\cosh(z/2)$ behavior of Eq. (3.64). We postpone analysis of the inferred π^0 distribution to a later section of this chapter.

The SU(3) relations both in the fragmentation and pionization regions have yet to be tested. An extensive experiment at Brookhaven should provide interesting information for the fragmentation of pseudoscalar mesons into pseudoscalar mesons (Beier et al., 1972).

D. Angular Distributions of Charged Particles at ISR

Barbiellini et al. (1972) and Breidenbach et al. (1972) have measured the angular distribution of charged particles at s = 910, 2000, and 2800 GeV^2. Breidenbach et al. have also measured the distribution at s = 450 GeV^2. The data of the two groups are consistent, except perhaps at s = 2000 GeV^2. The data of Breidenbach et al. are displayed in Fig. 8.10. There is no noticeable curvature to the data as a function of $\eta = \ell n(\cot \frac{\theta}{2})$. There is, however, a clear rise in

the cross section with increasing s. As we noted in Chapter Five, for distributions with a flat behavior in η the cross section is expected to be an increasing function of s. At $\eta = 0$, the data can be fitted with

$$\frac{1}{\sigma}\frac{d\sigma}{d\eta} = A' + B' s^{-\frac{1}{4}} \tag{8.11}$$

where plausible fits range from $A' = 2.0$, $B' = -4.0$ to $A' = 2.6$, $B' = -7.0$, with s measured in GeV^2. In Fig. 8.10, we compare the data with a fit assuming the charge particles have a transverse momentum distribution given by

$$f_{PP} \propto e^{-bp_\perp} \tag{8.12a}$$

$$f_{PR} \propto e^{-bp_\perp} . \tag{8.12b}$$

The normalizations are determined by Eq. (8.11). We have taken $b = 6$ GeV^{-1}, approximately the figure obtained by the Saclay Strasbourg group for pions at 90 degrees (Sens, 1972). The curves in Fig. 8.10 were obtained by evaluating Eq. (5.11) numerically. The quality of the fits is quite good.

E. Multiplicity at High Energies

From the angular distribution analysis above we can estimate the asymptotic multiplicity of charged particles. The coefficient of $\log s$ in the mean multiplicity is

$$A_0 = \sum_{c \text{ charged}} \int d^2p_{\perp c} \, \frac{d\sigma}{dz\, d^2p_\perp}(z = 0) \tag{8.13}$$

where A_0 is the variable of Eq. (5.19). We found above that $A_0' \simeq 2.0\text{-}2.6$. Now from (5.21b)

$$A_0 = A_0'/\langle p_\perp/m_\perp \rangle \quad . \tag{8.14}$$

For a pion distribution proportional to $\exp(-bp_\perp)$ with $b = 6\ \text{GeV}^{-1}$, we obtain $\langle p_\perp/m_\perp \rangle = 0.83$ and $A_0 = 2.4\text{-}3.1$. This is a surprisingly large number. Cosmic ray data indicated a value of about 0.7 (L. W. Jones et al., 1970). A naive interpretation of the photon data of Neuhofer et al. (1971, 1972) suggest a value of about 1.5 [see Eq. (8.26)].

We can check the consistency of the angular distributions against the Saclay Strasbourg results (Sens, 1972) for pion production at 90 degrees. Both the positive and negative pions can be fitted, independent of s in the range 900 to 2800 GeV^2, with

$$E\frac{d\sigma}{d^3p} = Ne^{-bp_\perp}$$

with

$$N = 140\ \text{mb/GeV}^2$$

$$b = 6.25\ \text{GeV}^{-1}$$

so that, for either π^+ or π^-,

$$\frac{d\sigma}{dz}(z = 0,\ s = 900\text{-}2800\ \text{GeV}^2) \simeq 22.5\ \text{mb} \quad .$$

We can apply a correction to relate this to the angular distribution, $\frac{d\sigma}{d\eta}$. As we noted above, this correction is about 0.83. Thus we have, with $\sigma_{\text{inel}} = 33$ mb,

$$\frac{1}{\sigma_{\text{inel}}}\frac{d\sigma}{d\eta}(\eta = 0,\ s = 900\text{-}2800\ \text{GeV}^2) \simeq 1.15 \quad .$$

On the other hand, the data of Breidenbach et al. (1972) for charged particles of all kinds increases from about 1.1 to about 1.5 as s increases from 450 to 2800 GeV^2. If these data were taken literally, they would mean that the increasing charged multiplicity was due entirely to nonpion sources.

F. Analysis of the ISR Photon Data

Data are available for photon distributions at $s = 900$, 2000, and 2800 GeV^2, at 10, 16, 24, and 90 degrees. Neuhofer et al. (1971, 1972) provide a parametrization of the data for photon energies between 100 MeV and 5 GeV as

$$\frac{k}{\sigma_{\text{inel}}}\frac{d\sigma}{d^3k} = \frac{A}{k_\perp}\exp\left(-\frac{k_\perp}{k_0} - \frac{x}{x_0}\right) \tag{8.19}$$

with $A = 1.48\ \text{GeV}^{-1}$, $k_0 = 0.162$ GeV, and $x_0 = 0.083$.

The parametrization in Eq. (8.19) clearly does not satisfy the requirements of Eq. (7.32). But it does permit a reasonable evaluation of the right-hand side of the equation. Thus we have the prediction

$$\lim_{k_\perp \to 0} \bar{f}_\gamma(x = 0, k_\perp) \simeq 53\ \text{GeV}^{-2} \quad . \tag{8.20}$$

Verification of this prediction is obscured by the bremsstrahlung. If at $s = 2800$ GeV^2, $\langle n_c \rangle \simeq 10$, then from Eq. (7.32)

$$\left.\frac{k}{\sigma_{\text{inel}}}\frac{d\sigma}{d^3k}\right)_{\text{Brems.}} \simeq 2 \times 10^{-3}\, k_\perp^{-2} \quad . \tag{8.21}$$

Comparing the bremsstrahlung prediction with the parametrization of the data, we see that the bremsstrahlung becomes significant in the region $k_\perp \simeq$ 1-10 MeV. The data cited above have been binned by total photon momentum into bins of 100 MeV. The bremsstrahlung contribution is primarily in the first bin. Formally, the integrated bremsstrahlung contribution diverges: the actual bremsstrahlung contribution to the measured cross section depends critically on the detection efficiency at low photon momenta. In principle, careful measurement of the photon spectrum at low transverse momentum could identify the bremsstrahlung by its characteristic $1/k_\perp^2$ behavior. After subtracting the bremsstrahlung, the remaining cross section should conform to the condition imposed by Eq. (7.32).

Figure 8.11 shows that the data of Neuhofer et al. are consistent with this interpretation. The cross section for the lowest transverse momenta lies above the curves anticipated on the basis of a spectrum like that of Eq. (7.36). Presumably this is a reflection of the bremsstrahlung contribution. The data shown in Fig. 8.12 are not exactly at $x = 0$. At fixed production angle, as $k_\perp$ increases, so does x. Since we expect a fall-off in x (c.f. Fig. 7.5), the data might be expected to be below the anticipated curve for $x = 0$ for larger values of k. Such a trend seems to be present in the 10 degree data. On the other hand, the choice of a hypothetical π^0 spectrum at $x = 0$ is quite arbitrary; different spectra would give somewhat different photon distributions. (See Fig. 7.4.)

Using the Sternheimer prescription and the parametrization of the photon data of Neuhofer et al., we deduce a neutral pion distribution

$$\frac{E}{\sigma_{inel}} \frac{d\sigma}{d^3p}(\underset{\sim}{p} = \underset{\sim}{k}, s) \simeq -\frac{1}{2}\left(1 + k_\perp \frac{\partial}{\partial k_\perp} + x\frac{\partial}{\partial x}\right)\left[\frac{A}{k_\perp} \exp\left(-\frac{k_\perp}{k_0} - \frac{x}{x_0}\right)\right]$$

$$\simeq \frac{1}{2}\left(\frac{x}{x_0} + \frac{k_\perp}{k_0}\right)\frac{A}{k_\perp} \exp\left(-\frac{x}{x_0} - \frac{k_\perp}{k_0}\right). \quad (8.22)$$

In particular, at $x = 0$, we have

$$\frac{E}{\sigma_{inel}} \frac{d\sigma}{d^3p}(x = 0, p_\perp) \simeq \frac{A}{2k_0} e^{-p_\perp/k_0} . \quad (8.23)$$

Using $\sigma_{inel} = 33$ mb, we have for the π^0 cross section

$$\frac{E}{\sigma_{inel}} \frac{d\sigma}{d^3p}(x = 0, p_\perp) \simeq 150\, e^{-6.2p_\perp} \text{ mb/GeV}^2 . \quad (8.24)$$

This distribution is closely similar to the charged pion cross section (8.15 and 8.16) of the Saclay Strasbourg collaboration, in confirmation of the prediction that at $x = 0$ the π^+, π^-, and π^0 distributions must coincide at very high energies.

For $x > 0$, isospin invariance requires for scaled fragmentation of protons [Eq. (4.9d)],

$$(p{:}\pi^0|p) = \frac{1}{2}\left[(p{:}\pi^+|p) + (p{:}\pi^-|p)\right] . \quad (8.25)$$

A comparison is shown in Fig. 8.12. The agreement is less satisfactory for $x > 0$ than for $x = 0$. The data shown are for $(p{:}\pi^-|p)$ and are taken from the Saclay-Strasbourg Collaboration ($x = 0$) (Sens, 1972) and Bertin et al. (1972) ($x > 0$). For $x > 0$, we would expect the π^0 curve to lie above the data, since the π^+ data of Ratner et al. (1971) are slightly higher. While the relation

in Eq. (8.25) does not appear to be satisfied by the data for $x > 0$, we should like to emphasize that this relation is on very good footing. It requires only the dominance of an $I = 0$ amplitude in the $b\bar{b}$ channel: factorization of the pomeron is not required. Thus the good agreement with the data at $x = 0$ is reassuring and we expect to see similar agreement for $x > 0$ as the accuracy of the experiments improves. Since Eq. (8.25) ignores η production, the number of photons observed should exceed the number of charged pions. With very precise measurements, this discrepancy could be used to deduce the magnitude of the η production.

A comparison similar to those made above has been performed by Charlton and Thomas (1972) who found good agreement between the charged and neutral pion data. In their comparison, however, they treated the data of Ratner et al. and Bertin et al. as if it were taken at 90 degrees, and compared it with the inferred spectrum at 90 degrees. Actually, the charged pion data they used were for $x > 0.05$ and should have been compared with the inferred pion spectrum for the same x values. Had this been done, the inferred π^0 spectrum would lie below the charged pion data as in Fig. 8.12. This is a strong reminder that in many instances a value of $x = 0.05$ is not necessarily small!

The parametrization of Neuhofer et al. gives us a means of evaluating the photon multiplicity and implicitly the charged pion multiplicity. From Eq. (8.14) we find

$$\langle n_\gamma \rangle \simeq 2\pi A k_0 \log\left(\frac{x_0^2}{k_0^2} s\right) \tag{8.26}$$

from which Neuhofer et al. deduced a photon multiplicity at $s = 2800$ GeV^2 of 9.4. By our isospin equality, Eq. (8.25), this means that the charged pion multiplicity is also 9.4. The photon data from $s = 900$ to 2800 GeV^2 showed no clear energy dependence while data on the production of charged particles appear to show energy dependence. A good deal of caution is called for under these circumstances. The Saclay-Strasbourg Collaboration found the charged pion production at 90° to be energy independent from $s = 910$ to 2800 GeV^2. This is consistent with the constancy of the photon spectrum, but it would require that the increasing charged particle multiplicity due entirely to nonpion sources.

CONCLUSION

Inclusive reactions are certain to be extensively studied for years to come, partly because of the impossibility of studying high multiplicity events as exclusive processes and partly as a result of the many theoretical problems which are associated with inclusive processes. The correctness of the Mueller picture has not been thoroughly established, but it seems to be in accord with existing data and provides a powerful means of analysis. In this paper we have exploited the Mueller picture to derive tests of its basic hypotheses and to isolate quantities of significant interest, such as symmetry breaking effects and the high-energy behavior of the mean multiplicity.

The use of the fundamental symmetries of the strong interactions provides a means of isolating certain crossed channel j-plane singularities. The energy dependence of these contributions to the inclusive cross section is a decisive test of the Mueller picture, independent of the factorization of the singularities. The failure of these contributions to exhibit behavior like that anticipated from two-body scattering would indicate the presence of important j-plane singularities outside the two-body framework. The experimental data available indicate that the dominant crossed channel singularity has $C = +1$, and probably $I = 0$, but little can be said about lower lying singularities.

The application of SU(3) leads to numerous predictions of equalities of inclusive cross sections. Each prediction offers an opportunity to measure the effects of SU(3) breaking. The potential here is very great in view of the scarcity of testable SU(3) predictions for two-body scattering.

The predictions of the Mueller picture for the behavior of particle distributions in the central rapidity region can be translated into predictions for wide-angle production. The data extant are consistent with these predictions and indicate, with a large uncertainty, an asymptotic multiplicity much greater than previously expected.

Inclusive photon production gives significant information on the inclusive π^0 distribution. This in turn can be used to check isospin relations. At low transverse momentum, the photon spectrum consists of two contributions, one coming from π^0 decays, and the other from bremsstrahlung associated with charged particle production. Both can be related to the magnitude of the charged particle production. The data from the CERN Intersecting Storage Rings are consistent with these predictions. More refined photon measurements at low transverse momentum would furnish valuable information about the charged multiplicity.

FOOTNOTES

Introduction

1. See Cocconi (1958) and references therein for earlier developments of "fireball" theories.

Chapter 3

1. D. Tow, private communication.

Chapter 4

1. This chapter is based on work done in collaboration with Dr. Martin B. Einhorn (Cahn and Einhorn, 1971).
2. We shall use $(a:c|b)$ to represent both the amplitude and the cross section for the process. This is slightly inaccurate since the kinematical factors relating the two may manifest some symmetry breaking in the instance of SU(3) symmetry. Since this is most likely not the entirety of the symmetry breaking, we may just as well ignore the effect since we make little effort to analyze possible symmetry breaking effects.
3. The notation is that of the standard reference (DeSwart, 1963). For a fine review of SU(3), see Carruthers (1966).

Chapter 5

1. This chapter is based on work done in collaboration with Dr. Martin B. Einhorn and Professor J. D. Jackson. This problem has also been treated in part by Lyon, Risk, and Tow (1971).

Chapter 6

1. For a review of the dual resonance model, see Mandelstam (1971).

Chapter 7

1. This chapter has appeared as a part of a report, LBL-943, with the same title.
2. See, for example, J. D. Jackson, Classical Electrodynamics (1962).

REFERENCES

Abarbanel, H. D. I., 1971a, Phys. Rev. D3, 2227.

Abarbanel, H. D. I., 1971b, Phys. Letters 34B, 69.

Abarbanel, H. D. I., G. F. Chew, M. L. Goldberger, and L. M. Saunders, 1971a, Phys. Rev. Letters 26, 937.

Abarbanel, H. D. I., G. F. Chew, M. L. Goldberger, and L. M. Saunders, 1971b, Phys. Rev. D4, 2988.

Albrow, M. G., D. P. Barber, A. Bogaerts, B. Bosnjakovic, J. R. Brooks, A. B. Clegg, F. C. Erne, C. N. P. Gee, A. D. Kanaris, A. Lacourt, D. H. Locke, P. G. Murphy, A. Rudge, J. C. Sens, and F. van der Veen, 1972, Phys. Letters 40B, 136.

Allaby, J. V., A. N. Diddens, R. W. Dobinson, A. Klovning, J. Litt, L. S. Rochester, and K. Schlupmann, 1972, CERN preprint.

Alston-Garnjost, M., 1972, Lawrence Berkeley Laboratory Report, LBL-735.

Alston-Garnjost, M., K. Barnham, M. S. Rabin, A. Barbaro-Galtieri, S. M. Flatte, F. H. Friedman, G. R. Lynch, J. N. MacNaughton, F. T. Solmitz, C. Risk, W. D. Shepard, J. T. Powers, N. N. Biswas, M. M. Cason, V. P. Kenney, and D. W. Thomas, 1972, Lawrence Berkeley Laboratory Report, LBL-733.

Arnold, R. C., 1971, Argonne National Laboratory Report ANL/HEP 7139.

Arnold, R. C., and E. L. Berger, 1971, Argonne National Laboratory Report, ANL/HEP 7131.

Barbiellini, G., M. Bozzo, P. Darriulat, G. Diambrini-Palazzi, G. De Zorzi, M. Holder, A. McFarland, G. Maderni, P. Mery, S. Orito, J. Pilcher, C. Rubbia, G. Sette, A. Staude, P. Strolin, K. Tittel, 1972, Phys. Letters 39B, 294.

Beier, H. Brody, G. Featherston, D. Kreinick, R. Van Berg, R. Warburton, and H. Weisberg, 1972, University of Pennsylvania preprint, UPR-00005E. Paper given at the Davis International Conference on Inclusive Scattering, Davis, Calif., Feb. 4-5, 1972.

Benecke, J., T. T. Chou, C. N. Yang, and E. Yen, 1969, Phys. Rev. 188, 2159.

Berger, E. L., 1971a, Argonne National Laboratory Report ANL/HEP 7148.

Berger, E. L., 1971b, Colloquium on Multiparticle Dynamics, Helsinki, May 25-28, 1971. Byckling et al. ed.

Bertin, A., P. Capiluppi, A. Cristallini, M. D'Agostino-Bruno, R. J. Ellis, G. Giacommelli, C. Maroni, F. Mercatali, A. M. Rossi, and G. Vannini, 1972, Phys. Letters 38B, 260.

Bjorken, J., 1971, Proceedings of the APS Division of Particles and Fields Meeting, Rochester, 30 Aug.-2 Sept. 1971 (American Institute of Physics, New York, 1971), p. 110.

Breidenbach, M., G. Charpak, G. Coignet, D. Drijard, G. Fischer, G. Flugge, Ch. Gottfried, H. Grote, A. Minten, F. Sauli, M. Szeptycka, and E. G. H. Williams, 1972, Phys. Letters 39B, 654.

Brower, R. C. and R. E. Waltz, 1972, CERN-TH-1335.

Brower, R. C. and J. Ellis, 1972, Phys. Rev. D5, 2253.

Brower, R. C. and J. H. Weis, 1972, MIT preprint.

Brown, L. W., 1972, Phys. Rev. D5, 748.

Cahn, R. N. and M. B. Einhorn, 1971, Phys. Rev. D4, 3337.

Cahn, R. N. and J. Koplik, 1972, unpublished.

Cahn, R. N., 1972, Lawrence Berkeley Laboratory Report LBL-943.

Caneschi, L., 1971, Phys. Letters 37B, 288.

Carruthers, P., 1966, Introduction to Unitary Symmetry (Interscience, New York, 1966).

Chan, H. M. and P. Hoyer, 1971, Phys. Letters 36B, 79.

Chan, H. M., C. S. Hsue, C. Quigg, and J-M. Wang, 1971, Phys. Rev. Letters 26, 672.

Charlton, G. R. and G. H. Thomas, Argonne National Laboratory Report, ANL/HEP 7217.

Chen, M. S., R. R. Kinsey, T. W. Morris, R. S. Panvini, L. L. Wang, T. F. Wong, S. L. Stone, T. Ferbel, P. Slattery, G. Werner, J. W. Elbert, and A. R. Erwin, 1971, Phys. Rev. Letters 26, 1585.

Chou, T. T. and C. N. Yang, 1970, Phys. Rev. Letters 25, 1072.

Cocconi, G., 1958, Phys. Rev. 111, 1699.

DeSwart, J. J., 1963, Rev. Mod. Phys. 35, 916.

DeTar, C. E., 1971, Phys. Rev. D3, 128.

DeTar, C. E. and J. H. Weis, 1971, Phys. Rev. D4, 3141.

DeTar, C. E., D. Z. Freedman, and G. Veneziano, 1971, Phys. Rev. D4, 906.

DeTar, C. E., C. E. Jones, F. E. Low, J. Weis, J. E. Young, and C-I Tan, 1971a, Phys. Rev. Letters 26, 675.

DeTar, C. E., K. Kang, C-I Tan, and J. H. Weis, 1971b, Phys. Rev. D4, 425.

Dias De Deus, J., and W. S. Lam, 1972, Phys. Letters 38B, 317.

Einhorn, M. B., M. B. Green, and M. A. Virasoro, 1971, Phys. Letters 37B, 292.

Einhorn, M. B., J. Ellis, and J. Finkelstein, 1972, Phys. Rev. D5, 2063.

Einhorn, M. B., M. B. Green, and M. A. Virasoro, 1972, Institute for Advanced Study Preprint.

Ellis, J., J. Finkelstein, P. H. Frampton, and M. Jacob, 1971, Phys. Letters 35B, 227.

Ellis, J., J. Finkelstein, and R. D. Peccei, 1972, Stanford Linear Accelerator Center report, SLAC-PUB-1020.

Erdelyi, A., W. Magnus, F. Oberhettinger, and F. G. Tricomi, 1953, Higher Transcendental Functions (McGraw Hill Book Co. Inc.) Vol. 1.

Feynman, R. P., 1969, High Energy Collisions (Gordon and Breach, New York, 1969), p. 237.

Frazer, W. R., L. Ingber, C. H. Mehta, C. H. Poon, D. Silverman, K. Stowe, P. D. Ting, and H. J. Yesian, 1972, Rev. Mod. Phys. 44, 284.

Gasiorowicz, S., 1971, University of Minnesota report COO-1764-119.

Goddard, P. and A. R. White, 1970, Nucl. Phys. B17, 45, and ibid 88.

Goddard, P. and A. R. White, 1971a, Nuovo Cimento 1A, 645.

Goddard, P. and A. R. White, 1971b, Nuovo Cimento 3A, 25.

Goddard, P. and A. R. White, 1972, Phys. Letters 38B, 93.

Gordon, D. and G. Veneziano, 1971, Phys. Rev. D3, 2116.

Grote, H., R. Hagedorn, and J. Ranft, 1971, Atlas of Particle Production Spectra, European Organization for Nuclear Research, Geneva.

Horn, D., 1971, Proceedings of the International Conference on Duality and Symmetry in Hadron Physics, E. Gotsman, ed. (The Weizmann Science Press of Israel, Jerusalem, 1971).

Hwa, R. S. and C. S. Lam, 1971, Phys. Rev. Letters 27, 1098.

Hwa, R. S. and C. S. Lam, 1972, Phys. Rev. D5, 766.

Jackson, J. D., 1962, Classical Electrodynamics (John Wiley and Sons, Inc., New York, 1962), p. 526.

Jacob, M. and R. Slansky, 1971, Phys. Letters 34B, 408.

Jacob, M. and R. Slansky, 1972, Phys. Rev. D5, 1847.

Jacob, M., R. Slansky and C. C. Wu, 1972, Phys. Letters 38B, 85.

Jones, C. E., F. E. Low, and J. E. Young, 1971, Phys. Rev. D4, 2358.

Jones, L. W., A. E. Bussian, G. D. DeMeester, B. W. Loo, D. E. Lyon, Jr., P. V. Ramana Murthy, R. F. Roth, F. E. Mills, J. G. Learned, D. D. Reeder, K. N. Erickson, and B. Cork, 1970, Phys. Rev. Letters 25, 1679.

Kwiecinski, J., 1972, Nuovo Cimento Letters 3, 619.

Lipkin, H. J. and M. Peshkin, 1972, Phys. Rev. Letters 28, 862.

Lyon, D. E., C. Risk, and D. Tow, 1971, Phys. Rev. D3, 104.

Mandelstam, S., 1970, Brandeis Lectures on Elementary Particles and Quantum Field Theory (The MIT Press, Cambridge, Mass., 1970), Vol. 1, p. 165.

Mueller, A. H., 1970, Phys. Rev. D2, 2963.

Mueller, A. H., 1971, Phys. Rev. D4, 150.

Neuhofer, G., F. Niebergall, J. Penzias, M. Regler, K. R. Schubert, P. E. Schumacher, W. Schmidt-Parzefall, and K. Winter, 1971, Phys. Letters 37B, 438.

Neuhofer, G., F. Niebergall, J. Penzias, M. Regler, W. Schmidt-Parzefall, K. R. Schubert, P. E. Schumacher, M. Steuer, and K. Winter, 1972, Phys. Letters 38B, 51.

Pignotti, A. and P. Ripa, 1971, Phys. Rev. Letters 27, 1538.

Polkinghorne, J. C., 1972, Nuovo Cimento 7A, 555.

Predazzi, E. and G. Veneziano, 1971, Nuovo Cimento Letters 2, 749.

Quigg, C., 1971a, Pasadena Meeting on Hadron Physics at Intermediate Energies, March 25, 1971, R. D. Field, Jr. ed., p. 277.

Quigg, C., 1971b, Proceedings of the APS Division of Particles and Fields Meeting, Rochester, 30 Aug. - 2 Sept., 1971 (American Institute of Physics, New York, 1971), p. 40

Ranft, G., 1971, Fortsch. d. Phys. 19, 393.

Ranft, J., 1971, Phys. Letters 36B, 225.

Ratner, L., R. Ellis, G. Vannini, B. Babcock, A. Krish, and J. Roberts, 1971, Phys. Rev. Letters 27, 68.

Sanda, A., 1972, National Accelerator Laboratory preprint.

Sanda, A. and S. D. Ellis, National Accelerator Laboratory preprint.

Sens, J. C., 1972, Proceedings of the Fourth International Conference on High Energy Collisions, Oxford, U.K., April 5-7, 1972.

Stapp, H. P., 1971, Phys. Rev. D3, 3177.

Sternheimer, R. M., 1955, Phys. Rev. 99, 277.

Tan, C-I, 1971, Phys. Rev. D4, 2412.

Thomas, G. H., 1972, Phys. Rev. D5, 2212.

Virasoro, M. A., 1971, Phys. Rev. D3, 2834.

Weis, J. H., 1971, Phys. Rev. D4, 1777.

Weis, J. H., 1972, Phys. Rev. D5, 1043.

White, A. R., 1972a, Nucl. Phys. 39, 432.

White, A. R., 1972b, Nucl. Phys. 39, 461.

Young, J. E., 1971, MIT preprint MIT-CTP-227.

FIGURE CAPTIONS

Fig. 3.1. A Mueller diagram representing the process $(b:c|a)$ and factors entering into the evaluation of the diagram.

Fig. 3.2. A Mueller diagram representing the process $(b|c|a)$ and factors entering into the evaluation of the diagram.

Fig. 3.3a. A diagram representing $a + b \to c +$ missing mass in a domain in which Regge exchange dominates in the $b\bar{c}$ channel.

Fig. 3.3b. A triple-Regge Mueller diagram and associated couplings.

Fig. 3.4. Schematic representation of $x\, d\sigma/dx$ for a triple-Regge dominated cross section. Curve (a) triple-pomeron with pomeron intercept $= 1$ and a linear zero in the triple-pomeron vertex, $g_{PPP}(t)$, at $t = 0$. Curve (b) reggeon-reggeon-pomeron with reggeon intecept $=1/2$. The actual curves plotted are $y = \left((1 - x)\log((1 - x)^{-1})\right)^{-1}$ and (b) $y = 5\left(\log((1 - x)^{-1})\right)$.

Fig. 4.1. A Mueller diagram in which there is double Regge exchange in the $b\bar{b}$ channel. The J-plane singularity thus generated does not factorize, but has a charge conjugation quantum number of C_iC_j where C_i and C_j are the C values for reggeons i and j, similarly for G, etc.

Fig. 5.1. The ratio $A_\perp'/A_0'$ vs. am^2 for a transverse momentum distribution proportional to $\exp(-ap_\perp^2)$. See Eqs. (5.20), (5.24), and (5.32).

Fig. 5.2. The ratio $B_\perp'/B_0'$ vs. am^2 for a transverse momentum distribution proportional to $\exp(-ap_\perp^2)$. See Eqs.(5.20), (5.25), and (5.33).

Fig. 5.3. The angular distribution $\frac{d\sigma}{d\eta}$ resulting from the asymptotic, PP term in Eq. (5.5), with a transverse momentum dependence proportional to $\exp(-ap_\perp^2)$ for various values of am^2. The normalization is such that the rapidity distribution, $d\sigma/dz$ is unity for all z.

Fig. 5.4. The angular distributions $\frac{d\sigma}{d\eta}$ resulting from the asymptotic, PP, term in Eq. (5.5) with a transverse momentum dependence proportional to $\exp(-bp_\perp)$ for various values of $(bm)^2$. The normalization is such that the rapidity distribution, $d\sigma/dz$ is unity for all z.

Fig. 5.5. The angular distributions $\frac{d\sigma}{d\eta}$ resulting from the non-asymptotic, P-R, term in Eq. (5.5), with a transverse momentum dependence proportional to $\exp(-ap_\perp^2)$ for various values of am^2. The normalization is such that the rapidity distribution, $d\sigma/dz(P - R)$ is $\cosh(z/2)$.

Fig. 5.6. The angular distributions $\frac{d\sigma}{d\eta}$ resulting from the non-asymptotic, P - R, term in Eq. (5.5), with a transverse momentum dependence proportional to $\exp(-bp_\perp)$ for various values of $(bm)^2$. The normalization is such that the rapidity distribution, $d\sigma/dz(P - R)$ is $\cosh(z/2)$.

Fig. 6.1a. The two-body optical theorem for $a + b \to$ anything.

Fig. 6.1b. The inclusive cross section for $a + b \to c +$ anything as sum of squares of amplitudes.

Fig. 6.1c. A discontinuity equation for the six-point function. The summations indicate permutations of initial or final particles. The equation holds for nonforward amplitudes so the momenta of the primed particles need not be the same as those of the unprimed particles. (Tan, 1971.)

Fig. 6.1d. The discontinuity equation in Fig. 6.1c below threshold for all but the $ab\bar{c}$ channel. (Tan, 1971.)

Fig. 6.1e. The inclusive cross section as a discontinuity of the six-point amplitude.

Fig. 6.2. Four tree diagrams in the dual resonance model contributing to $(a{:}x|b)$. The diagrams are distinct because the ordering determines which channels have resonances and Regge behavior.

Fig. 6.3. The inclusive distribution, $\bar{f}(y,p_\perp)$, of the dual resonance model using only the diagram of Fig. 6.2a. The curves are for fixed $p_\perp$ as a function of the lab rapidity, y. The vacuum intercept is taken to be one-half.

Fig. 6.4. The pionization function, $\bar{f}(x = 0,p_\perp)$, of the dual resonance model vs. $p_\perp$, with the vacuum intercept taken to be 0.5 and 0.9.

Fig. 7.1. Cross sections of the paraboloids in momentum space on which π^0's must lie to contribute at given values of photon momentum.

Fig. 7.2. The geometry for determining the photon spectrum from a given pion spectrum.

Fig. 7.3. The photon spectrum as a function of $(k_\perp/m)$ at $x = 0$ resulting from a pion spectrum given by $\exp(-ap_\perp^2)$ with $am = 0.3$. The behavior at extremeley small values of $k_\perp$ is shown in more detail in Fig. 7.4.

Fig. 7.4. Photon spectra as functions of $k_\perp/m$ at $x = 0$ resulting from two pion spectra having the same $\langle p_\perp^2\rangle$: solid line, $\exp(-ap_\perp)$ with $am^2 = 0.3$; dashed line, $\exp(-bp_\perp)$ with $(bm)^2 = 1.8$. Both spectra are normalized to unity at $k_\perp = 0$.

Fig. 7.5. The photon spectrum $f_\gamma(x,k_\perp^2)$ as a function of x for various fixed values of $k_\perp$ in GeV/c. The original pion spectrum is $\exp(-ap_\perp^2)$ with $am^2 = 0.3$.

Fig. 7.6. A typical bremsstrahlung diagram in charged particle production.

Fig. 8.1. Data for $(p{:}\pi^+|p)$ at $p_{inc} = 14.25$ and 24.04 GeV/c: $\frac{2E}{\sigma_{tot}}\frac{d\sigma}{d^3p}$ as a function of x at fixed $p_\perp = 0.1$ GeV/c. (Allaby, 1971).

Fig. 8.2. Invariant cross section for $(p{:}\pi^+|p)$ at various fixed values of $p_\perp$ as a function of lab rapidity, y. From the compilation of Sens (1972).

Fig. 8.3. Invariant cross section for $(p{:}\pi^-|p)$ at various fixed values of $p_\perp$ as a function of lab rapidity, y. From the compilation of Sens (1972).

Fig. 8.4. A schematic representation of scaled distributions, $x\,d\sigma/dx$, for $(\pi^\pm|\pi^+{:}p)$, $(\pi^\pm|\pi^-{:}p)$, $(\pi^\pm{:}\pi^\pm|p)$, and $(\pi^\pm{:}\pi^\mp|p)$ as functions of x.

Fig. 8.5. Low-energy data for $(\pi^+{:}\pi^\pm|p)$, $(\pi^+|\pi^\pm{:}p)$, $(\pi^-{:}\pi^-|p)$, and $(\pi^-|\pi^-{:}p)$. The quantity plotted is $F(x) = \frac{x}{\pi\sigma}\frac{d\sigma}{dx}$ as a function of x.

Fig. 8.6. A test of factorization and scaling: $\frac{1}{\sigma_{tot}}\frac{d\sigma}{dp_{||}}$ vs $p_{||}$ for $(a|\pi^-{:}p)$ with $a = \pi^-(A)$, $p(B)$, $K^+(C)$ and $\pi^+(D)$, in the proton rest frame. The incident momenta are 24.8, 28.5, 12.7, and 7 GeV/c respectively. If the distributions had scaled and if the leading singularity factorized, the curves would coincide. Chen et al. (1971).

Fig. 8.7. Data of the Saclay-Strasbourg Group as presented by Sens (1972) on the invariant cross section for $(p|p|p)$ (circles) and $(p|\bar{p}|p)$ (triangles) as a function of $p_\perp$ at p_{inc} = 1500 GeV/c-equivalent. Charge conjugation invariance requires the distributions to coincide asymptotically.

Fig. 8.8a. Data on the invariant cross section as a function of p for $(p|\pi^-|p)$, x = 0, from the Saclay-Strasbourg Group as presented by Sens (1972). Also shown is the data of Bertin et al. (1972) for $(p:\pi^-|p)$ at x = 0.076. The solid curve is a fit (Sens, 1972) given by $140\exp(-6.25p_\perp)$. The dashed curve is a dual resonance pionization function with $\alpha_V = 0.9$. The normalization was determined by fitting to the data at $p_\perp^2 = 0.3$ GeV^2. See Fig. 6.4.

Fig. 8.8b. Data on the invariant cross section as a function of $p_\perp$ for $(p|\pi^+|p)$, x = 0, from the Saclay-Strasbourg Group as presented by Sens (1972). Also shown is the data of Ratner et al. (1971) for $(p:\pi^+|p)$ at x = 0.07.

Fig. 8.9. Particle ratios π^+/π^- and $\bar{p}/\pi^-$ from p-p collisions at ISR energies as a function of x. From the data and compilation of Albrow et al. (1972).

Fig. 8.10. Data for the angular distribution $\frac{1}{\sigma_{inel}}\frac{d\sigma}{d\eta}$ vs. η of charged particles (Breidenbach et al., 1972). The center-of-mass energy squared is (a) 450 GeV^2, (b) 910 GeV^2, (c) 2000 GeV^2, and (d) 2820 GeV^2. The curves were obtained by assuming a transverse momentum dependence in the PP and PR terms [Eq. (5.5)] of $\exp(-bp_\perp)$ with $b = 6(\text{GeV/c})^{-1}$, and using Eqs. (5.11c) and (5.11d).

Fig. 8.11. Some of the data of Neuhofer et al. (1972) for $\frac{k}{\sigma_{inel}}\frac{d\sigma}{d^3k}$ at low transverse photon momentum and fixed angles of 10 and 24 degrees away from the beam direction. The curves are predictions for x = 0 photons based on an assumed pion spectrum proportional to $\exp(-ap_\perp^2)$ with $am^2 = 0.3$. The normalization for the curve is determined by Eq. (7.32). See Eq. (8.20). The data pions have values of x between zero and 0.05.

Fig. 8.12. The data of Bertin et al. (1972) and the Saclay-Strasbourg Group as reported by Sens (1972) for $(p:\pi^-|p)$. The solid curves are fits to lower energy data for $(p:\pi^-|p)$. The dashed curve is the value of the invariant cross section for $(p:\pi^0|p)$ at $p_\perp = 0.4$ GeV/c derived with the Sternheimer approximation, Eq. (8.22). The data of Ratner et al. (1971) for $(p:\pi^+|p)$ are slightly higher than those shown for $(p:\pi^-|p)$. Isospin invariance, together with the assumption that the leading J-plane singularity has I = 0, requires that asymptotically, $(p:\pi^0|p) = [(p:\pi^+|p) + (p:\pi^-|p)]/2$. Cahn (1972).

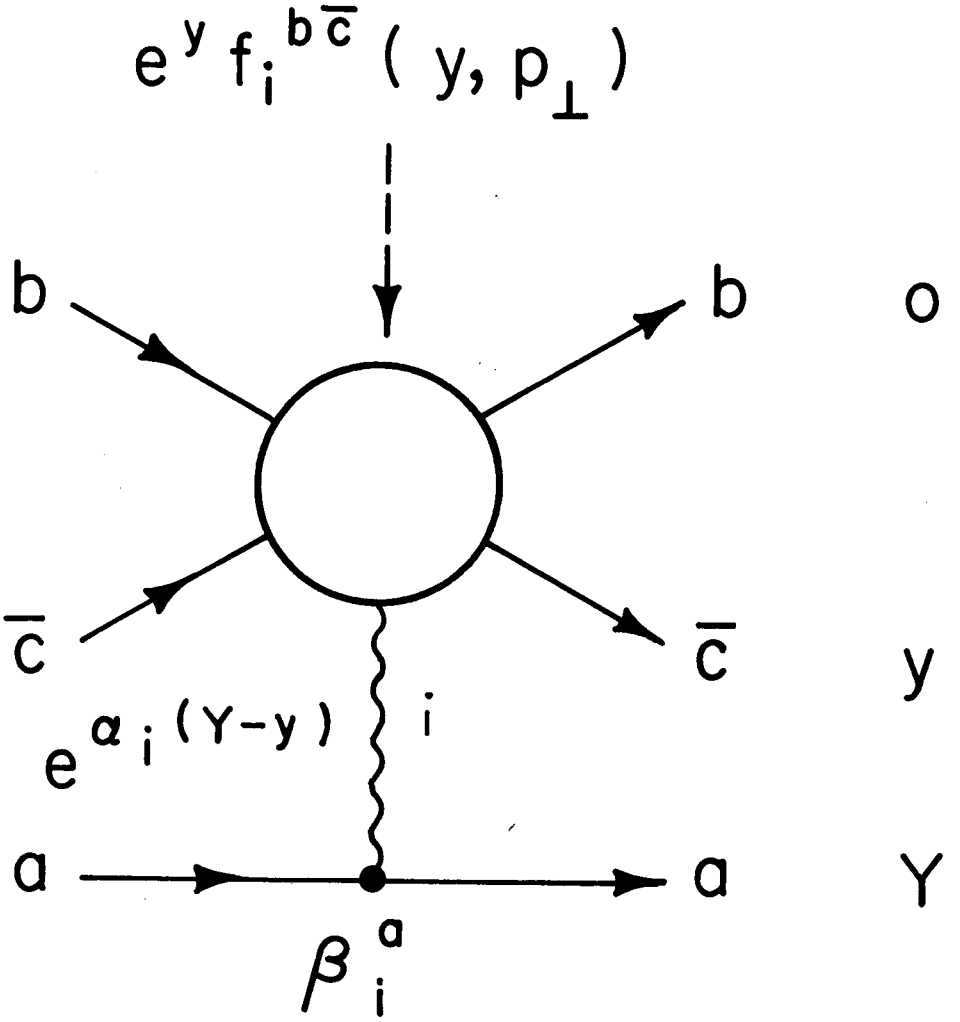

XBL 726 - 3351

Fig. 3.1.

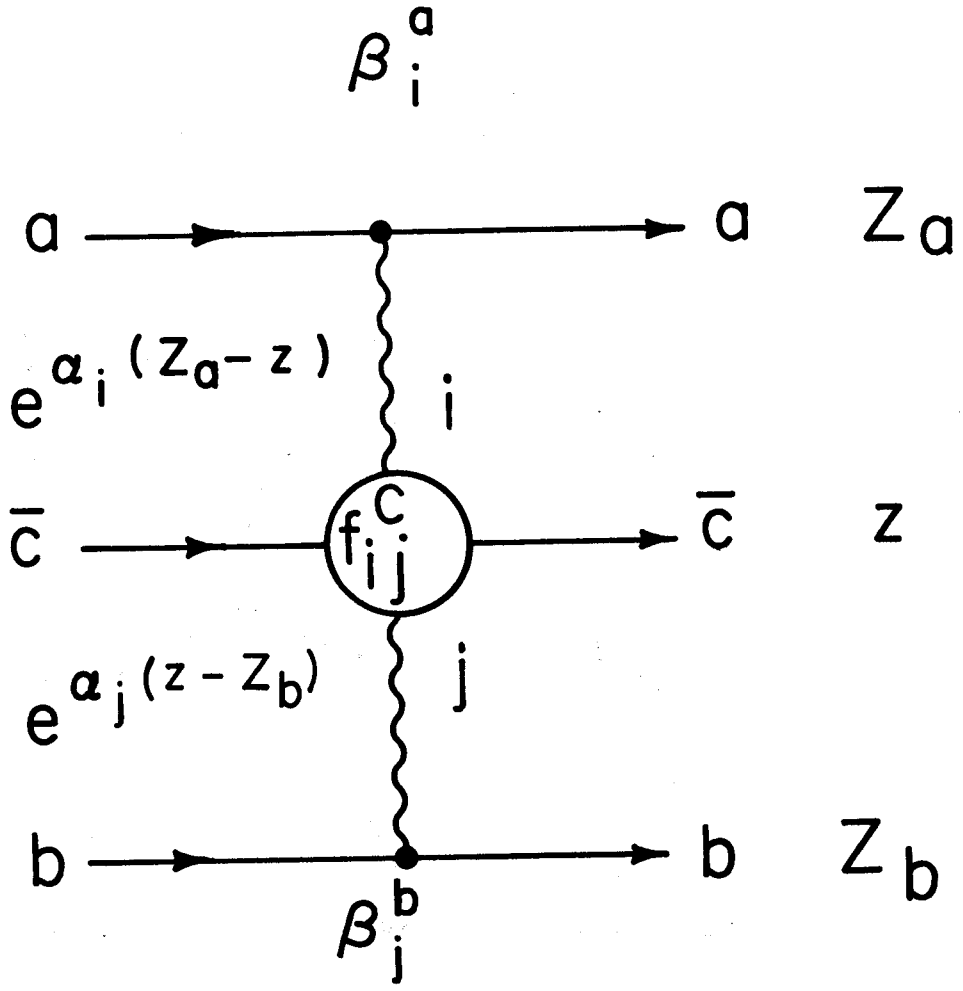

XBL726-3352

Fig. 3.2.

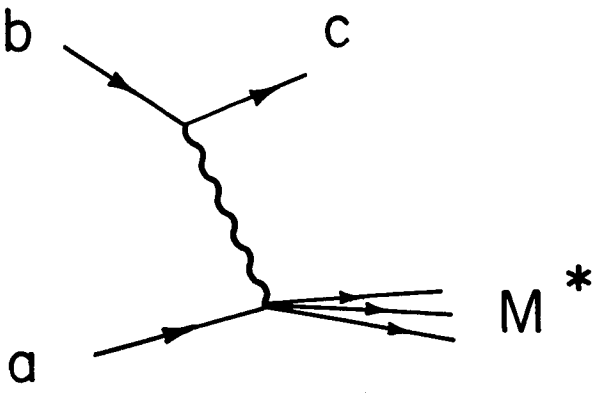

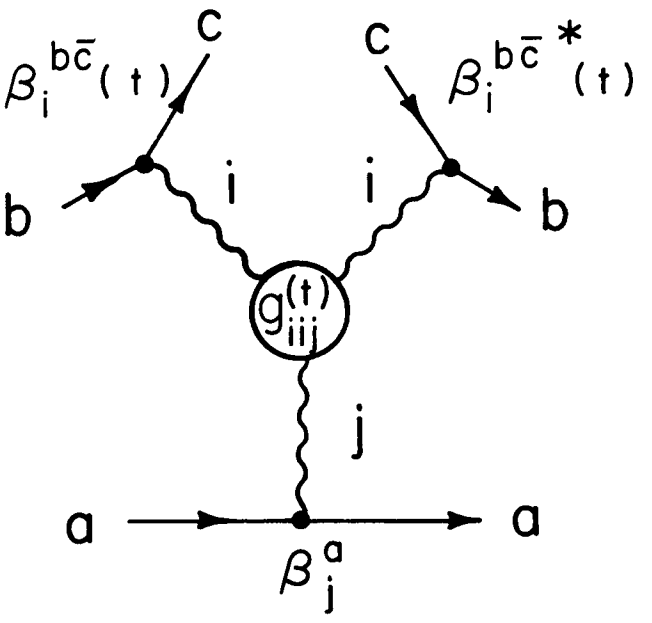

XBL726-3350

Fig. 3.3.

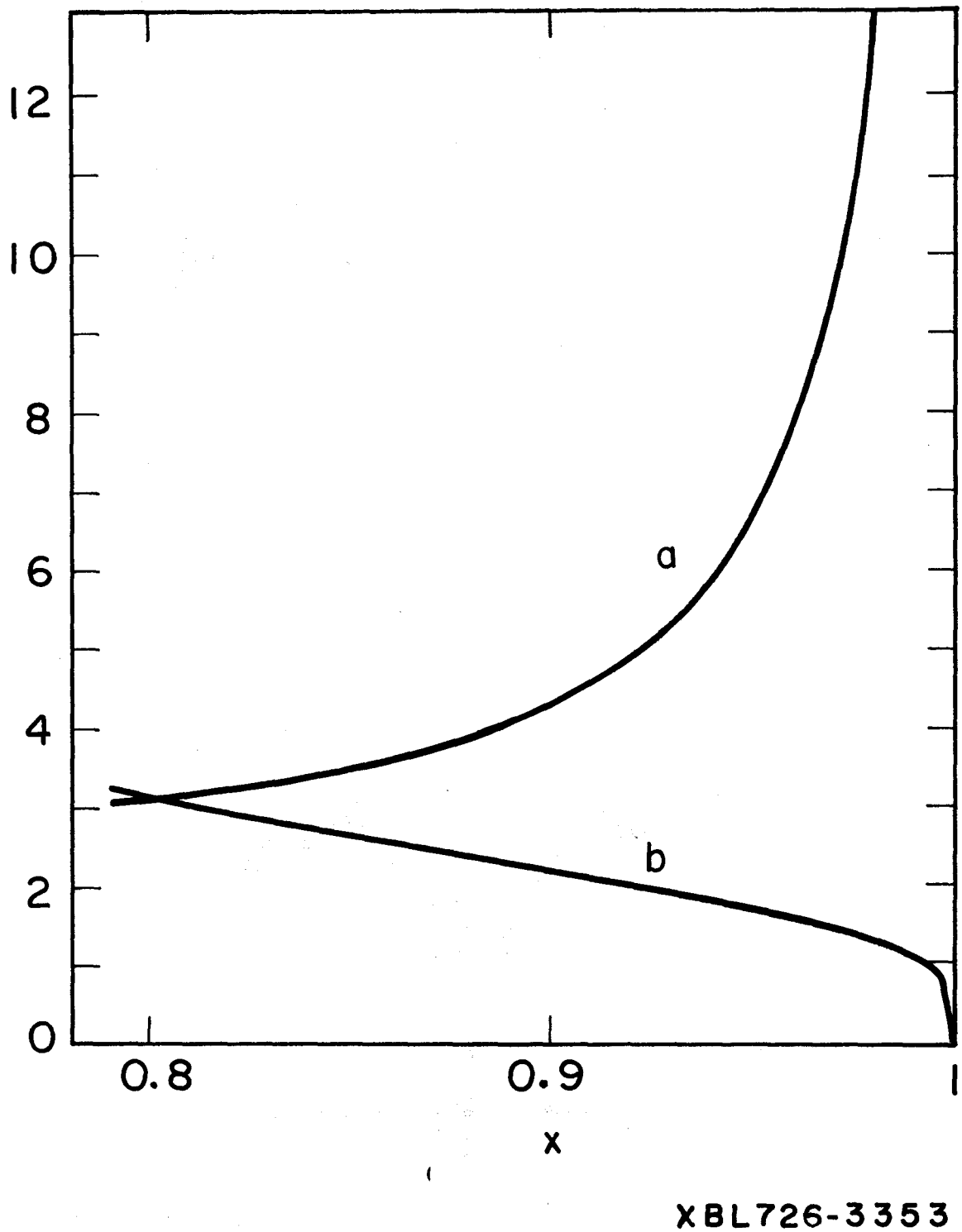

Fig. 3.4.

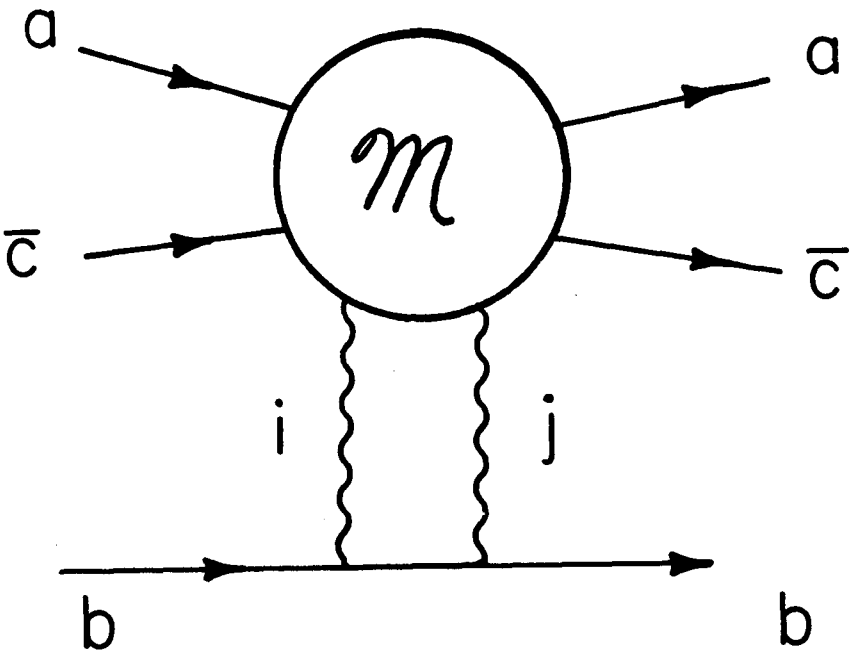

XBL726-3354

Fig. 4.1.

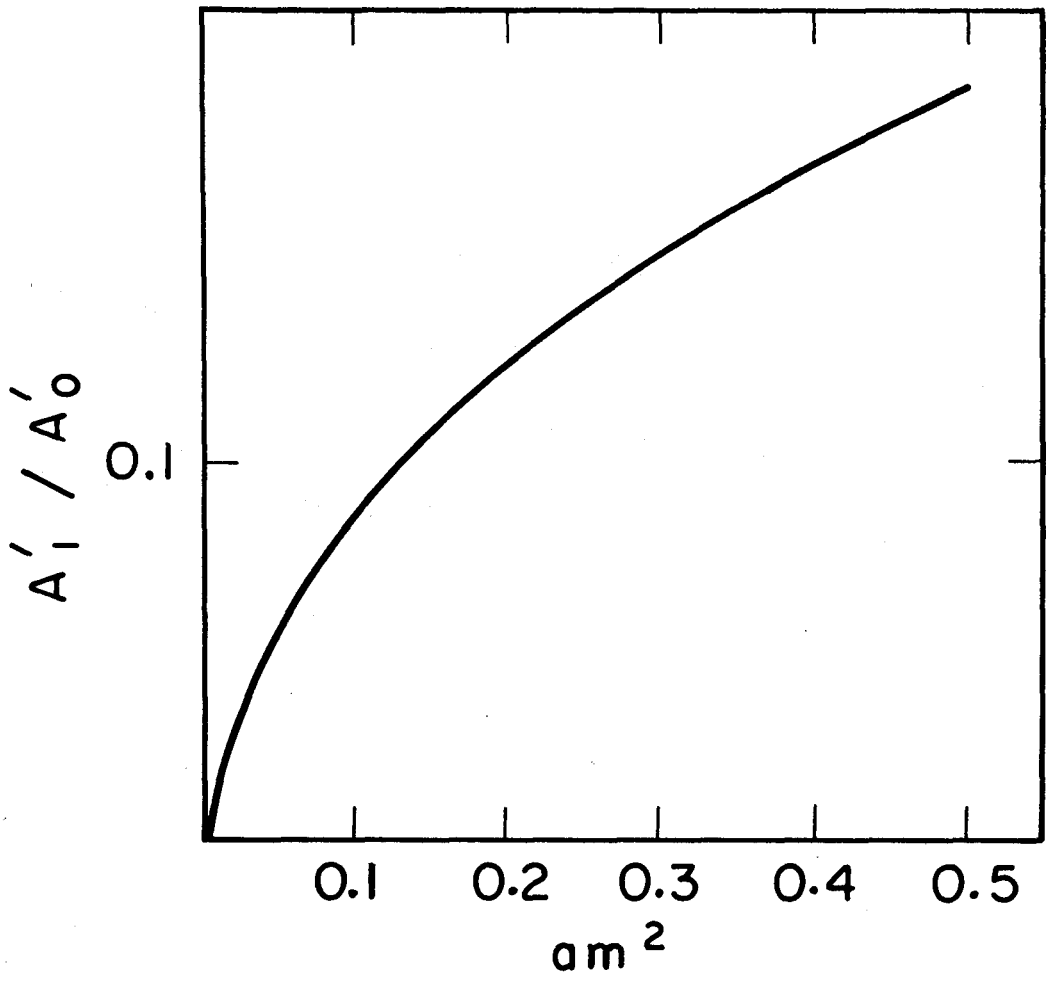

Fig. 5.1.

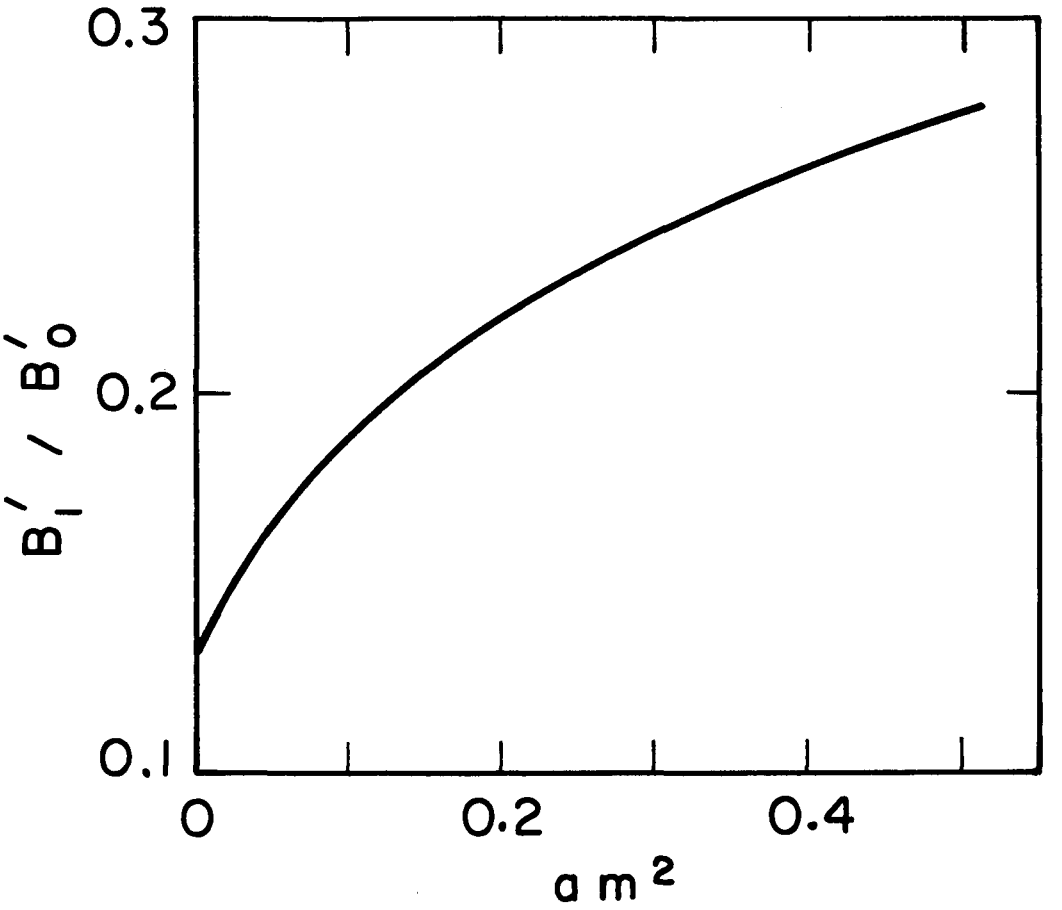

XBL726-3356

Fig. 5.2.

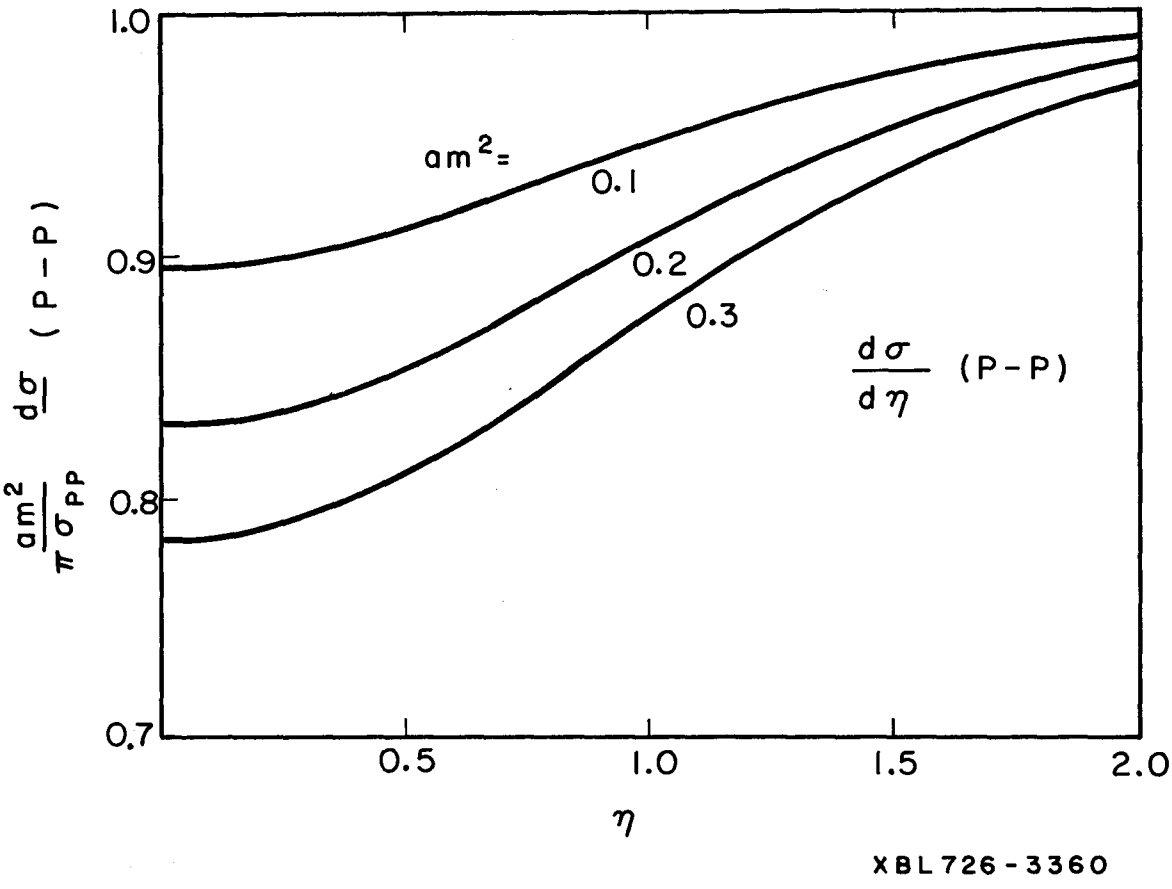
1.0
0.9
0.8
0.7
0.5
1.0
1.5
2.0
η
am² =
0.1
0.2
0.3
dσ/dη (P-P)
am²/π σ_PP dσ/dη (P-P)
XBL726-3360

Fig. 5.3.

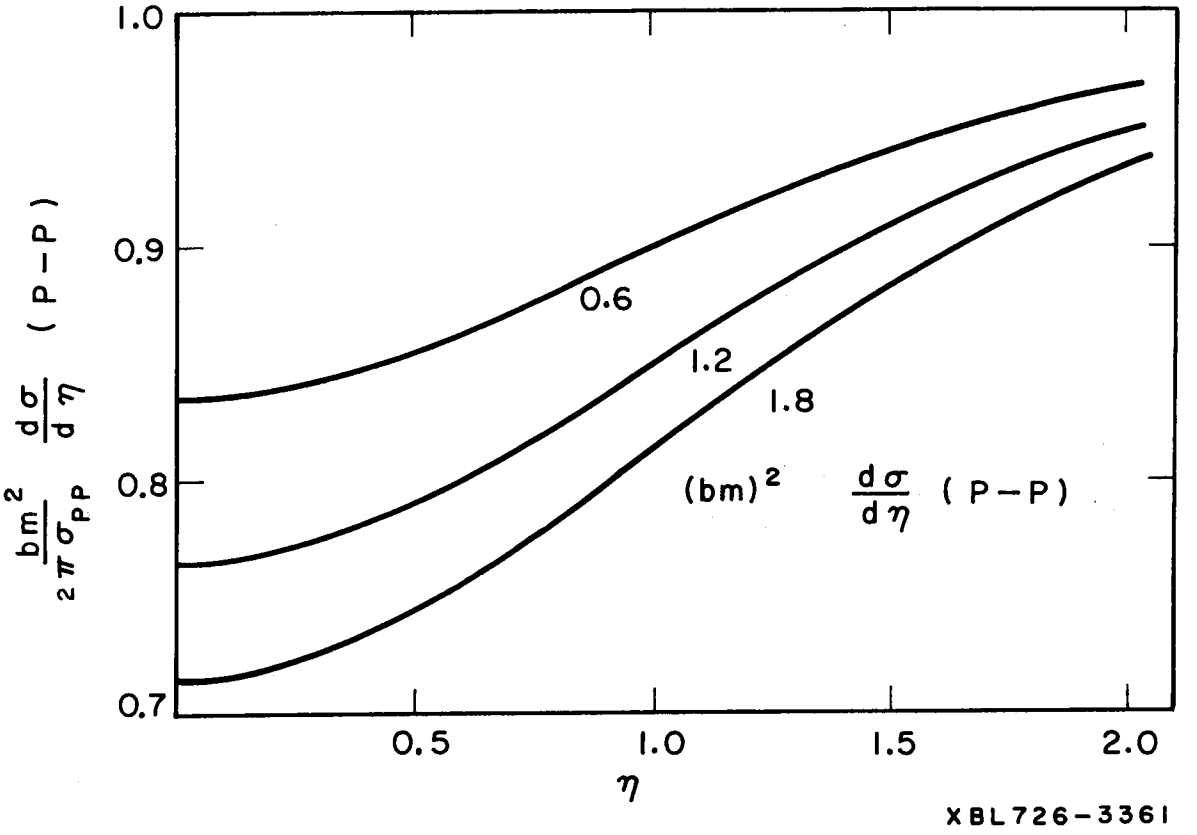
1.0
0.9
0.8
0.7
0.5
1.0
1.5
2.0
η
0.6
1.2
1.8
(bm)² dσ/dη (P−P)
bm²/2πσPP dσ/dη (P−P)
XBL726-3361

Fig. 5.4.

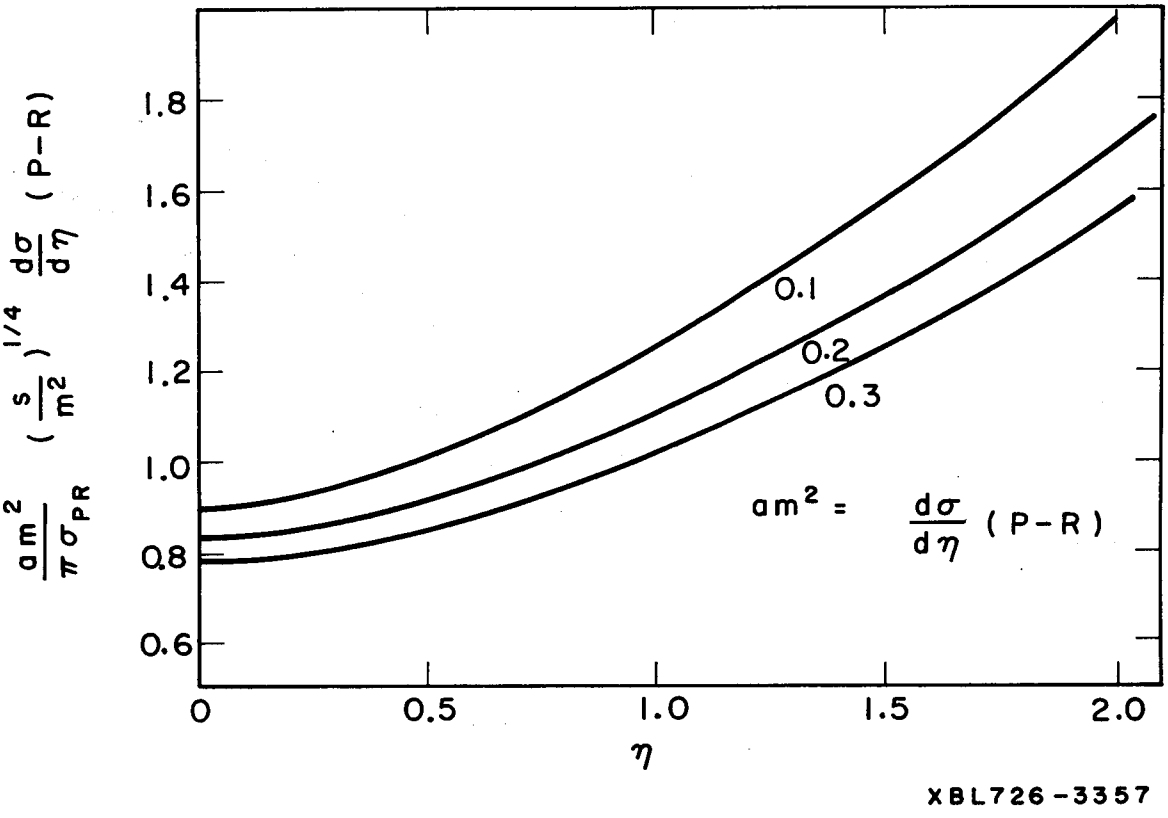
$\frac{am^2}{\pi\sigma_{PR}}\left(\frac{s}{m^2}\right)^{1/4}\frac{d\sigma}{d\eta}\,(P-R)$
1.8
1.6
1.4
1.2
1.0
0.8
0.6
0
0.5
1.0
1.5
2.0
η
0.1
0.2
0.3
$am^2 = \frac{d\sigma}{d\eta}\,(P-R)$
XBL726-3357

Fig. 5.5.

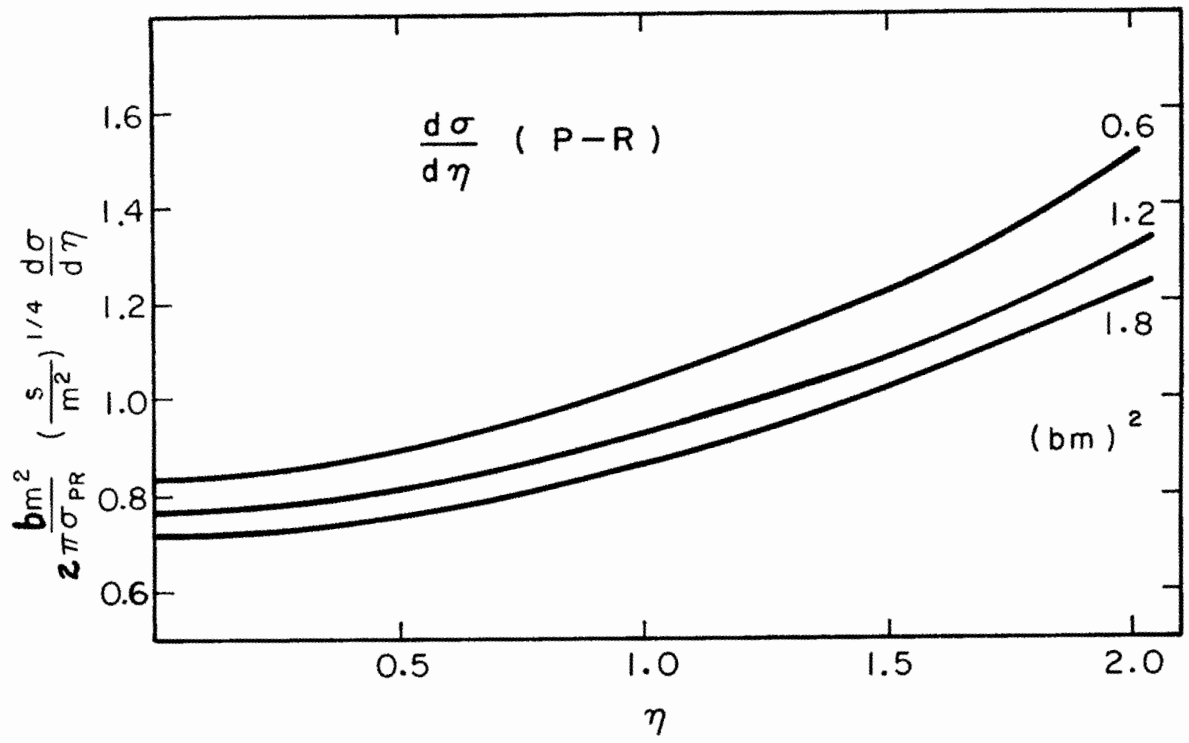

XBL726-3362

Fig. 5.6.

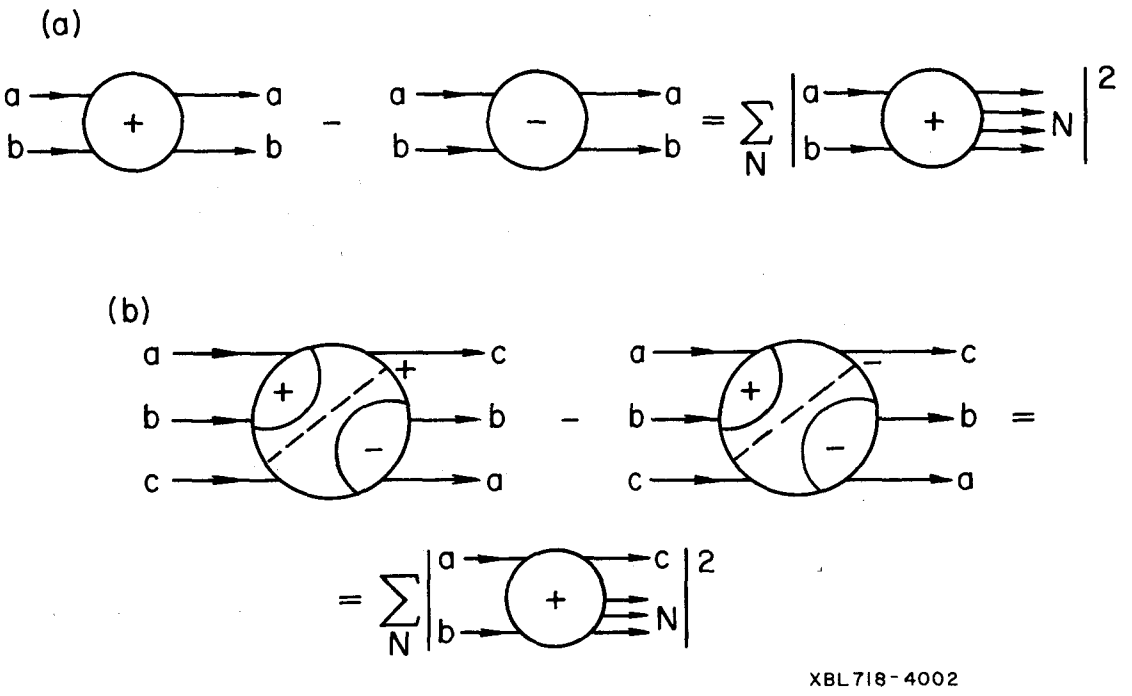

Figs. 6.1a. and 6.1e.

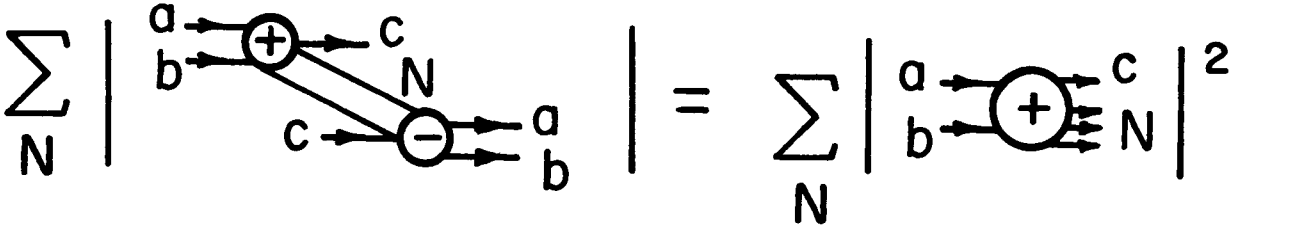

XBL726-3364

Fig. 6.1b.

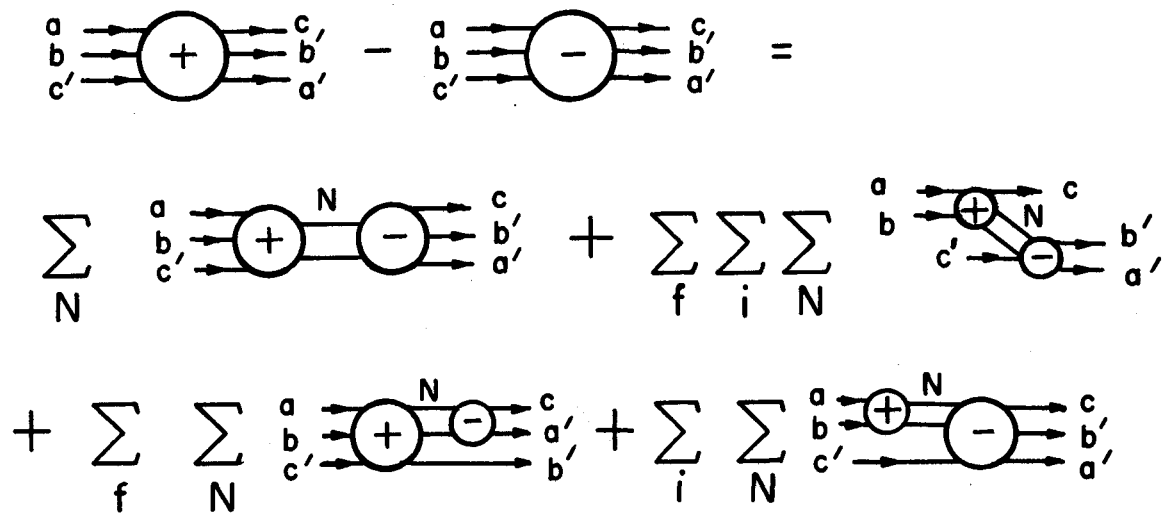

Fig. 6.1c.

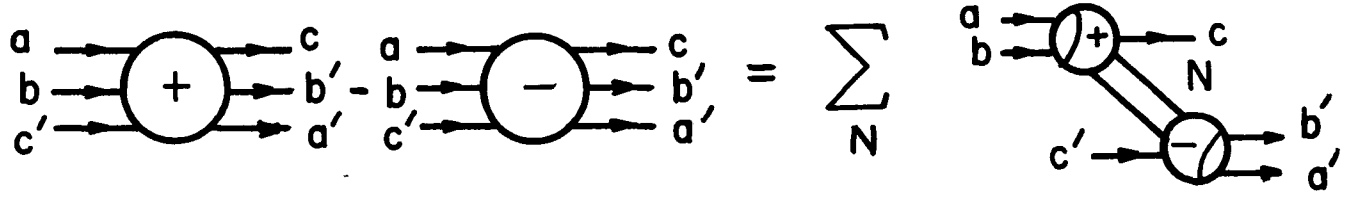

XBL726 - 3366

Fig. 6.1d.

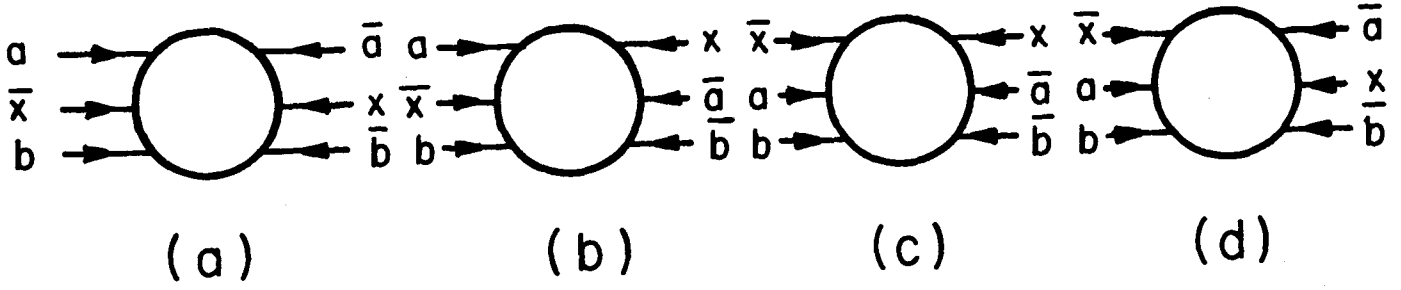

XBL726-3363

Fig. 6.2.

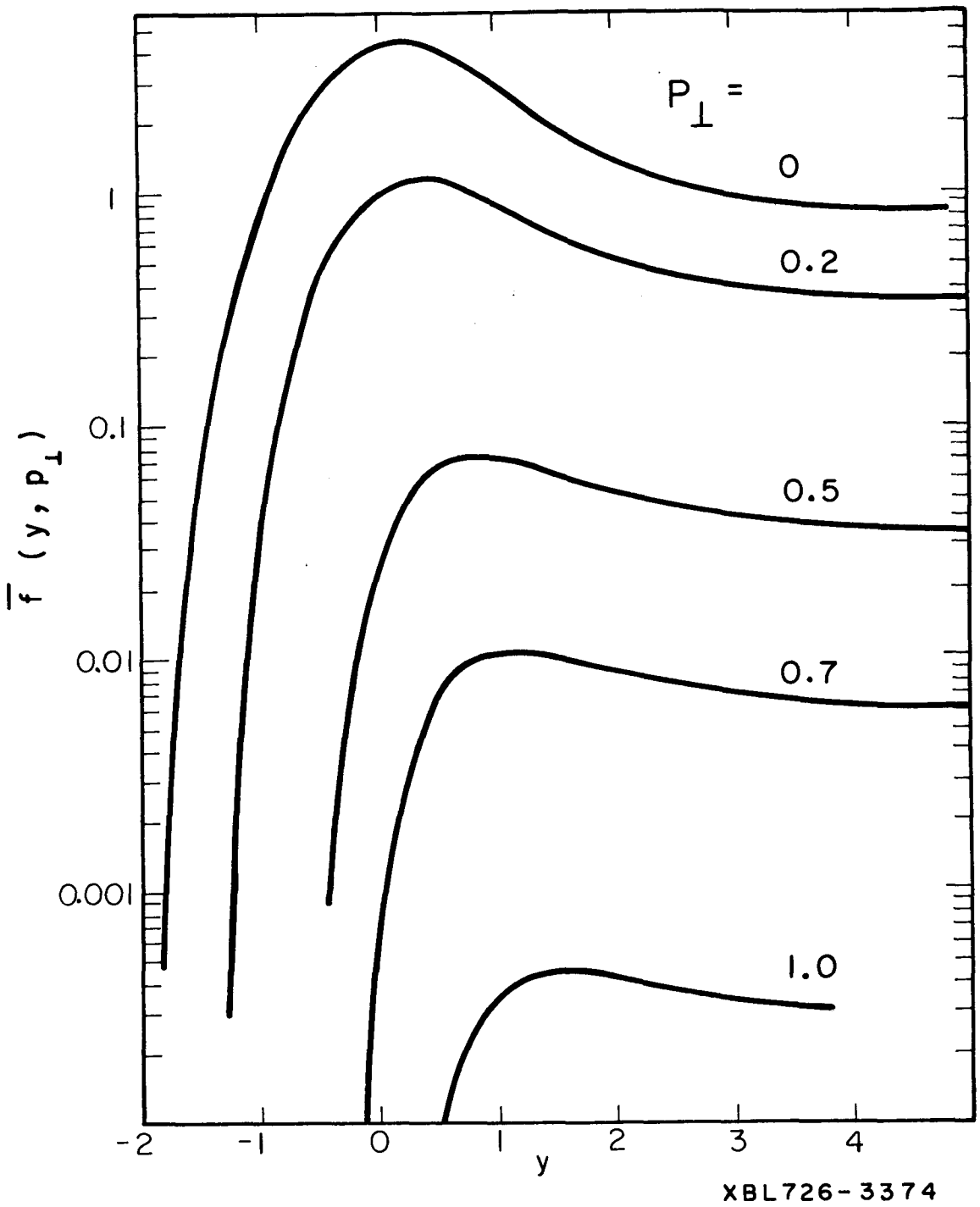
$P_\perp$ =
0
0.2
0.5
0.7
1.0
1
0.1
0.01
0.001
$\bar{f}(y, p_\perp)$
-2
-1
0
1
2
3
4
y
XBL726-3374

Fig. 6.3.

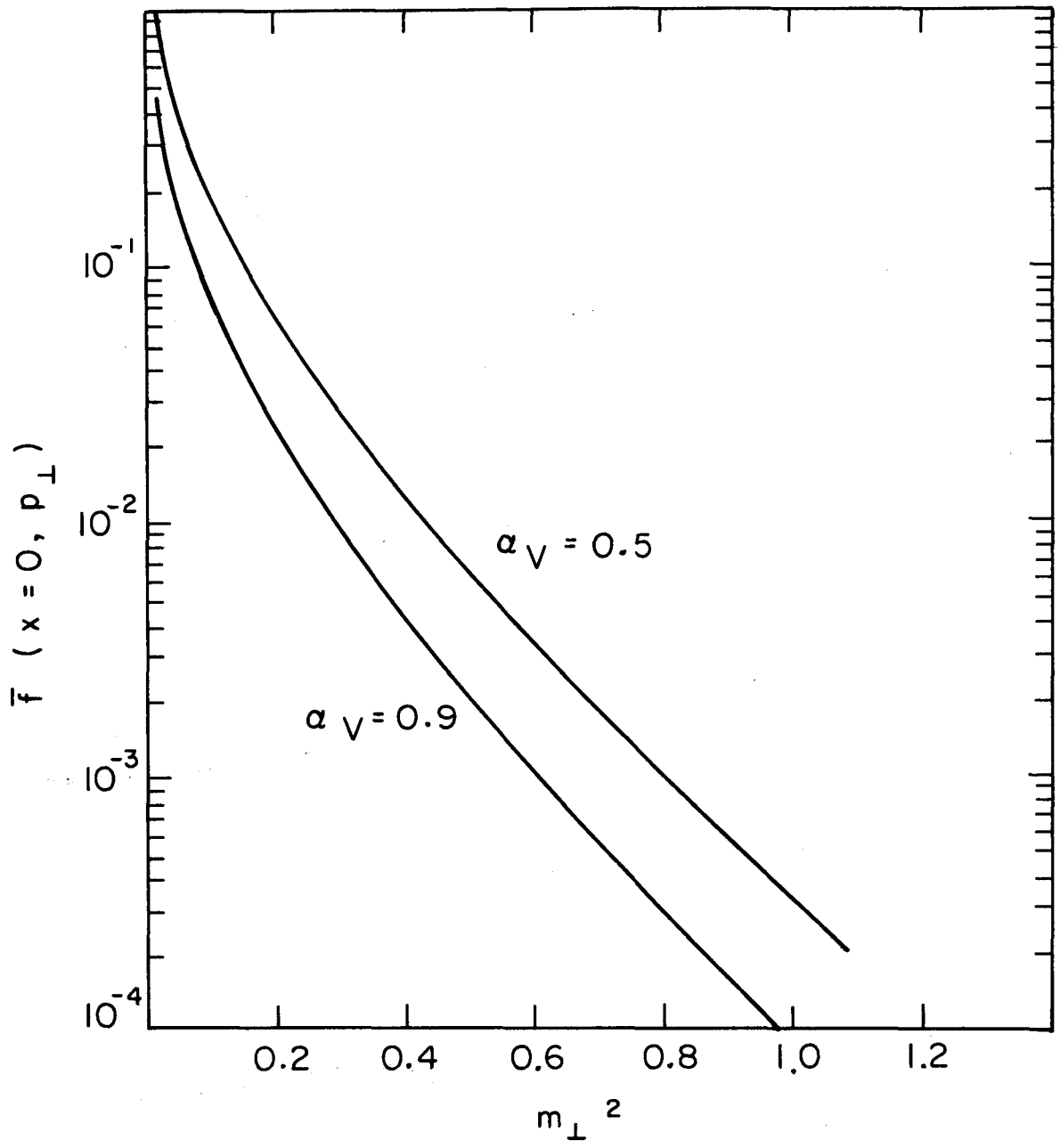

XBL726 - 3367

Fig. 6.4.

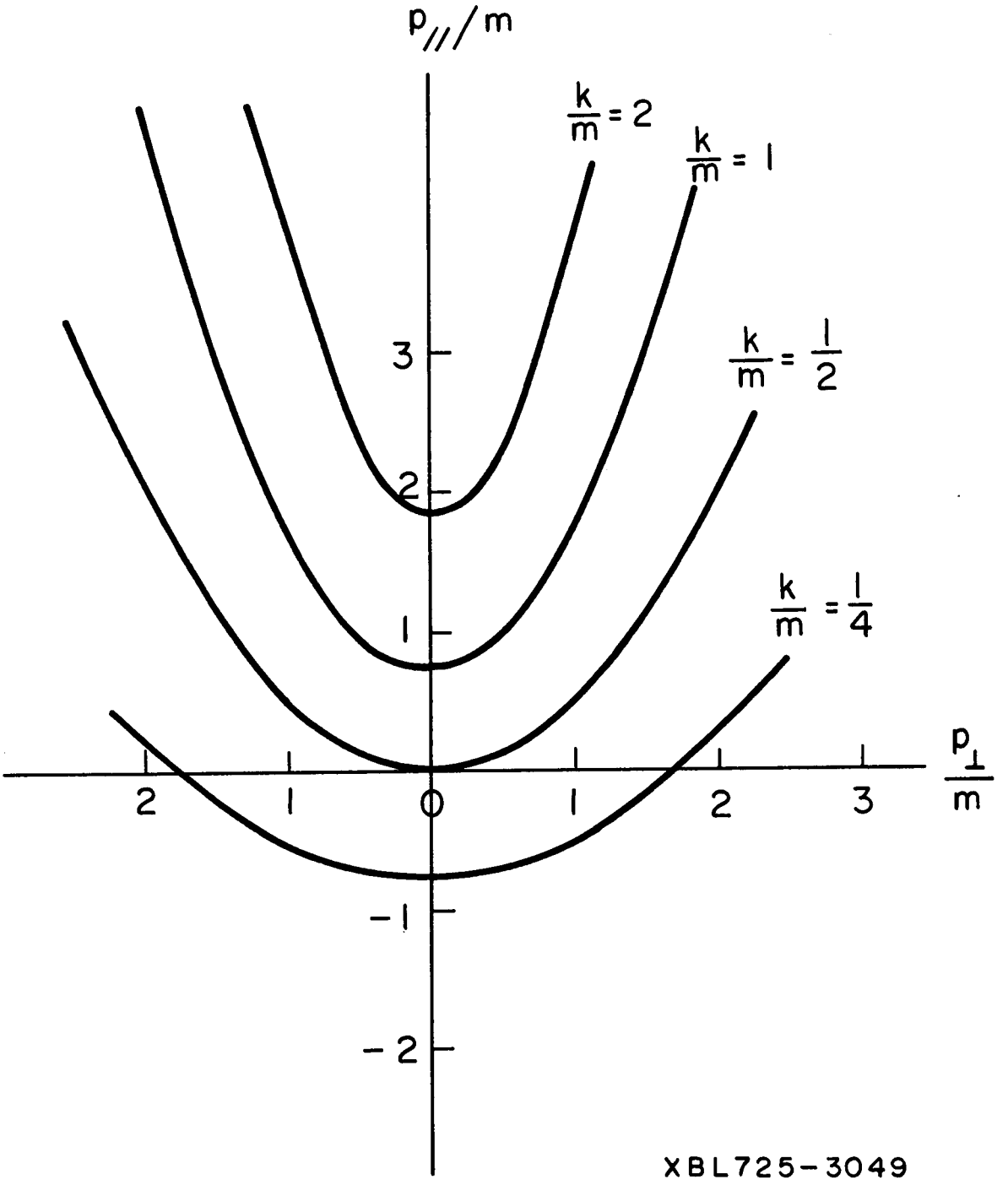
$p_{///}/m$
$\frac{k}{m} = 2$
$\frac{k}{m} = 1$
$\frac{k}{m} = \frac{1}{2}$
$\frac{k}{m} = \frac{1}{4}$
3
2
1
-1
-2
2
1
0
1
2
3
$\frac{p_\perp}{m}$
XBL725-3049

Fig. 7.1.

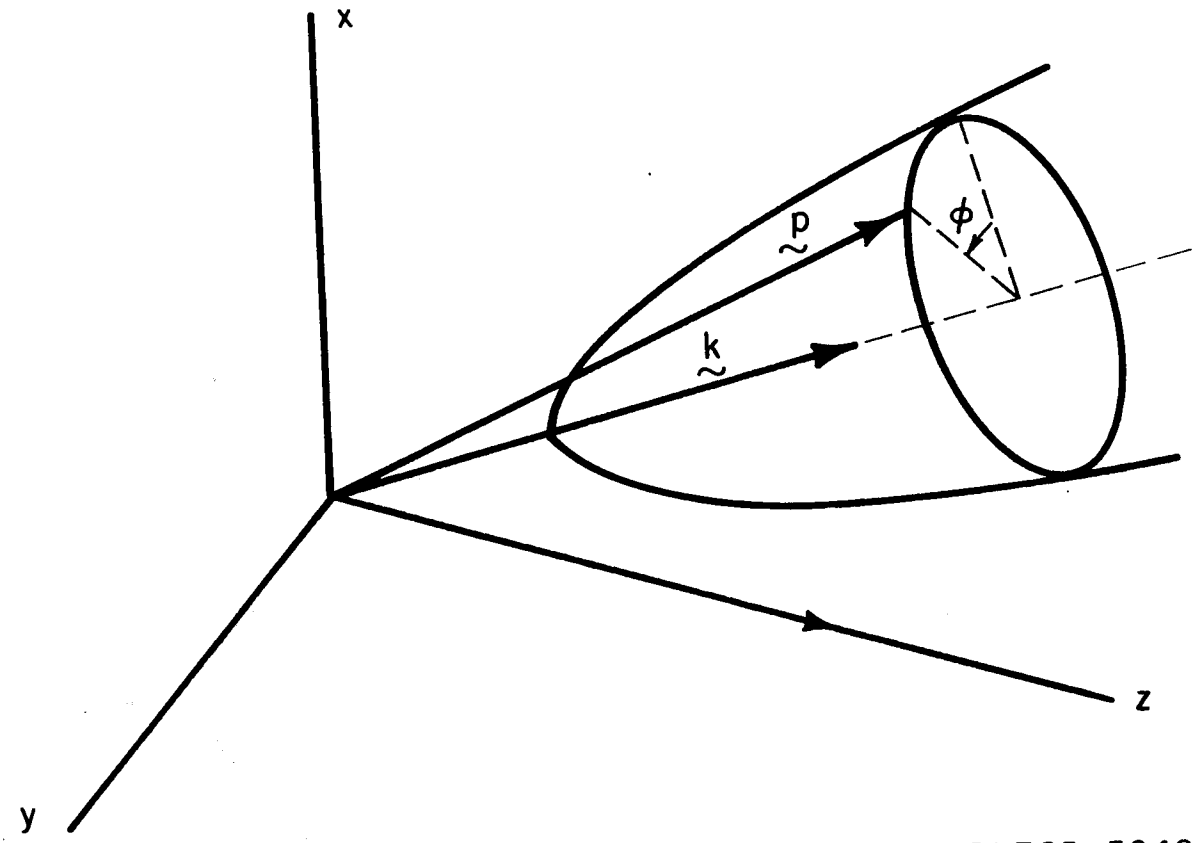

Fig. 7.2.

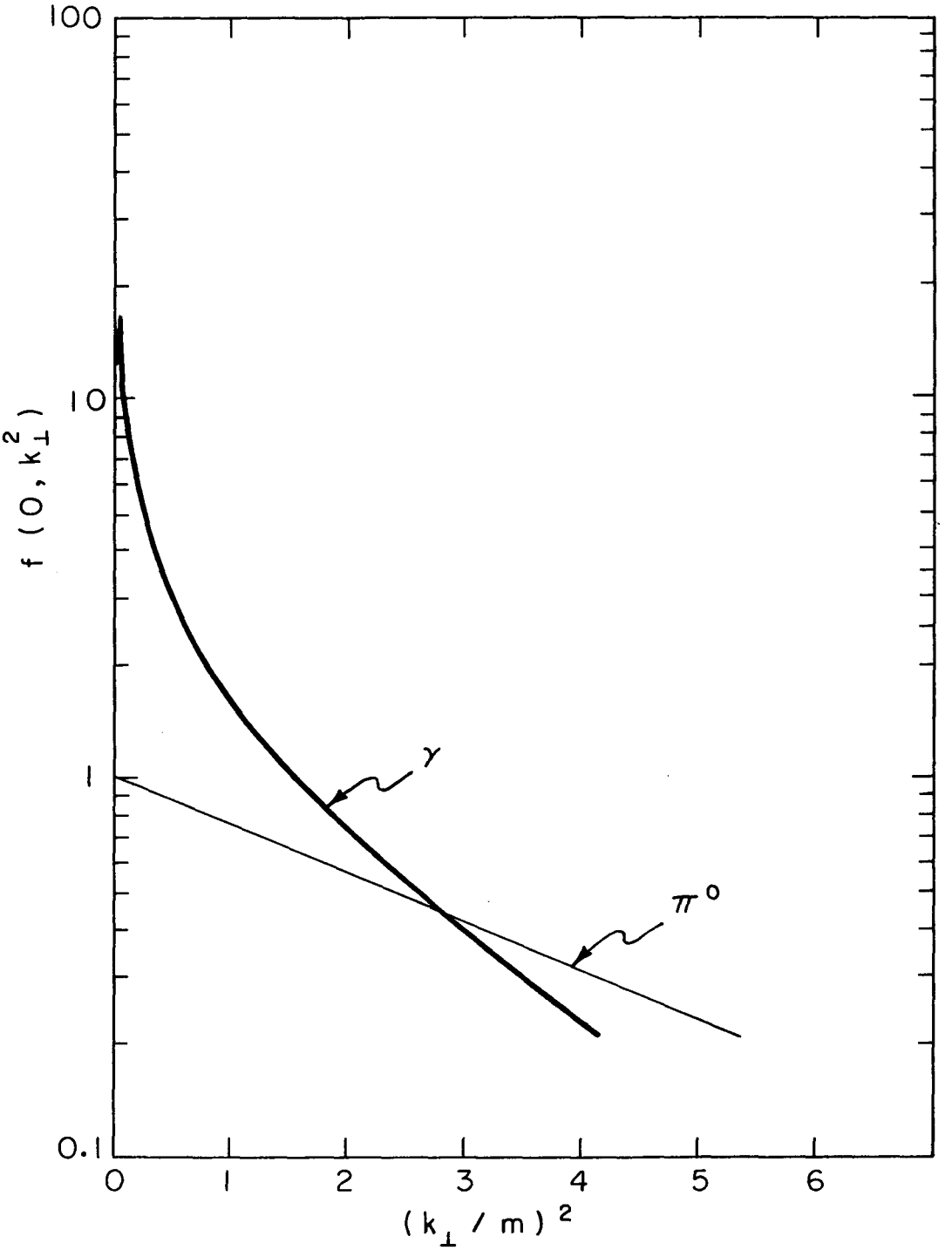

XBL725-3056

Fig. 7.3.

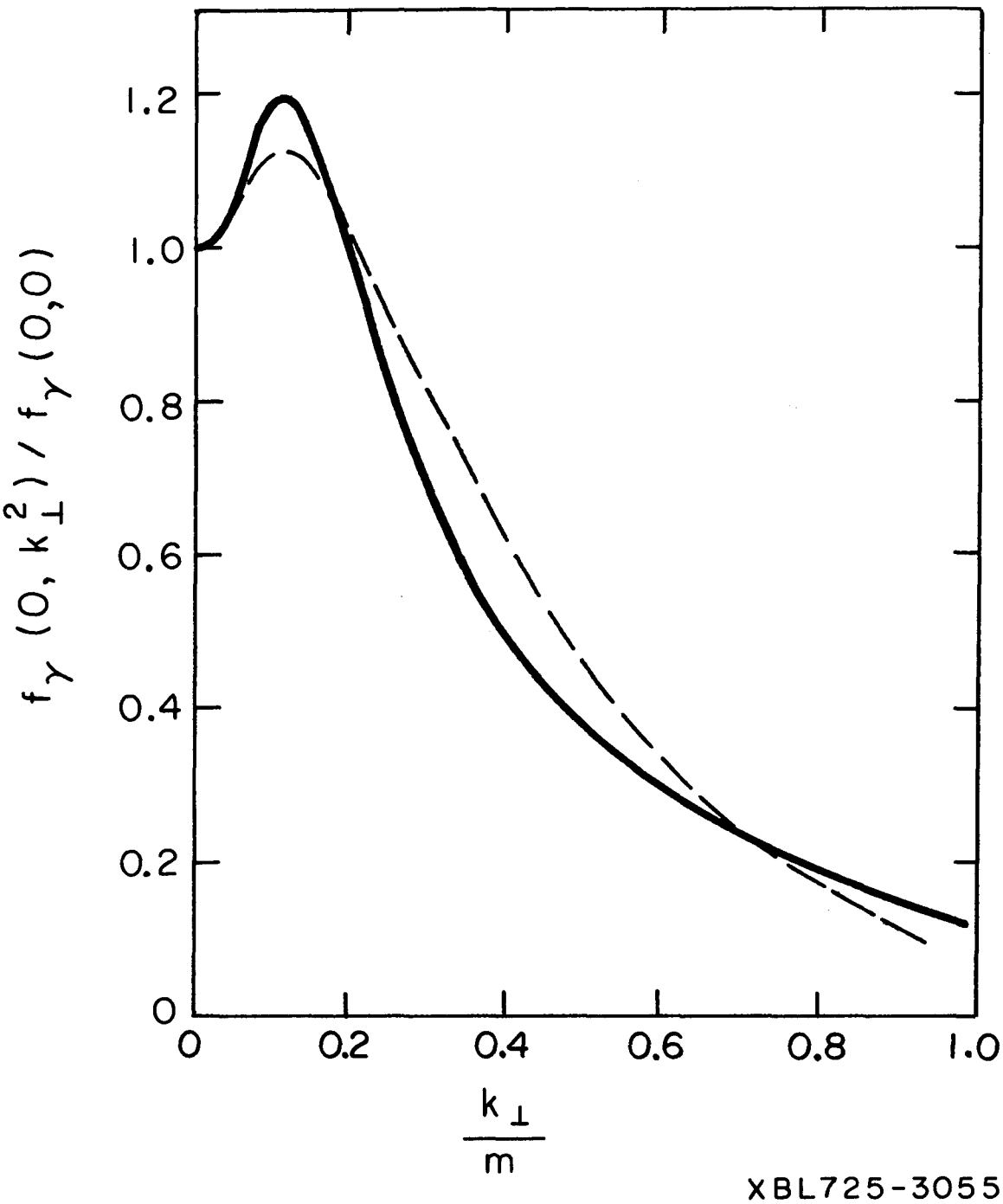
1.2
1.0
0.8
0.6
0.4
0.2
0
0
0.2
0.4
0.6
0.8
1.0
$f_\gamma(0, k_\perp^2) / f_\gamma(0,0)$
$\frac{k_\perp}{m}$
XBL725-3055

Fig. 7.4.

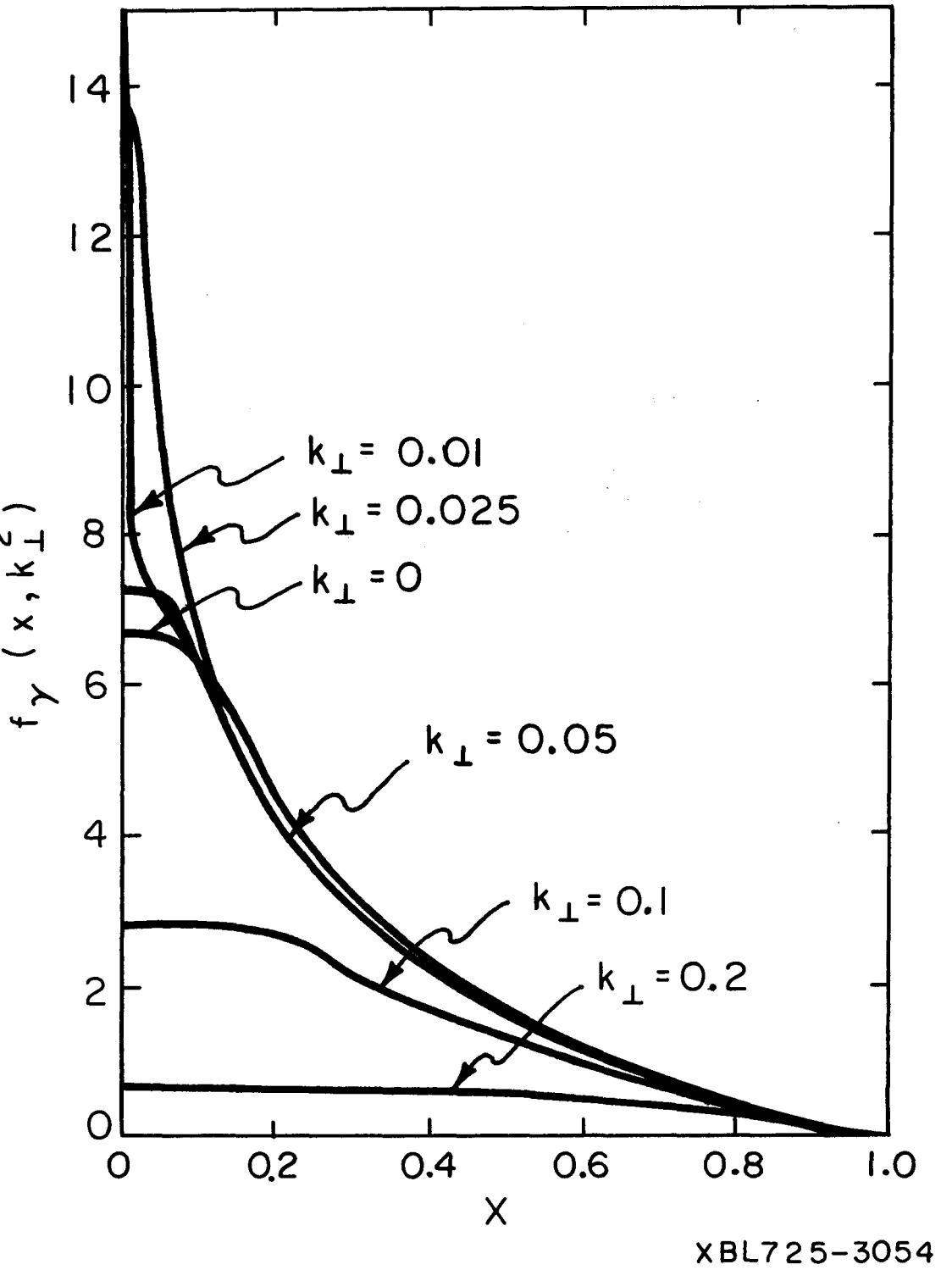
14
12
10
8
6
4
2
0
0
0.2
0.4
0.6
0.8
1.0
X
$f_\gamma(x, k_\perp^2)$
$k_\perp = 0.01$
$k_\perp = 0.025$
$k_\perp = 0$
$k_\perp = 0.05$
$k_\perp = 0.1$
$k_\perp = 0.2$
XBL725-3054

Fig.7.5.

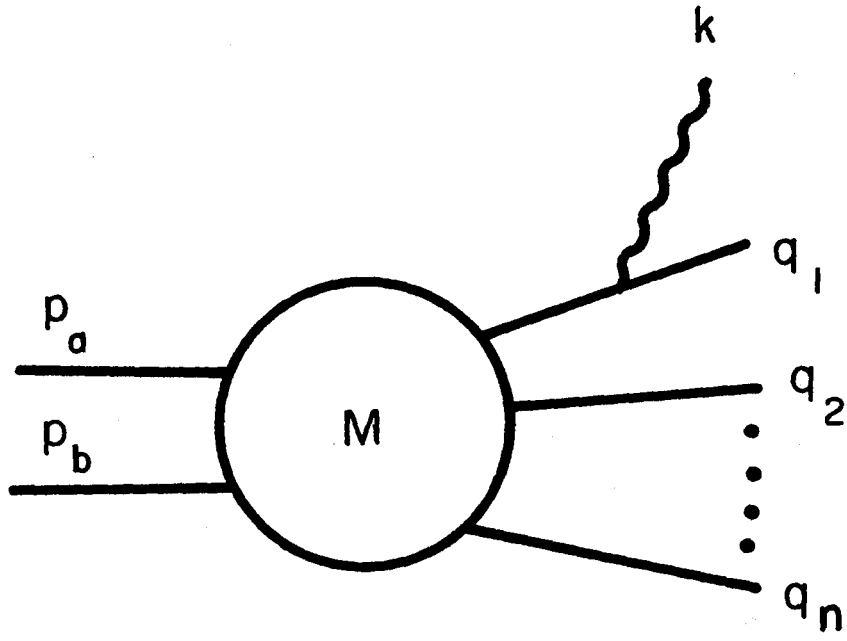

XBL725-3053

Fig. 7.6.

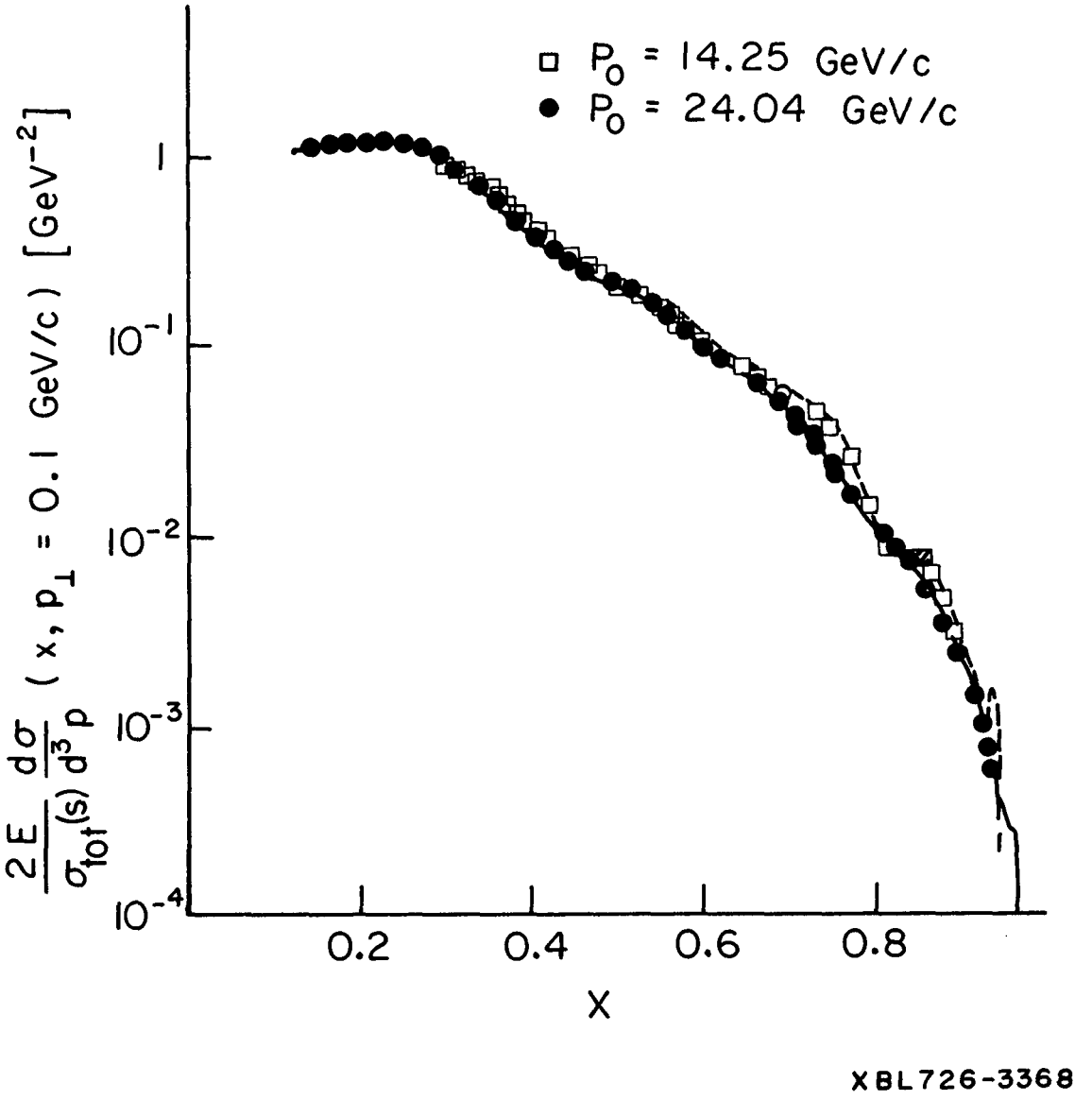

XBL726-3368

Fig. 8.1.

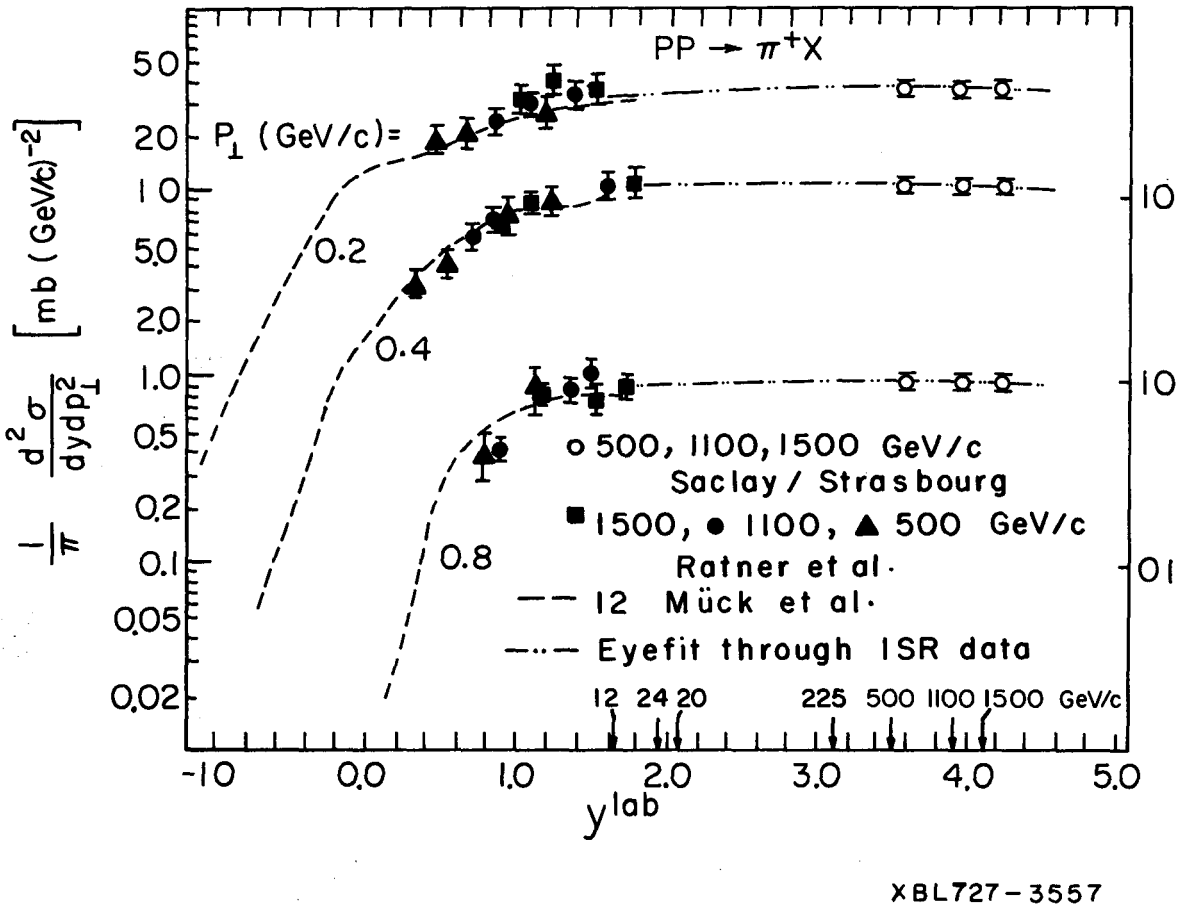
PP → π⁺X
P⊥ (GeV/c)=
0.2
0.4
0.8
o 500, 1100, 1500 GeV/c
Saclay / Strasbourg
■ 1500, ● 1100, ▲ 500 GeV/c
Ratner et al.
12 Mück et al.
Eyefit through ISR data
12 24 20 225 500 1100 1500 GeV/c
1/π d²σ/dydp²⊥ [mb (GeV/c)⁻²]
ylab
XBL727-3557

Fig. 8.2.

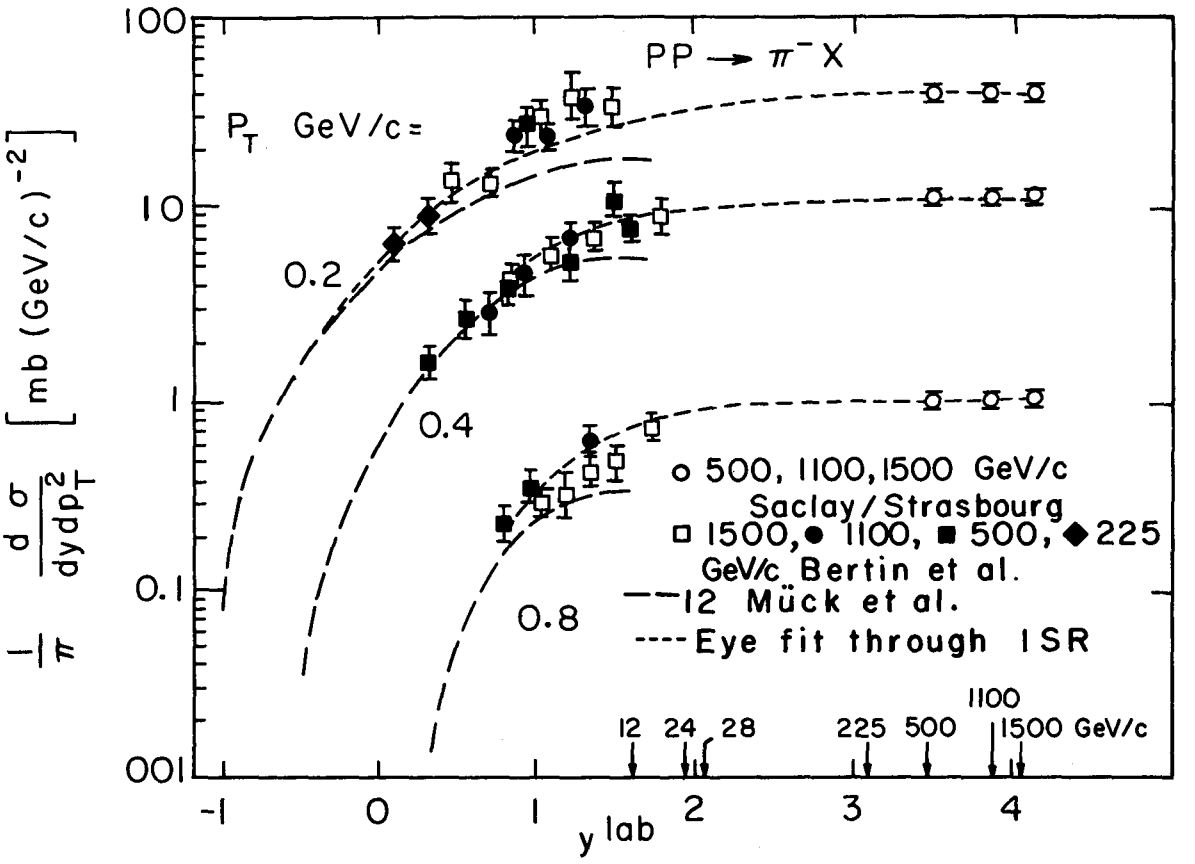

XBL727 – 3558

Fig. 8.3.

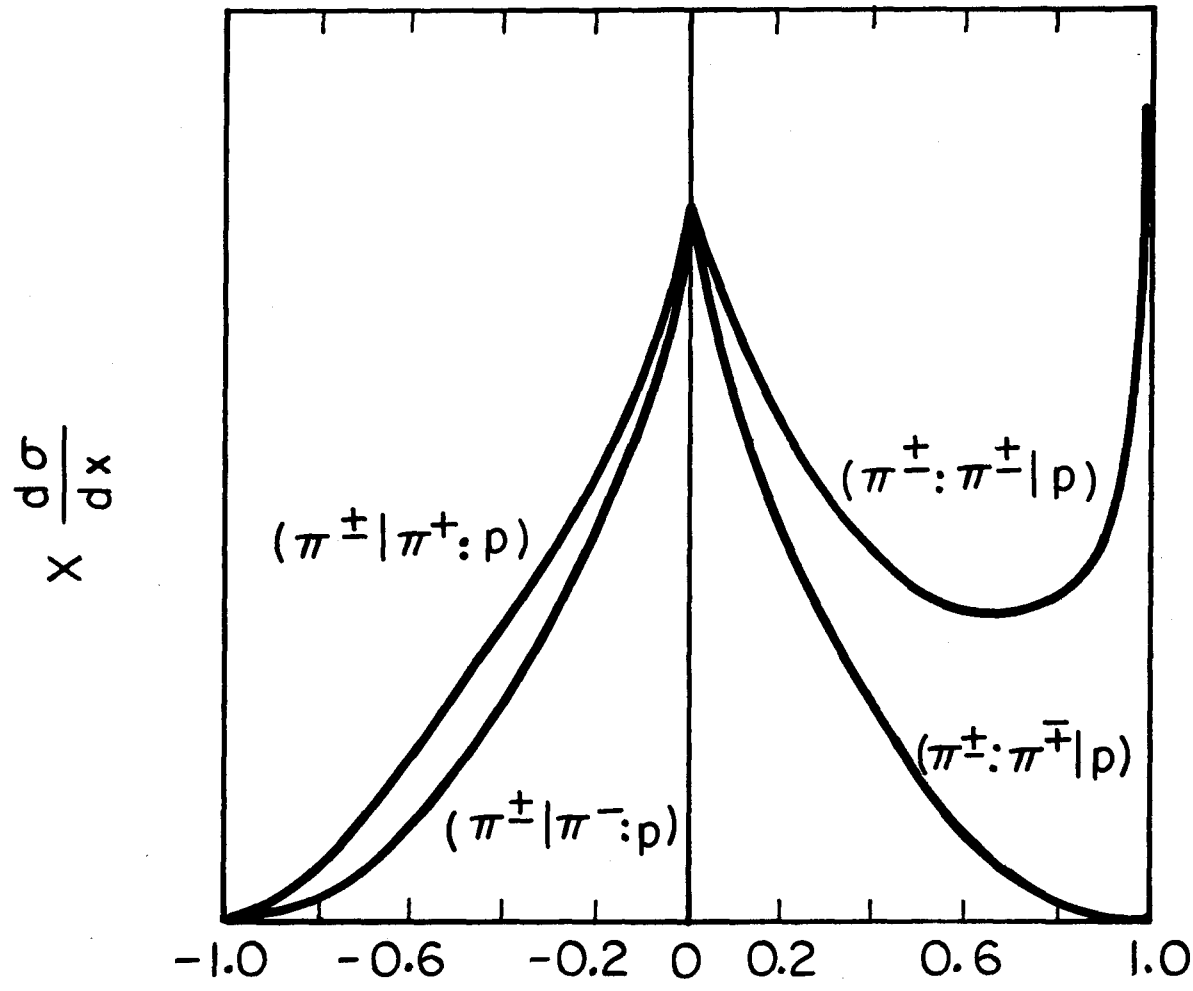
$\frac{d\sigma}{dx}$ x
$(\pi^{\pm}|\pi^{+}:p)$
$(\pi^{\pm}|\pi^{-}:p)$
$(\pi^{\pm}:\pi^{\pm}|p)$
$(\pi^{\pm}:\pi^{\mp}|p)$
-1.0
-0.6
-0.2
0
0.2
0.6
1.0
XBL726-3369

Fig. 8.4.

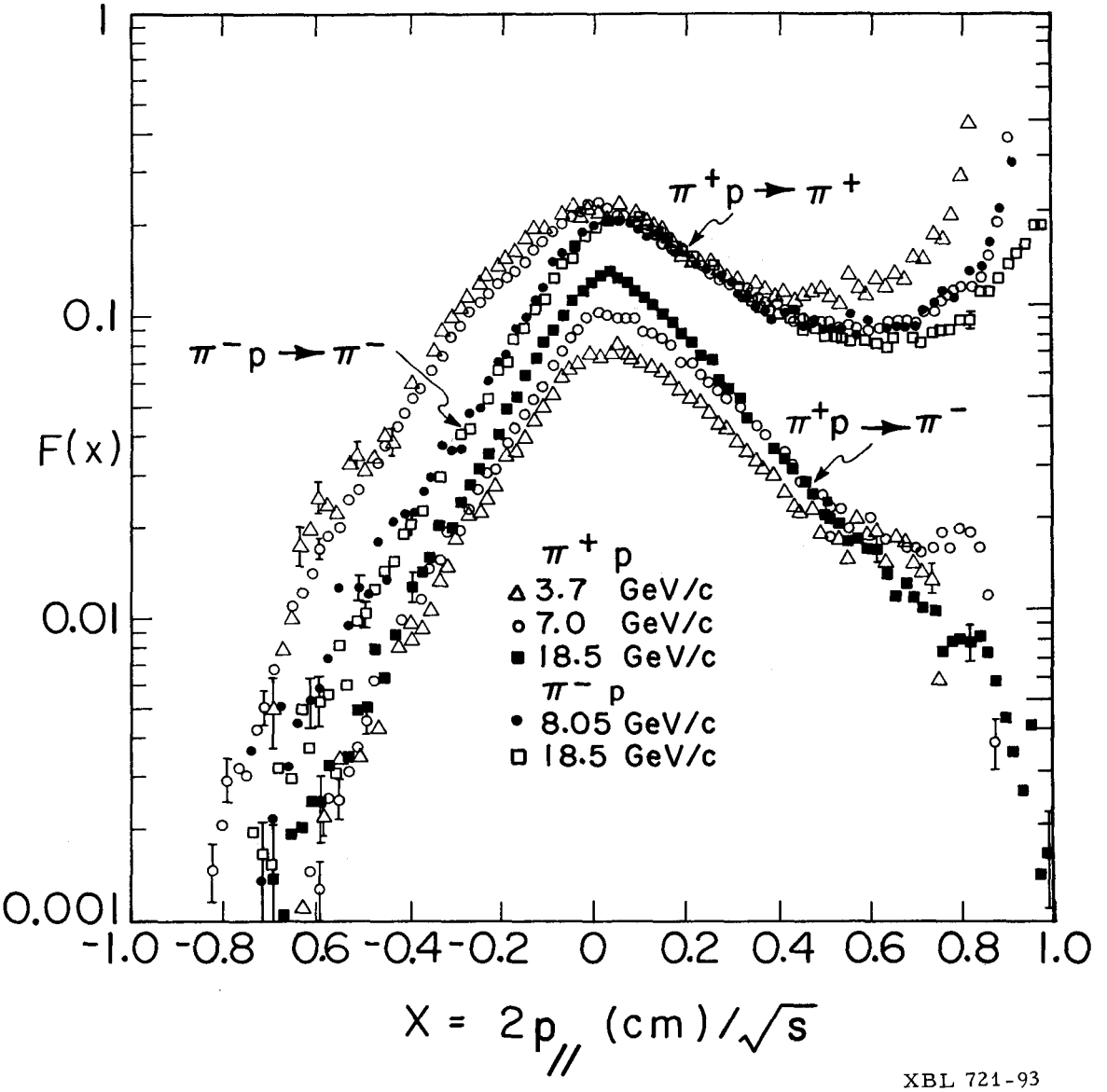
1
0.1
0.01
0.001
F(x)
$\pi^+ p \to \pi^+$
$\pi^- p \to \pi^-$
$\pi^+ p \to \pi^-$
π^+ p
3.7 GeV/c
7.0 GeV/c
18.5 GeV/c
π^- p
8.05 GeV/c
18.5 GeV/c
-1.0 -0.8 -0.6 -0.4 -0.2 0 0.2 0.4 0.6 0.8 1.0
$X = 2p_{//}\,(cm)/\sqrt{s}$
XBL 721-93

Fig. 8.5.

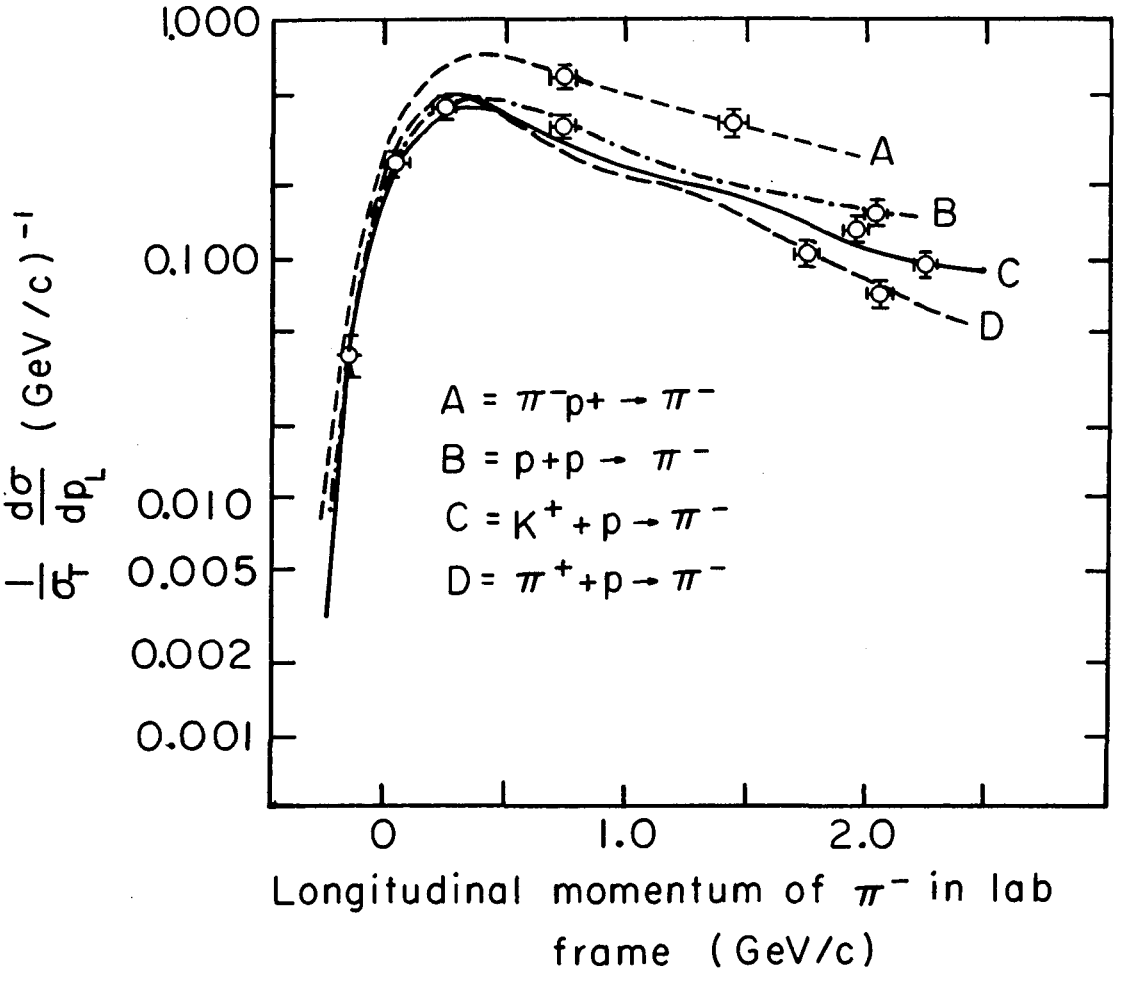
1.000
0.100
0.010
0.005
0.002
0.001
$-\frac{1}{\sigma_T}\frac{d\sigma}{dp_L}$ (GeV/c)$^{-1}$
A = $\pi^- p+ \rightarrow \pi^-$
B = $p+p \rightarrow \pi^-$
C = $K^+ + p \rightarrow \pi^-$
D = $\pi^+ + p \rightarrow \pi^-$
A
B
C
D
0
1.0
2.0
Longitudinal momentum of π^- in lab frame (GeV/c)
XBL726-3358

Fig. 8.6.

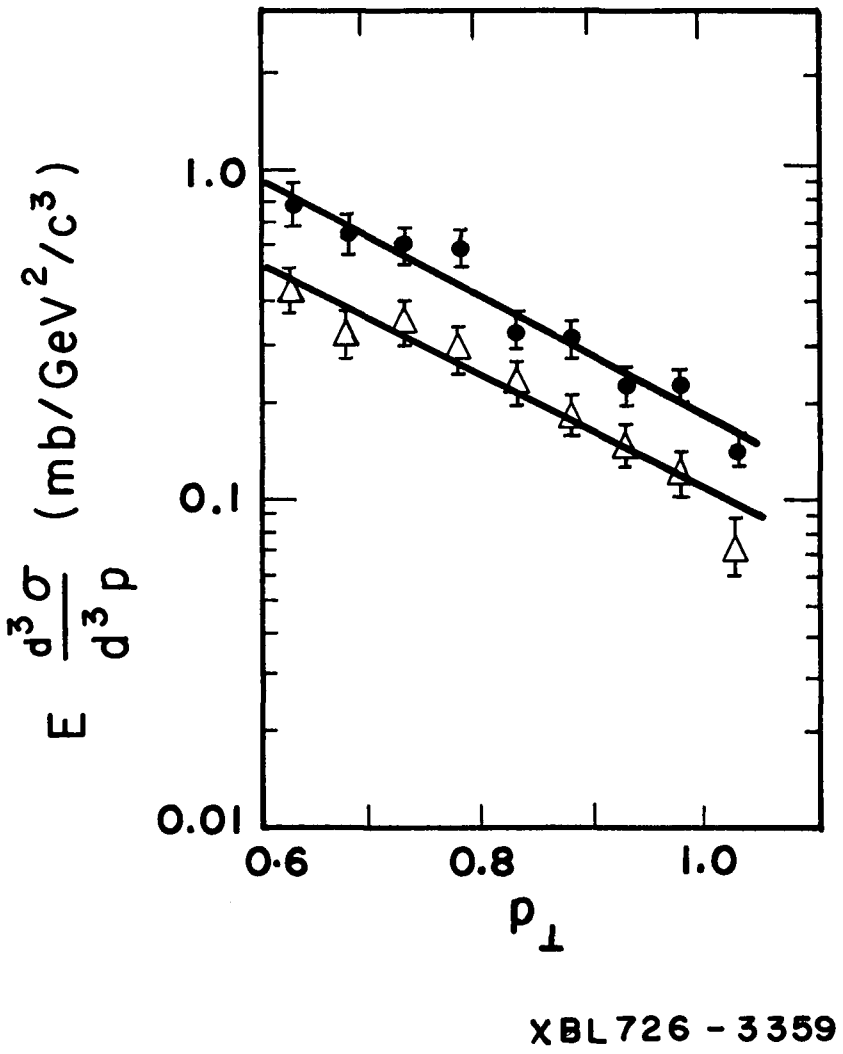

XBL726-3359

Fig. 8.7.

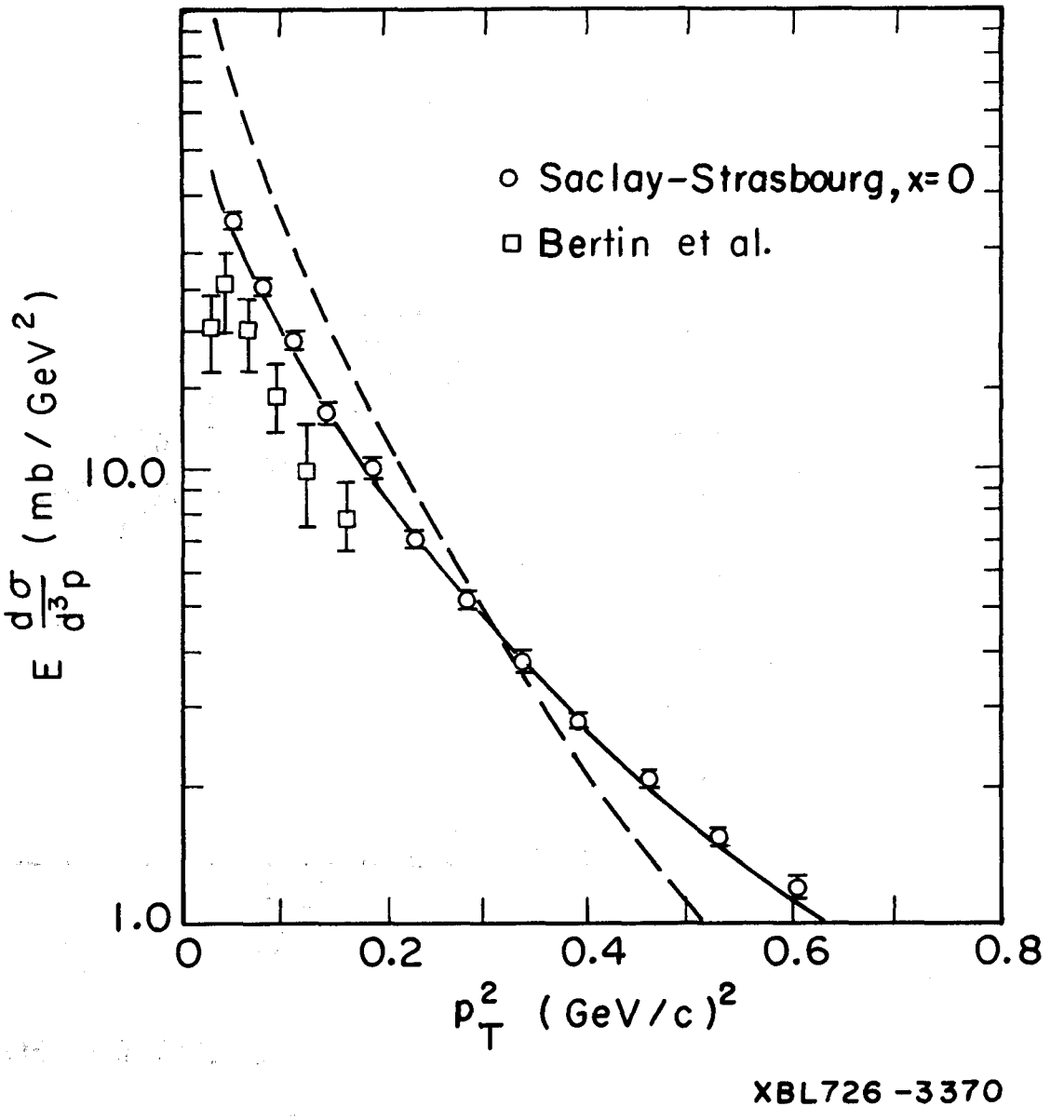
o Saclay-Strasbourg, x=0
□ Bertin et al.
$E\frac{d\sigma}{d^3p}$ (mb / GeV^2)
10.0
1.0
0
0.2
0.4
0.6
0.8
p_T^2 (GeV/c)^2
XBL726-3370

Fig. 8.8a.

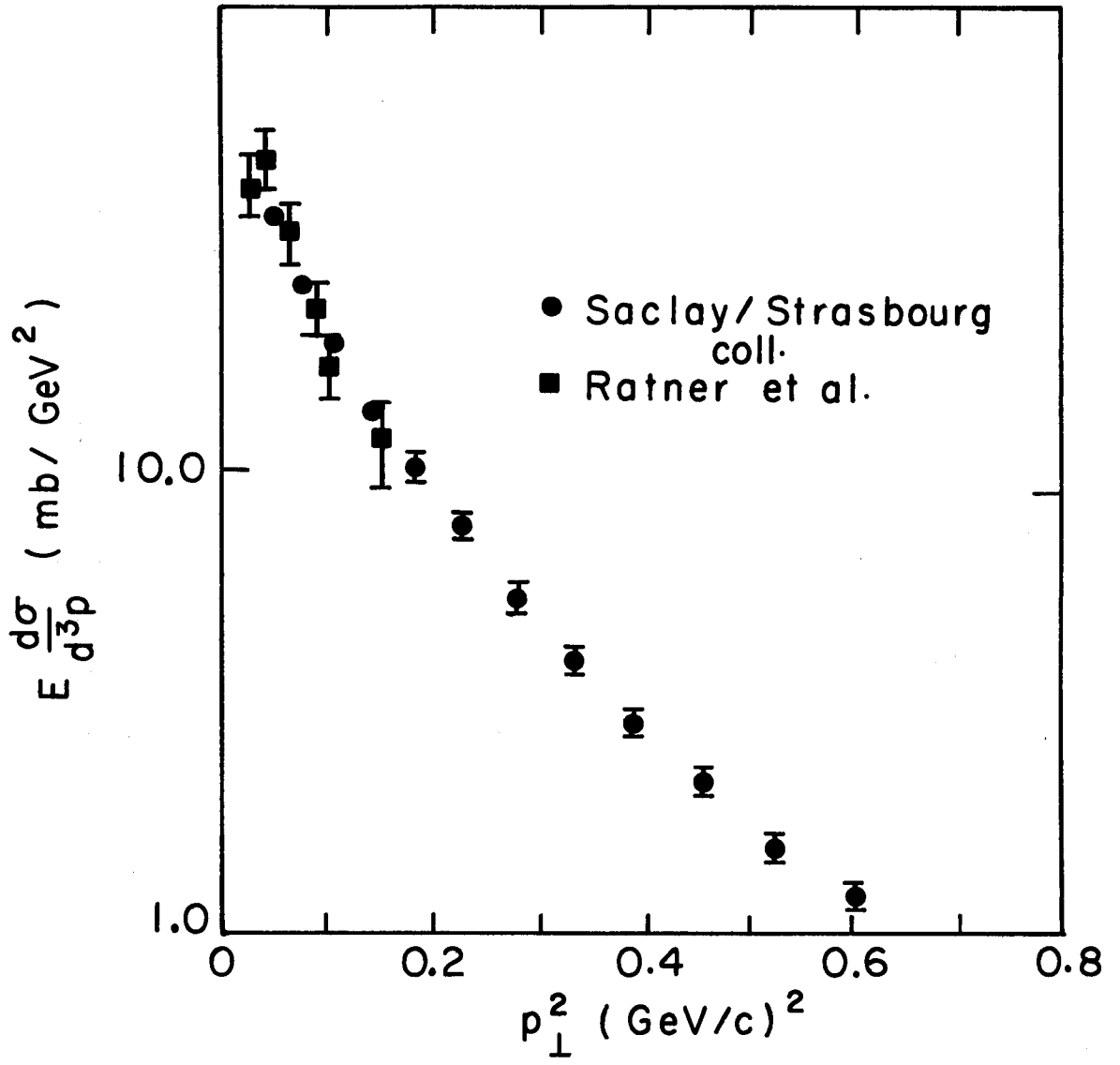
Saclay/Strasbourg coll.
Ratner et al.
10.0
1.0
0
0.2
0.4
0.6
0.8
$E\frac{d\sigma}{d^3p}$ (mb/ GeV^2)
$p_\perp^2$ (GeV/c)^2
XBL726-3371

Fig. 8.8b.

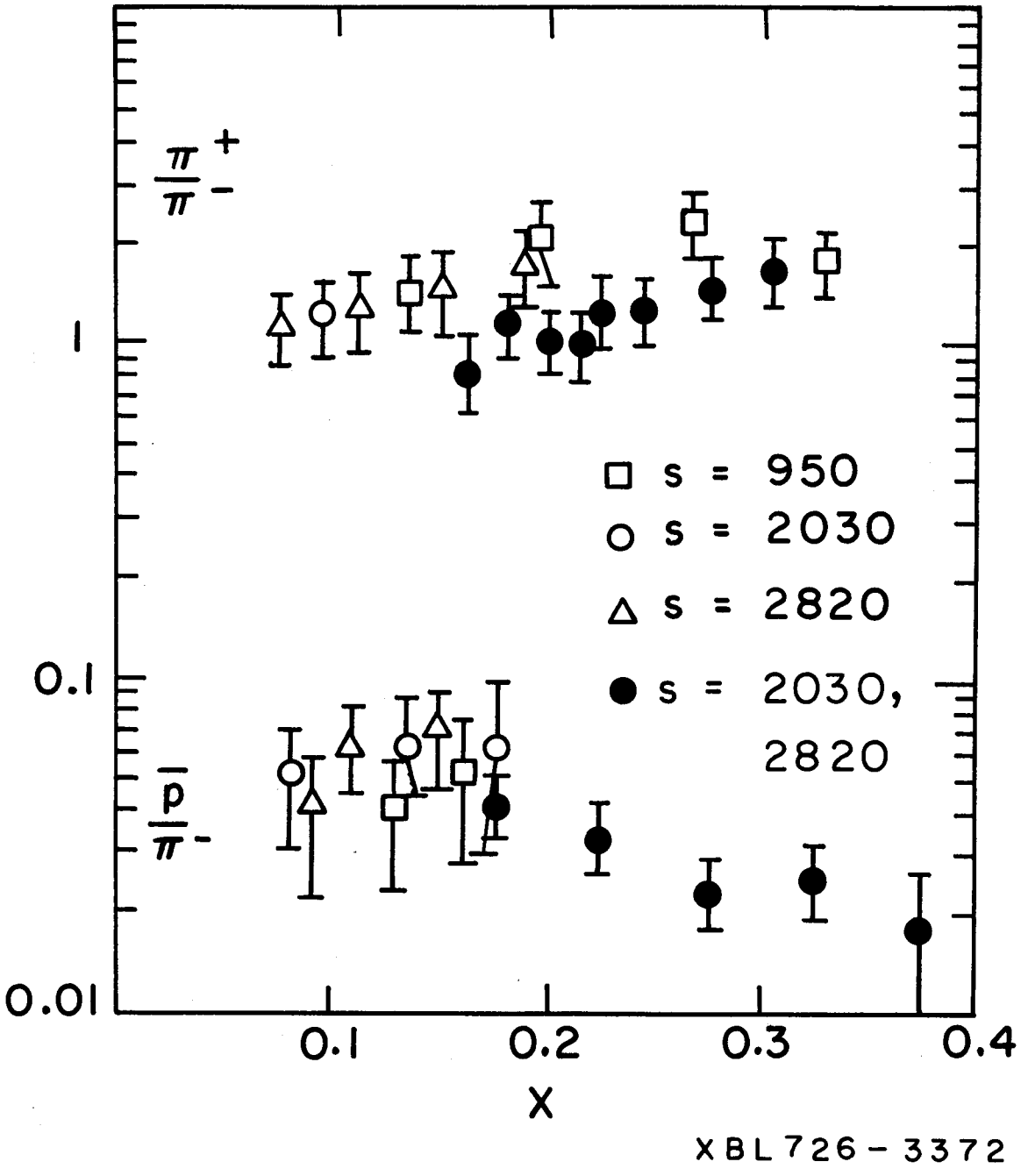
$\frac{\pi^+}{\pi^-}$
$\frac{\bar{p}}{\pi^-}$
1
0.1
0.01
0.1
0.2
0.3
0.4
X
□ s = 950
○ s = 2030
△ s = 2820
● s = 2030, 2820
XBL726-3372

Fig. 8.9.

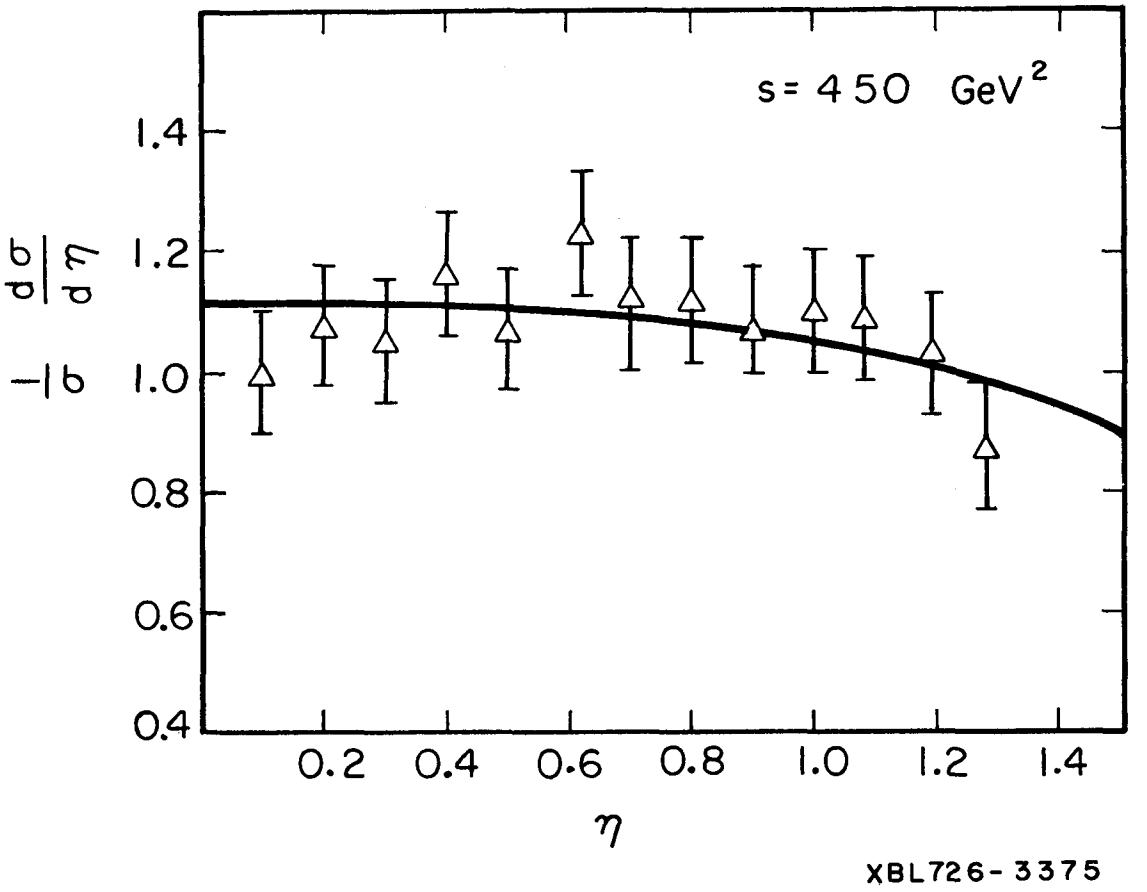

Fig. 8.10a.

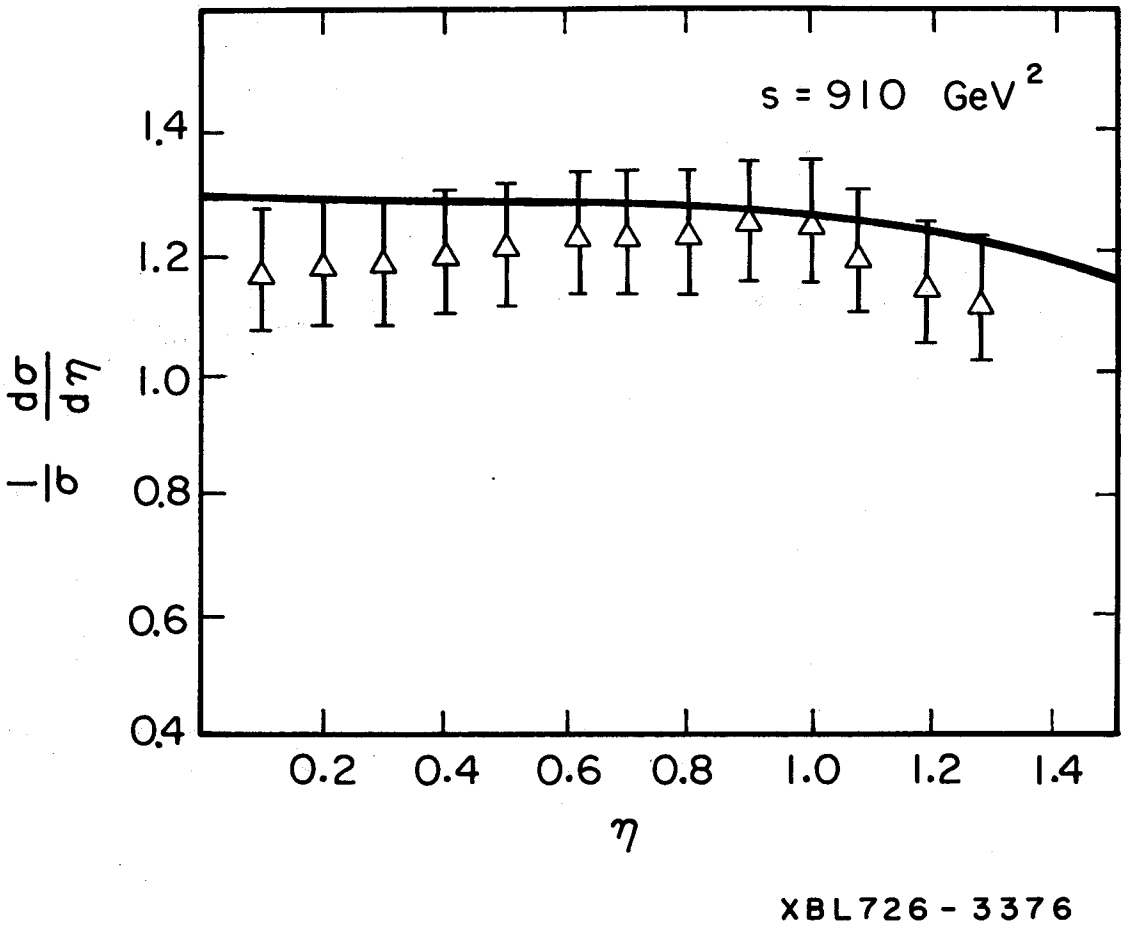
s = 910 GeV²
1.4
1.2
1.0
0.8
0.6
0.4
0.2
0.4
0.6
0.8
1.0
1.2
1.4
η
dσ/dη
−|b
XBL726-3376

Fig. 8.10b.

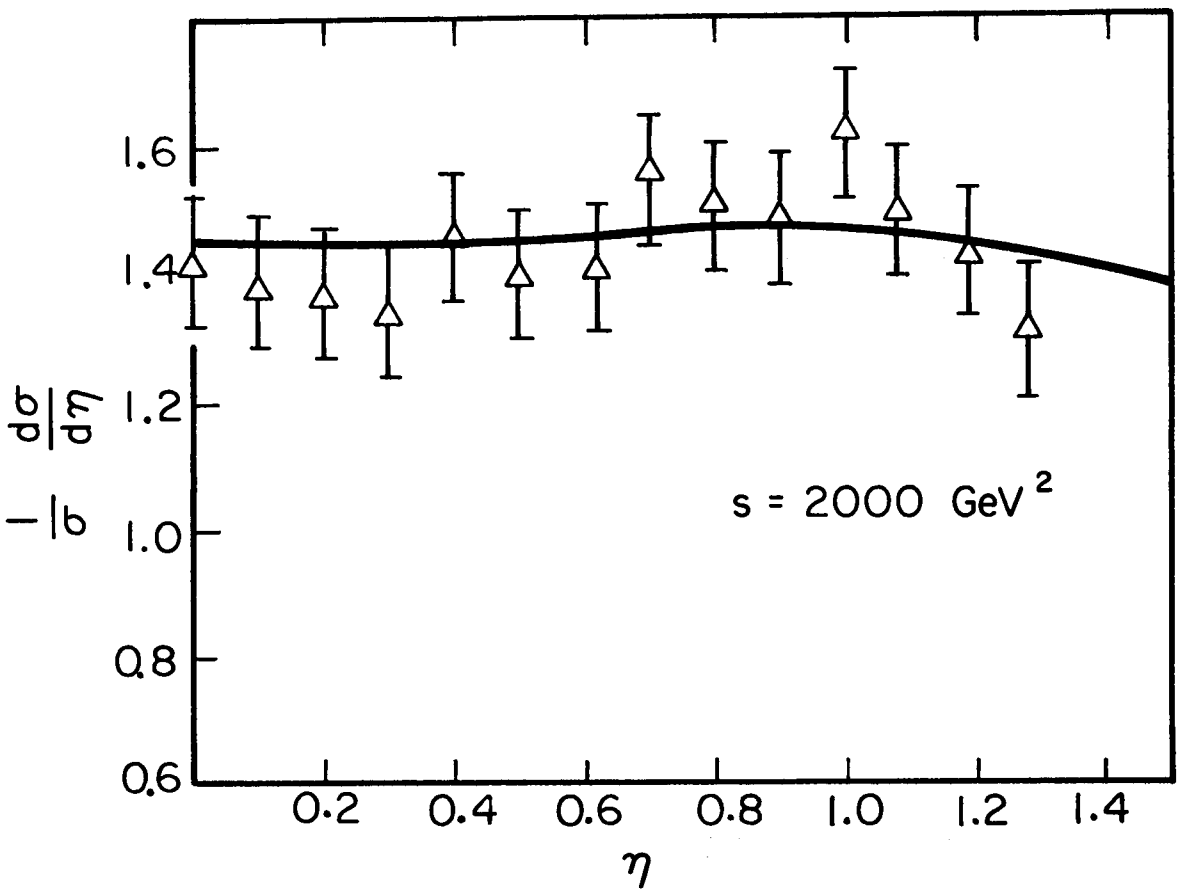

XBL726-3377

Fig. 8.10c.

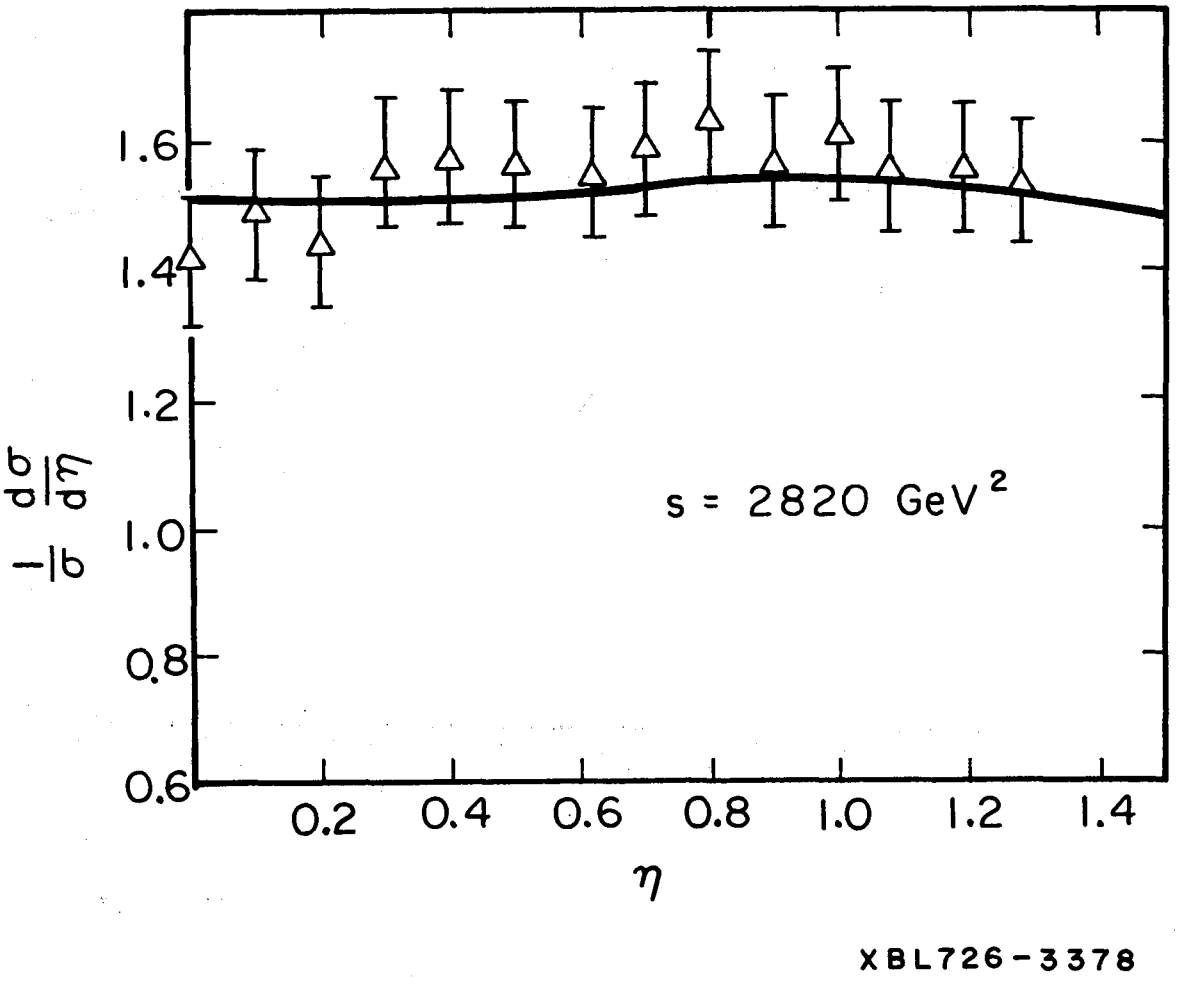
1.6
1.4
1.2
1.0
0.8
0.6
0.2
0.4
0.6
0.8
1.0
1.2
1.4
η
s = 2820 GeV²
dσ/dη
XBL726-3378

Fig. 8.10d.

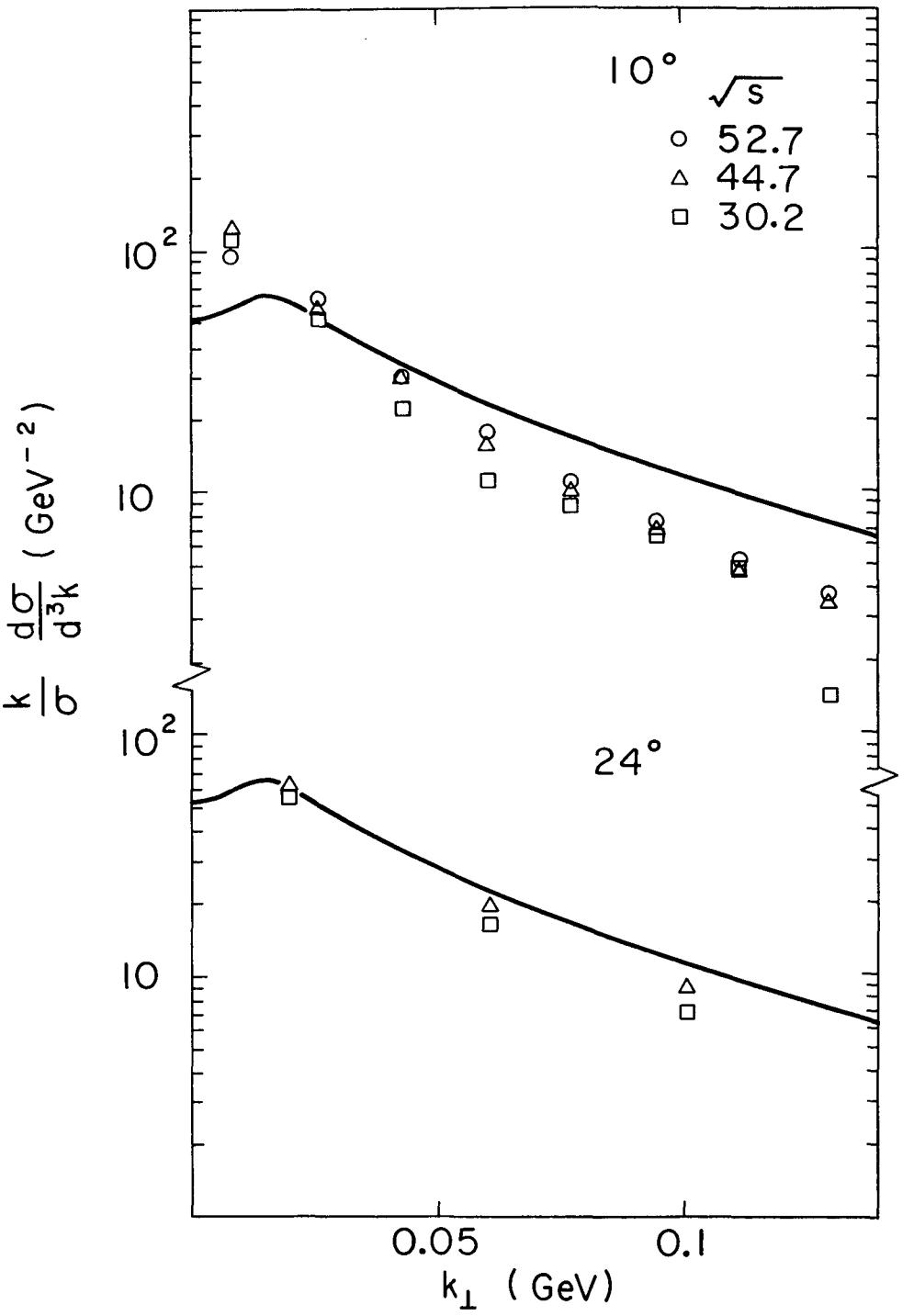
10°
√s
52.7
44.7
30.2
10²
10
10²
10
24°
0.05
0.1
k⊥ (GeV)
k/σ dσ/d³k (GeV⁻²)
XBL725-3052

Fig. 8.11.

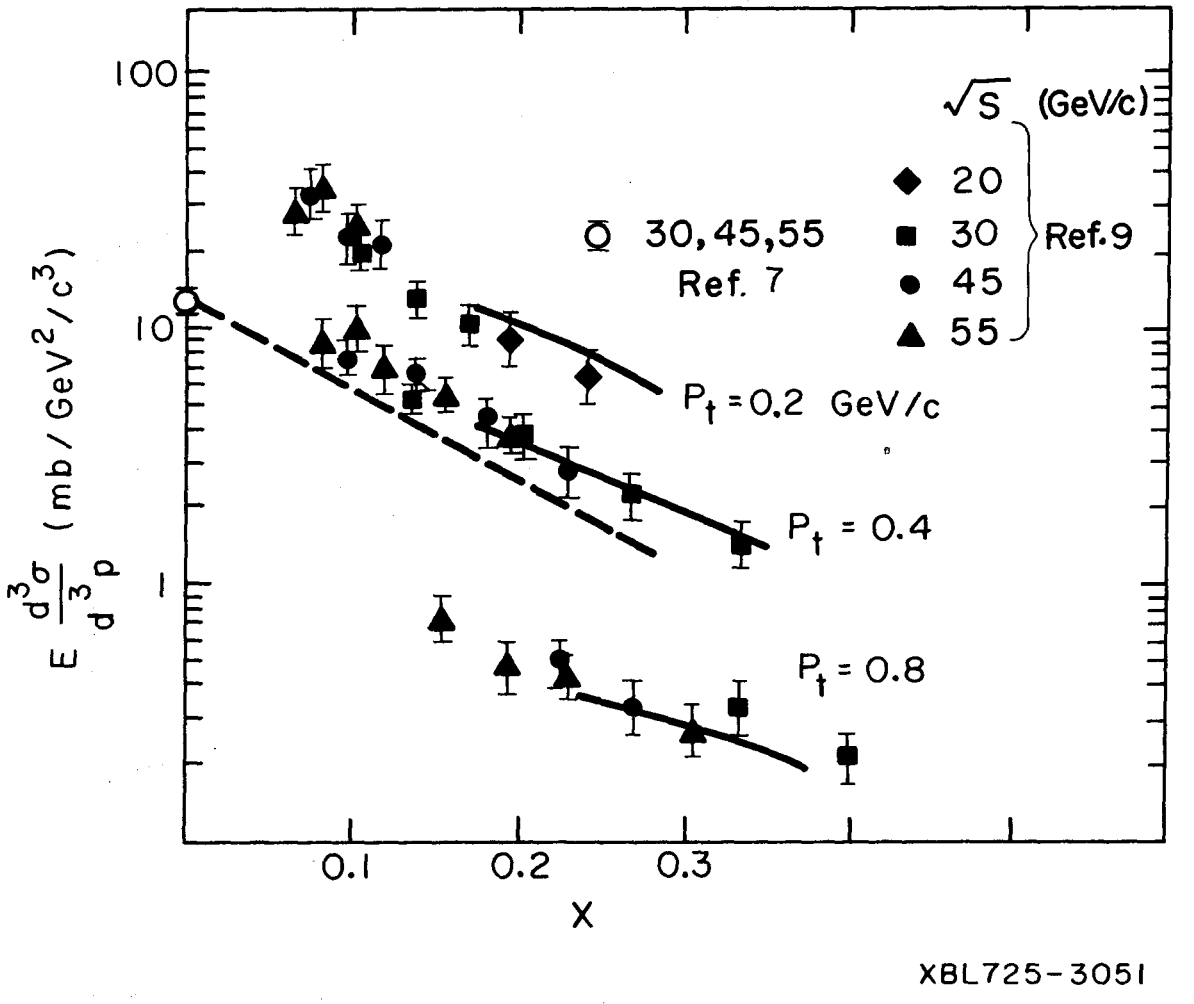
100
10
1
$E\frac{d^3\sigma}{d^3p}$ (mb/GeV^2/c^3)
0.1
0.2
0.3
X
$\sqrt{S}$ (GeV/c)
20
30
45
55
Ref.9
30,45,55
Ref. 7
P_t = 0.2 GeV/c
P_t = 0.4
P_t = 0.8
XBL725-3051

Fig. 8.12.